Title

Low-cost Retrofit of Ventilation and Filtration Systems to Improve Indoor Air Quality and Energy Efficiency in Buildings

Author

Pistochini, Theresa E

Publication Date

2024

Peer reviewed|Thesis/dissertation

Low-cost Retrofit of Ventilation and Filtration Systems to Improve Indoor Air Quality and Energy Efficiency in Buildings

By

THERESA PISTOCHINI
DISSERTATION

Submitted in partial satisfaction of the requirements for the degree of

DOCTOR OF PHILOSOPHY

in

Civil and Environmental Engineering

in the

OFFICE OF GRADUATE STUDIES

of the

UNIVERSITY OF CALIFORNIA

DAVIS

Approved:

Christopher Cappa, Co-Chair

Richard Corsi, Co-Chair

Deborah Bennett

Matthew Ellis

Committee in Charge

2024

Acknowledgements

I entered the PhD program with 12 years invested as a Research and Development Engineer at the UC Davis Western Cooling Efficiency Center (WCEC). WCEC aims to bridge the gap between industry and academia through research, development, and testing of technologies that reduce energy use in buildings, with a focus on heating, ventilation, and air conditioning (HVAC). In 2019, I concluded a study on energy efficiency and indoor air quality (IAQ) in schools working with Dr. Debbie Bennett and researchers at Lawrence Berkeley National Laboratory. While the study concluded, my interest did not, and I began to lay out a research agenda of all the things I wanted to do next. At this point, I decided to enter the PhD program to increase my subject matter knowledge and obtain the credentials needed to lead future research. A decade of experience laid the foundation for the work presented here.

My experience at WCEC greatly benefited me and made working through the PhD process faster and much smoother than it otherwise would have been. It would be difficult to acknowledge all the team members that have positively impacted me over the years. I appreciate the support of the leadership team (Mark, Vinod, Dave, Curtis, and Sarah) that stepped up so I could step back and focus more time on my PhD. In support of this work specifically, graduate student Antonea Fraiser and R&D Engineer Fredrick Meyers executed much of the laboratory testing described in Chapter 2, R&D Engineer Caton Mande gave me a crash course in running the Energy Plus simulations with Python that are described in Chapter 3, and student assistant Graham Jaeger tirelessly repeated experiments and analyzed data in support of Chapter 4. I am grateful to my committee Dr. Cappa, Dr. Corsi, Dr. Ellis, and Dr. Bennett for the continuous collaboration and support of this work.

It's not easy to juggle work, school, and family. I am thankful and proud of my awesome children, Hailey and Kyle, who are creative, honest, and hardworking (which makes it so much easier to be a parent)! I am grateful to my husband Ryan, who is the stabilizing force of the family and yet jumps on board in support of all the wild ideas I come up with. Life is brighter traveling through it with you. Friends and family often stepped in throughout the years to help us keep the train on the tracks. Amber, thank you for always having our backs. Cherie, thank you for spending time with the kids when we were traveling.

When I'm stuck on a problem, my first call for brainstorming solutions is often to my dad John, who is an endless source of skills and knowledge. Thank you for always being a sounding board. Obtaining a PhD requires grit and resilience. For those qualities, I credit my mom Rochelle, who taught me that important things are worth fighting for.

Funding

The work was supported by the California Energy Commission (Agreement EPC-17-034) and Flu Lab, LLC (Agreement A22-2462).

Material Previously Published or Pending Publishing

Chapter 2 of this work was published in 2023 with the following citation:

Pistochini, T, Ellis, M, Meyers, F, Frasier, A, Cappa, C, and Bennett, D. Method of Test for CO2-Based Demand Control Ventilation Systems: Benchmarking the State-of-the-Art and the Undervalued Potential of Proportional-Integral Control. *Energy and Buildings*. 2023 Dec;301:113717. https://doi.org/10.1016/j.enbuild.2023.113717

Chapter 4 of this work is currently under review with the following citation:

Submitted: Pistochini, T, Jaeger, G, Cappa, C, and Corsi, L. Longevity of size-dependent particle removal performance of do-it-yourself box fan air filters. Environmental Science: Processes & Impacts.

Abstract

Low-cost approaches are needed to retrofit existing heating, ventilation, and air conditioning (HVAC) systems in buildings to improve indoor air quality and reduce energy use. This dissertation describes three approaches to improve existing ventilation and filtration systems and evaluates their impacts in terms of energy use and indoor air quality. While the approaches described are generally relevant to all most types of commercial building stock, the work primarily studies the impact to classrooms due to the importance of indoor air quality in schools and the lack of resources faced by public school districts in the US.

In Chapter 2, an improvement to existing carbon dioxide (CO_2) based demand control ventilation (DCV) systems is proposed and demonstrated through laboratory testing and modeling. DCV adjusts a building's outdoor air ventilation rate in response to indoor CO_2 concentration to save energy while maintaining indoor air quality. Packaged HVAC systems often contain DCV controllers with embedded proprietary algorithms that lack transparent performance data. A test method was developed to assess the ability of a DCV controller to maintain the indoor CO_2 concentration at a setpoint in response to a series of CO_2 generation functions that represent three different building occupancy densities and two occupancy schedules. Six commercially available controllers were tested to demonstrate the method and provide directly comparable results. The performance (in terms of CO_2 control and damper movement) of each controller tested was compared to the performance of an ideal controller which knows the CO_2 generation function. Finally, the performance of a proportional-integral (PI) controller with preset gains was developed and tested to determine the potential maximum performance achievable with this control strategy. The best performing commercially available controller achieved CO_2 control (within 75 ppm of the setpoint) approximately 80% of the time with damper movement

slightly less than an ideal controller. However, most of the commercially available controllers had marginal or poor performance for CO_2 control and damper movement. Two controllers had damper movement more than three times the ideal controller. Notably, a PI algorithm configured and tested by the research team achieved superior performance with CO_2 control 92% of the time and damper movement 1.5 times the ideal controller.

DCV systems are often paired with an economizer function that increases outdoor air to save cooling energy when the outdoor air is within temperature and/or enthalpy conditions set by the controller. While this additional outside air will dilute any sources of indoor pollutants, a major shortcoming of economizer controls is they do not consider outdoor air pollution levels. Thus, temporarily increasing outside air for free cooling may worsen indoor air quality (IAQ), especially when wildfire smoke is present. In Chapter 3, the rule-based IAQ-Energy Controller, which includes an economizer and DCV and consideration of outdoor particulate matter with particle diameter less than 2.5 µm ($PM_{2.5}$) in the control architecture, is proposed. The performance of the IAQ-Energy Controller is modeled for a single-zone HVAC system in a classroom environment in 14 US cities. In addition to optimizing ventilation rate control, the IAQ-Energy controller approach includes modulating the speed of an internet-connected a portable air cleaner (PAC) in about half the modeled cities (those that contain small central HVAC systems with the least filtration capacity) to meet ASHRAE Standard 241 for controlling infectious aerosols.

In each city simulated, five years of historical weather (2018 to 2022) were applied to an EnergyPlus model to calculate HVAC energy use and outdoor air rates at each timestep. Then, the dynamic outdoor air rates and five years of outdoor $PM_{2.5}$ data (2018 to 2022) for the same location were applied to a box model (which included filtration and deposition) to calculate dynamic indoor $PM_{2.5}$ concentrations. In each city simulated, the proposed IAQ-Energy Controller was compared to a fixed rate ventilation system and a state-of-the-art Economizer + DCV system to consider how energy use, indoor exposure to $PM_{2.5}$, and removal rates for infectious respiratory aerosols varied across 14 cities in the US. Overall, the IAQ-Energy Controller reduced electricity use compared to the fixed rate ventilation system in 12 cities (range 5 to 16%), which was less than the savings from the Economizer + DCV system (range 6 to 22%), due disabling of the economizer function when outdoor $PM_{2.5}$ levels were above 12 μg/m^3. There was no change to electricity use in San Francisco and Seattle increased by 8% due to the small central HVAC system and resulting portable air cleaner use to company with ASHRAE Standard 241. Compared to the Economizer + DCV system, the maximum indoor $PM_{2.5}$ exposure decreased substantially with the IAQ-Energy Controller. For example, on the highest average outdoor $PM_{2.5}$ day of the year, the IAQ-Energy Controller reduced average $PM_{2.5}$ indoor exposure in Stockton, San Francisco, and Seattle by 10.8, 19.0, and 24.3 μg/m^3, respectively. The IAQ-Energy controller also resulted in consistent attainment of ASHRAE Standard 241 for infectious respiratory aerosol removal. The biggest increases in infectious aerosol removal rates (relative to the Economizer + DCV system) were seen in the cities with small central HVAC systems and larger portable air cleaning systems (San Francisco and Seattle).

While optimizing ventilation rates is an important approach to improving indoor air quality and energy efficiency, HVAC control system upgrades require implementation by the owner and operator of the facility. In Chapter 4, an approach that anyone can take to improve their indoor environment is evaluated. Filtration performance of do-it-yourself (DIY) box fan filters deployed across a university campus was assessed over an academic year. Four DIY air filters were constructed from box fans and air filters with a minimum efficiency reporting value (MERV) of 13 and deployed in four spaces (including two laboratories that include large sources of particles and two offices). They were operated 9-hours daily with programmable timers and were continuously monitored with power meters. Particle concentrations in the spaces were continuously monitored with low-cost nephelometers. The particle size dependent clean air delivery rate (CADR) and single pass filtration efficiency for each box was measured in a laboratory before deployment and every 10 weeks, for a total of five measurements over 40 weeks.

We found that these DIY box fan filters maintain robust performance over time, with each air filter maintaining at least 60% of its initial CADR at the end of the 40-week study, even with daily operation in environments with modest particle concentrations. CADR values for particles of 1.0-3.0 µm optical diameter averaged 34% higher than CADR values for 0.35-1.0 µm particles, aligning with MERV 13 filter size-dependent filtration expectations. Reductions in CADR over time were attributed to a reduction in filtration efficiency, likely due to a loss of filter electrostatic charge over time. There was no strong indication that increased resistance due to particle accumulation on filters appreciably decreased flow rates over time for any of the fans. The long-term robustness of DIY box fan air filters demonstrates their validity as a cost-effective, high performance, alternative to portable high efficiency particulate air (HEPA) filters.

Table of Contents

Table of Figures

Table of Tables

Abbreviations

ACH – Air changes per hour

AHAM – American Home Appliance Manufacturers

AHU – Air handling unit

ASHRAE – American Society for Heating, Refrigeration, and Air Conditioning Engineers

API – Application programming interface

APS – Aerodynamic particle sizer

BMS – Building management system

CADR – Clean air delivery rate

CR – Corsi-Rosenthal

CO_2 – Carbon dioxide

DCV – Demand control ventilation

DIY – Do-it-yourself

ECA – Equivalent clean airflow

EPA – Environmental protection agency

HEPA – High efficiency particulate air

HVAC - Heating, ventilation, and air conditioning

IAQ – Indoor air quality

MERV – Minimum efficiency reporting value

OPC – Optical particle counter

PAC – Portable air cleaner

PI – Proportional-integral

$PM_{2.5}$ – Particulate matter with aerodynamic diameter less than 2.5 µm

SPFE – Single pass filtration efficiency

WCEC – Western Cooling Efficiency Center

Chapter 1 Introduction

Children spend 1,000 hours per year in classrooms and are especially sensitive to the impacts of indoor air quality (IAQ) so ensuring proper ventilation and filtration is critical [1, 2]. Ventilation and filtration impact indoor comfort, airborne disease transmission, indoor particulate matter (PM) concentrations, indoor concentrations of inorganic pollutants (e.g. nitrogen dioxide and ozone), and indoor volatile organic compound concentrations (e.g. emissions from off-gassing from building materials and interior furnishings). Despite the evidence for the importance of ventilation in schools, ventilation rates in classrooms frequently fall short of standards [3, 4]. Ventilation and filtration standards in classrooms are generally designed to be met through central heating, ventilation, and air conditioning (HVAC) systems. Approximately 60% of HVAC systems in educational facilities are packaged systems [5] that contain all mechanical components in a wall-mounted or roof-top box. A packaged system contains a filter and a set of dampers that control the outdoor air rate (Figure 1-1). Since HVAC systems are replaced infrequently (every 15 to 20 years), solutions are needed to improve the ventilation and filtration delivered by existing systems. There are benefits and drawbacks to increased ventilation and filtration (Table 1-1) [3, 6], and all of these must be considered when engineering improvements to ventilation and filtration systems.

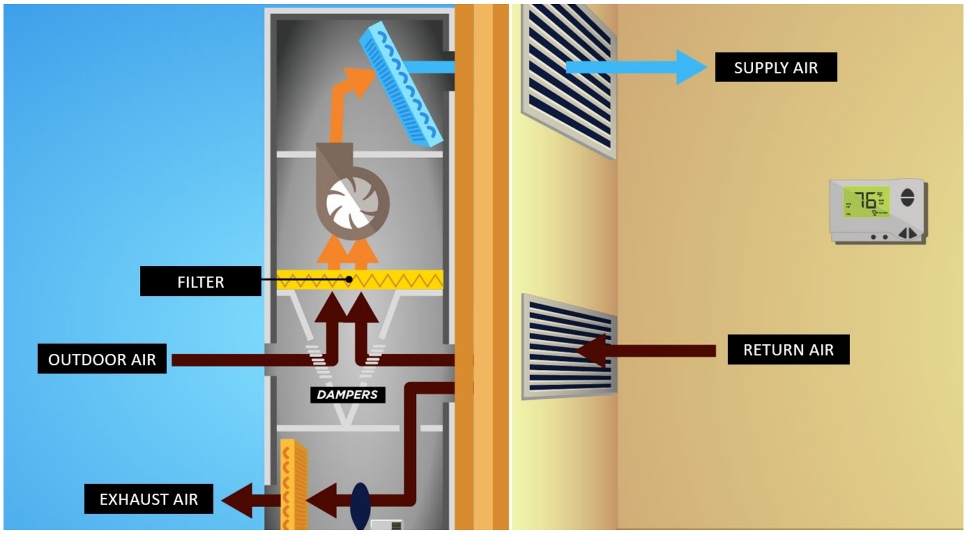

Figure 1-1: Mechanical Components of Packaged HVAC System. Figure credit: Paul Fortunato, University of California Davis

Table 1-1: Benefits and drawbacks of increased ventilation and filtration

Potential benefits of increased ventilation	**Potential drawbacks of increased ventilation**
• Reduced indoor concentration of respiratory aerosols • Reduced indoor concentration of volatile organic compounds of indoor origin • Reduced energy use at certain outdoor air temperature and humidity conditions (ventilative cooling) • Increased student performance and reduced absence	• Increased indoor concentration of particulate matter of outdoor origin • Increased concentration of ozone and ozone reaction products indoors • Increased energy use at certain outdoor air temperature and humidity conditions • Increased filter maintenance
Potential Benefits of Increased Filtration	**Potential Drawbacks of Increased Filtration**
• Reduced indoor concentration of respiratory aerosols • Reduced indoor concentration of particulate matter of indoor and outdoor origin	• Increased energy use • Increased filter maintenance • Noise from portable air cleaners

Another challenge is that HVAC system technology development is notoriously slow moving. It has not yet adapted to threats that have become more apparent over the past decade. In 2020, widespread recognition that the SARS-CoV-2 virus was primarily spread indoors through airborne transmission [7] resulted in recommendations from government agencies to increase outdoor air “as much as possible”

[8]. However, this can increase exposure to outdoor pollution, use more energy, and reduce thermal comfort [6].

The number of acres destroyed by wildfires in the US has more than doubled in the past twenty years, from 3.4 million (1983 to 2002) to 7.2 million (2003 to 2023) acres annually [9], polluting outdoor air that is drawn into HVAC outdoor air intakes. School districts are advised to temporarily close outdoor air intakes during wildfire events, but this may not be practical when outdoor air damper controls are located across hundreds of rooftops in a school district and are not remotely accessible. An optimized approach to automate ventilation and filtration-system operation in existing HVAC systems is needed to minimize airborne infectious disease transmission, pollutant exposure, and energy consumption. In Chapter 2 of this work, an improvement to existing carbon dioxide (CO_2) based demand control ventilation (DCV) systems for single-zone HVAC systems is proposed and demonstrated through laboratory testing and modeling. In Chapter 3, the rule-based IAQ-Energy Controller, which includes an economizer and DCV and consideration of outdoor particulate matter less than 2.5 µm ($PM_{2.5}$) in the control architecture, is proposed and its modeled performance is evaluated for a single-zone HVAC system in a classroom environment in 14 US cities. In addition to optimizing ventilation rate control, the IAQ-Energy Controller approach includes modulating the speed of an internet-connected a portable air cleaner (PAC) in about half the modeled cities (those that contain small central HVAC systems and thus less filtration capacity) to meet ASHRAE Standard 241 for controlling concentrations of infectious aerosols.

In addition to central HVAC control retrofits, portable filtration is an important tool to reduce exposure to indoor particles. Filtration of indoor air with portable air filters reduces particle concentrations indoors, which is expected to have health benefits for building occupants [10]. Most portable air cleaners that are applied in intervention studies use high efficiency particulate air (HEPA) filters that remove 99.97% of the most penetrating particles from the airstream [11]. Low-cost do-it-yourself portable air cleaners can be built from a box fan and standard filters used in HVAC systems. When filters are arranged in a box configuration, termed a Corsi-Rosenthal box (CR box), the airflow resistance is low, the airflow rates are high, and the particle removal rates exceed most commercially available portable HEPA filters [12]. The CR box offers a first-cost that is an order of magnitude below HEPA at \$0.05 to \$0.07 per m^3/h of CADR [12]. While multiple papers have been published documenting the filtration performance of new CR boxes [12-17], there is no published data on their long-term performance. In Chapter 4, the size dependent filtration performance of CR boxes operated daily over a 9-month academic year is assessed to determine how well these low-cost do-it-yourself filters perform over time.

Chapter 2 Method of Test for CO_2-Based Demand Control Ventilation Systems: Benchmarking the State-of-the-Art and the Undervalued Potential of Proportional-Integral Control

2.1 Introduction

Carbon dioxide (CO_2) based demand control ventilation (DCV) adjusts a building's outdoor air ventilation rate in response to indoor CO_2 concentration to save energy while maintaining indoor air quality when the occupancy density is below the design level. Demand control ventilation gained popularity in the 1990s with the commercialization of low-cost CO_2 sensors for heating, ventilation, and air-conditioning (HVAC) systems [18] [19]. The strategy saves energy when outdoor air requires heating or cooling to maintain thermal comfort. Thus, it has the largest energy savings potential in very cold and hot/humid climates and in densely, yet intermittently, occupied buildings (e.g. classrooms, retail, theatres) [20]. Use of DCV is required in certain occupied spaces by ANSI/ASHRAE Standard 90.1 Energy Standard for Buildings Except Low Rise Residential Buildings, which is adopted as the Energy Standard for most of the US [21]. ASHRAE Standard 90.1 first required DCV in densely occupied spaces of 0.40 people/m^2 or more in 1999 and reduced the required threshold to 0.25 people/m^2 in 2013 [19].

With DCV, mechanical ventilation rates can be reduced during periods of decreased occupancy and when CO_2 levels are reduced by natural ventilation (i.e., with open windows) and infiltration. When at least one occupant is present, DCV systems may not reduce ventilation below the value required to remove contaminants that are not occupancy dependent (e.g., volatile organic compounds released from building materials and interior furnishings), which is a calculation based on floor area [22]. When occupants are present and the ventilation required exceeds the floor area requirement, DCV systems are designed to control the indoor CO_2 concentration to a maximum level to provide the desired per-person ventilation rate. The maximum indoor CO_2 concentration setpoint may vary based on jurisdiction and building operator. For reference, California's Building Energy Efficiency Standards specify a DCV setpoint of 600 ppm above the outdoor concentration of CO_2 while a range of international building standards specify maximum concentrations of 350 to 1350 ppm above outdoors depending on indoor air quality category [19, 23]. Carbon dioxide emissions from people (which vary by age, sex, and activity level) are an indicator of respiratory aerosol generation and control strategies to manage CO_2 concentrations help assure adequate ventilation and are one way to reduce exposure to infectious aerosols and respiratory illness transmission risk [24, 25].

It is important to assess the CO_2-control performance of DCV systems given the occupant health implications. Acker et al. (2021) examined six DCV systems in the field (two commercial offices, two medical offices, and two schools) and found none to be functioning properly for one or more of the following reasons: lack of specification of control parameters, lack of sensor communication, poor sensor placement, and supply fan not operating continuously [26]. In a study of packaged HVAC systems with DCV controllers from two manufacturers installed in two California classrooms each, Pistochini et al. (2019) observed that CO_2 concentrations in the classrooms were not well controlled and had greater variation than expected, even after ensuring none of the problems identified by Acker were present [27]. Furthermore, the DCV controllers did not allow for technician programming or adjustments that would improve their performance. Preliminary testing of one DCV controller in the laboratory by Fraiser et al. (2021) demonstrated that its control algorithm achieved CO_2 control within 75 ppm of the setpoint only 66-73% of the time for six different occupancy functions as a result of initial overshoot of the CO_2 setpoint (attributed to under-ventilation) followed by steady-state period of lowered CO_2 attributed to over-ventilation [28].

While more sophisticated building management systems may accommodate custom programming and specification of control parameters, these systems currently require an experienced engineer to tune the system in an occupied building [29]. Proportional-integral (PI) control is a type of feedback control that determines the control input based on the current error from the setpoint and the integral of the error over time. Proportional-integral-derivative (PID) control is similar and considers the derivative of the error. Shell et. al. (1998) describes that PI control is applied to DCV [30], but no sources were found that describe the relationship between proportional gain, integral gain, and controller performance as a function of building occupancy density and patterns. Johnson Controls employs a patented adaptive control algorithm for automatically adjusting the gains in PI control and has published field data demonstrating good performance for controlling supply air temperature and fan speed in an air handler, however results for DCV were not included [31]. It is currently unclear how most commercially available packaged DCV controllers function as they are "black boxes" with proprietary control algorithms. There is a lack of performance data in terms of how successful a particular DCV controller will be in maintaining the programmed CO_2 setpoint and quantification of actuator movements required to achieve the result.

Lu et al. (2022) reviewed approaches for CO_2-based DCV and categorized them as rule-based, model-based, and learning-based, where rule-based controls (which include PI control) are noted to result in potential air quality problems [32]. Due to the capacitance of the building air volume, CO_2 levels take minutes to increase, while the time required to change an outdoor air damper position to respond to the CO_2 signal is on the order of seconds. Therefore, it is expected that well-designed feedback controllers would be sufficient for the job. However, as described by Lu et al. (2022), there is increasing research into more sophisticated DCV approaches including model-based control and learning-based control. Several of the included studies compared results of new control methods to PI/PID control. Lu et al. (2013) compared an open-loop control method (called Psuedo Session DCV) that predicted occupancy based on CO_2 concentrations and concluded that performance was similar to PI control, with both managing CO_2 to within 10 ppm of the setpoint. Liu et al. (2014) developed and simulated a model predictive controller for temperature and CO_2 control and concluded the performance was improved compared to the PI controller, which overshot the CO_2 setpoint by 600 ppm and took hours to return to the setpoint [33]. Zhigang et al. (2010) developed a feedback linearization strategy and presented simulation results demonstrating that the proposed controller achieved better CO_2 control (within 10 ppm of setpoint) than a PID controller (within 50 ppm of setpoint) [34], although the improvement was small (less than 5 % of the setpoint). Lachhab et al. (2019) showed that a state-feedback controller, formulated based on a linearized single-zone ventilation system, achieved slightly better CO_2 control performance than a PID controller, although both approaches overshot the CO_2 setpoint by 100-150 ppm [35]. Finally, Zhu et al. (2014) showed that a reinforcement learning controller achieved better CO_2 control (within 15 ppm of setpoint) than the PI controller (within 30 ppm of setpoint), but these differences were small and unlikely to be meaningful in the field [36]. It is unclear why Zhigang et al. (2010), Lu et al. (2013) and Zhu et al. (2014) achieved much better results with PI/PID controllers compared to Liu et al. (2014) and Lachhab et al. (2019) as the papers do not describe the gains used for PI/PID control. Finally, all studies except Lachhab et al. (2019) were simulations only, so it is unclear how well the simulations represent the dynamics of physical systems. For studies that achieve good results with PI control, the main improvement cited from more sophisticated approaches was eliminating the need for building-specific tuning. In general, it is difficult to assess the potential benefits of a proposed new control method when the performance of the simulated baseline PI/PID control varied widely.

A test method for DCV controllers is important to benchmark commercially available controllers, motivate industry improvements, and provide a direct comparison for new control approaches. The specifics of DCV control vary with design of the air handling unit (AHU). The most straightforward application of DCV is to a single-zone constant air volume (CAV) AHU, where the air handler fan runs at a fixed speed and the supply air serves a single space with one CO_2 sensor. This is commonly found in wall-mount and packaged rooftop HVAC systems that are prevalent in light commercial buildings and schools [5]. These systems often contain a local controller for the outdoor and return air damper assembly that has DCV capabilities. These local controllers are often referred to as “economizer controllers” because they can increase outdoor airflow to 100% of the supply airflow for “free” cooling when the building requires cooling and outdoor air conditions meet certain criteria. The method of test and subsequent evaluation of DCV controllers presented here is limited to local controllers for single-zone CAV AHU systems; the term DCV controller used hereafter refers to this limited subset of DCV controllers.

This paper presents a method of test to assess the performance of single-zone CAV DCV controllers that receive a CO_2 sensor input and modulate the outdoor and return air dampers for an HVAC system to maintain an indoor CO_2 setpoint. Each controller tested was challenged with three CO2 generation profiles that represent three different occupancy densities and two building occupancy schedules. The system performance (in terms of CO_2 concentration and total damper movement) was compared to the performance of an ideal feed-forward controller, which determines the required ventilation rate to achieve the desired CO_2 concentration based on the CO_2 generation function. Six commercially available controllers were tested to demonstrate the method and benchmark the state-of-the-art.

Finally, a model of a PI controller for a single-zone CAV system was developed and simulated to evaluate the impact of proportional and integral gain selection on controller performance for the same series of CO_2 generation functions. The model was validated with the laboratory method of test and the performance achievable with fixed gain (i.e. not tuned, non-adaptive) PI control was evaluated and quantified.

2.2 CO_2-Based Demand Control Ventilation Method of Test

2.2.1 Chamber Design and Construction

A test chamber constructed from a walk-in freezer case (with no refrigeration system) was built to represent a scaled room with a constant volume air handling unit (AHU) plus a CO_2 distribution system to mimic CO_2 exhaled by building occupants (Figure 2-1). The chamber had an interior height of 2.4 m and a floor area of 5.2 m^2. The AHU mixed the return air from the chamber with outdoor air and supplied the mixed air to the chamber. The fraction of outdoor air to return air was controlled by the voltage to the outdoor air damper actuator (Belimo TFB24-SR) (fully open at 10V, closed at 2V) and return air damper actuator (Belimo TFB24-SR) (fully open at 2V, closed at 10V). The control voltage was output from the DCV controller under test.

The mixed air was supplied to the chamber at a constant flow rate using a multi-speed supply fan (AC Infinity Cloudline T6) set to the desired flowrate. Additionally, a supply air damper actuator (Belimo TFB24-SR) controlled by a PI controller was used to fine-tune the supply airflow rate to the setpoint based on differential pressure (TEC DG-700) across a custom orifice plate calibrated using tracer gas measurement techniques. The outdoor air rate was measured based on the differential pressure (TEC DG-700) across a second custom orifice plate, calibrated using a carbon dioxide tracer gas measurement technique, where carbon dioxide is injected into the air duct at a known rate and the measured change in carbon dioxide concentration in the air stream is used to calculate the airflow rate [37]. Uncertainty of the supply and outdoor air rates measured with the tracer gas system was estimated at less than 3% of the measurement using an error propagation method [37]. A pressure relief damper was used to exhaust air from the chamber to maintain a differential pressure in the chamber of 1-10 Pa above the surrounding environment.

Within the chamber, a wall-mounted high accuracy, calibrated HVAC-grade CO_2 sensor (Vaisala GMP251) was installed on the wall four feet from the floor to measure the chamber CO_2 concentration. The outdoor air and exhaust air CO_2 concentrations were monitored with Vaisala GMP251 and GMW90 sensors, respectively. A ceiling fan operated clockwise at high-speed mixed the chamber air during the test. A wall-mounted mini-split heat pump (Panasonic RX09RMVJU9/FTXR09TVJUW) with thermostat was used to condition the chamber air to meet the test conditions (Table 2-2). The chamber air temperature and humidity were continuously monitored (Vaisala HMP110).

When compatible, the chamber CO_2 sensor was used in all tests to send the CO_2 signal to the DCV controller. The goal of using a calibrated CO_2 sensor was to isolate testing of the DCV controller response characteristics. If the DCV controller's manufacturer's CO_2 sensor had to be used with the controller due to compatibility requirements, then all manufacturer recommendations for the operation of the CO_2 sensor were followed. In this case, the chamber CO_2 sensor was still used to record the CO_2 concentration during the tests for consistency. Of six controllers tested (Table 2-3), only the Pelican Wireless system required use of the manufacturer's CO_2 sensor. In this case, the accuracy of the manufacturer's CO_2 sensor was evaluated using a calibration test protocol [28]. Accuracy for the manufacturer's CO_2 sensor was within 5% of the sensor reading.

Carbon dioxide from a compressed gas cylinder was regulated to 30 psi and plumbed to a mass flow controller (Alicat MC-1slpm-D/5M). The supply from the mass flow controller was plumbed to the chamber, where a manifold split the flow into nine small tubes which were attached to nine ends of a distribution frame 1.2 m above the floor to simulate the height of seated occupants. The nine distribution points were arranged in a three-by-three rectangular pattern such that the distance between the chamber walls and each distribution point was the same. Each distribution tube had an identical length for equal flow resistance. The mass flow controller injected the CO_2 following a time-based occupancy density function for each test (Figure 2-3).

Data acquisition of the chamber CO_2, temperature, and humidity sensors, control command and position feedback of the three damper actuators, and CO_2 generation rate was performed with a NI Compact DAQ Chassis (NI cDAQ-9174) and serial data communication interface and LabVIEW software (NI LabVIEW 2019 SP1). Data was acquired at 10 Hz, averaged, and logged at 0.1 Hz.

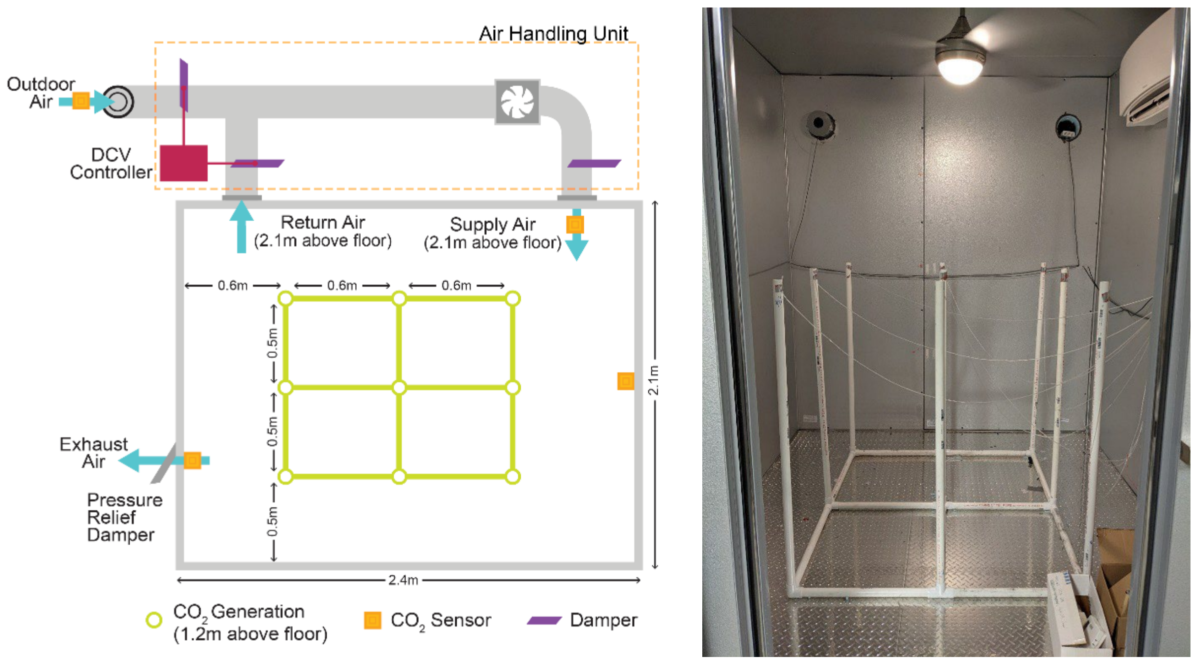

Figure 2-1: Top view schematic of chamber and AHU (left) and photo of chamber interior showing CO_2 distribution system (right).

2.2.2 Test Conditions and Configuration

DCV controllers need to adjust ventilation in response to changing occupancy. To represent occupancy patterns encountered in typical buildings, a step occupancy schedule and gradual occupancy schedule were developed (Figure 2-2). The step occupancy function was intended to reflect use cases where occupants enter and exit a space in groups (e.g., classroom and conference room) and the gradual occupancy pattern is intended to reflect use cases where occupancy gradually builds in a space with a peak occupancy period (e.g., restaurant and grocery store). Testing DCV controllers in response to a step change and gradual change is expected to cover the range of operating conditions, since building occupancy schedules are a combination of step and gradual changes.

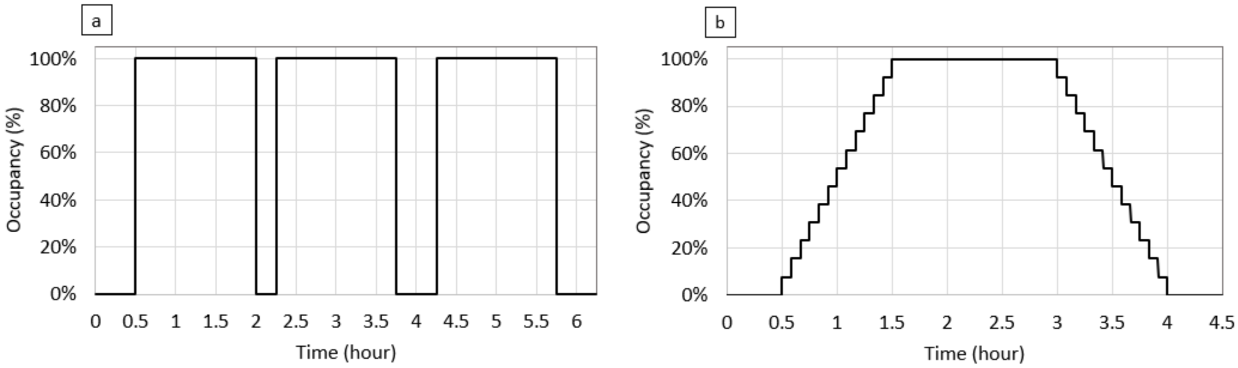

Figure 2-2: Occupancy schedule for the (a) step change and (b) gradual change in occupancy.

For each occupancy schedule (step and gradual), three occupancy densities (low, medium, and high) were considered to cover a range of ventilation rates from ASHRAE Standard 62.1-2019 [22] (Table 2-1). To set the maximum (100%) CO_2 generation rate for the laboratory test, the occupancy density was scaled by the floor area of the chamber (5.2 m^2) and multiplied by an average CO_2 generation rate of 4.72 mL/s-person (Table 2-1). Carbon dioxide generation rates per person vary widely from 3.6 to 9.1 mL/s based on age, body mass, sex, and level of physical activity, where 4.72 mL/s is representative of seated occupants [38]. Three different maximum CO_2 generation rates were calculated based on the assumption of varying occupancy density. However, the range could also reflect variance in occupant CO_2 generation rate for the same occupancy density. Each occupancy schedule type (step and gradual) was then multiplied by the maximum CO_2 generation rate to obtain six CO_2 generation schedules (Figure 2-3).

Table 2-1: Maximum CO_2 generation rate, ventilation, and supply airflow rates for the test chamber. For reference, a typical classroom is approximately 100 m^2 and medium density.

Maximum Occupancy Density		Test Chamber (5.2 m^2)			
Category	People per 100 m^2 of floor area	People per chamber floor area	Maximum CO_2 generate rate (mL/s)	Minimum Floor Area Ventilation Rate (L/s)	Supply Airflow Rate (L/s)
Low	16	0.84	3.96	4.0	26.4
Medium	38	1.96	9.24	4.0	26.4
High	54	2.80	13.20	4.0	26.4

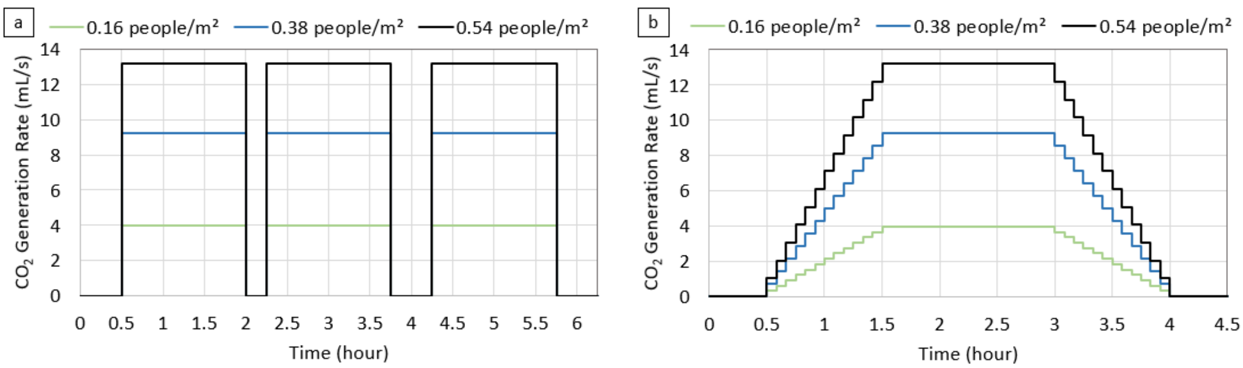

Figure 2-3: CO_2 generation rate for the (a) step change occupancy profile and (b) a gradual change occupancy profile for three occupancy densities.

When a DCV system is implemented, building codes require that a minimum ventilation rate be supplied to the building during typical occupancy hours (even when no occupants are present) to remove indoor pollutants that are emitted from building materials and furnishings. The minimum ventilation is a function of floor area and for this test procedure was set to 0.76 L/s-m^2 (4.0 L/s for the chamber used), which is the standard in California [39], and is within the range of requirements set by ASHRAE Standard 62.1-2019 [22]. Finally, the total supply airflow rate of the AHU, which is the sum of the return air and the outdoor air, was set to a constant of 5.1 L/s-m^2 (26.4 L/s for the chamber used), which is a typical supply airflow rate used in constant air volume systems to meet heating and cooling loads in commercial buildings [40]. This test method can be executed with any chamber size by sizing the mechanical components and scaling the CO_2 generation rate, minimum ventilation rate, and supply airflow rate accordingly.

Prior to testing a DCV controller, the supply fan and PI-controlled supply air damper were configured to provide the required airflow of 26.4 L/s using the AHU controls described in Section 2.2.1. The minimum outdoor and return air damper position were set in the controller under test to be 4.2 V, which provided a 4 L/s ventilation rate based on the calibration described in Section 2.2.1. The maximum outdoor and return air damper position were set to 10 V to allow up to 100% outdoor air.

To ensure that each DCV controller test was consistent and repeatable, a set of test conditions and tolerances were developed that cover the important environmental parameters and the accuracy of the instruments used to measure these parameters is reported (Table 2-2). Within Table 2-2, the test operating tolerance specifies the allowed difference from the test condition at each 10 s time step. The test condition tolerance specifies the allowed difference from the test condition for the measured parameter averaged over the entire test. Atmospheric pressure is included since changes in atmospheric pressure affect air density. The test laboratory was near sea level (16 m) and all tests were conducted at ambient pressure. The difference in the indoor and exhaust CO_2 concentrations was used as a metric to monitor the uniformity of the chamber CO_2 concentration during the test. Since completely uniform CO_2 concentrations are not achievable in practice, an operating tolerance of 50 ppm was set on the absolute value of the five-minute moving-average difference of the indoor and exhaust CO_2 concentration. The moving-average was applied to smooth out sensor noise from the difference calculation. All test data was post-processed to ensure that tolerances were met and any test that failed was repeated.

Table 2-2: Test operating conditions and tolerances. *Calculated as a five-minute moving average

Chamber Measurement	Units	Test Condition	Instrument Accuracy	Test Operating Tolerance	Test Condition Tolerance
Absolute pressure	kPa	101	±2.5% of reading	±3	±1.5
Dry-bulb temperature	°F	75	±1	±5	±3
Relative humidity	%RH	40	±5	±20	±10
CO_2 generation rate	SLPM	Figure 3	±2% of reading	±5% of test condition	±3% of test condition
Outdoor air CO_2 concentration[1]	PPM	≤ 425	Greater of ±30 PPM or ±2% of reading	+25	+10
Indoor and exhaust CO_2 concentrations	PPM	-	Greater of ±30 PPM or ±2% of reading	Indoor – Exhaust* ≤ 50	-

2.2.3 Test Protocol

For each evaluation, the DCV controller was installed and connected to the chamber CO_2 sensor (unless a specific manufacturer's CO_2 sensor was required) and the control output was connected to outdoor and return air damper actuators. The DCV controller was programmed with a chamber CO_2 concentration setpoint of 600 ppm above the outdoor air consistent with the specification in California's Building Energy Efficiency Standards. The DCV controller was programmed for an actuator voltage range of 2 to 10 V with a minimum setting of 4.2 V.

Once the preliminary setup tasks were complete, the six tests were executed with the CO_2 generation profiles shown in Figure 2-3. Upon completion of a test, the chamber was flushed with outdoor air to return the indoor CO_2 concentration below 425 ppm to begin the next test. The automated process was repeated until the tests for all six profiles were complete and all test conditions were met.

2.2.4 Ideal DCV Controller

To quantify the performance of each DCV controller, the time-series chamber CO_2 concentration for each test was compared to the expected concentration under an ideal DCV controller. The ideal DCV controller is a theoretical feedforward controller with inputs of outdoor CO_2 concentration, CO_2

generation rate, initial chamber CO_2 concentration, and chamber CO_2 concentration setpoint. Comparing the results obtained from the DCV controller laboratory test method with that obtained from the closed-loop simulation under the ideal DCV strategy gives a measure of how close the DCV controller performance is relative to the optimal performance, where optimal performance is the minimum amount of ventilation required to maintain the CO_2 concentration at or below the setpoint. Assuming that the chamber CO_2 concentration is spatially uniform such that it can be characterized by a single value, an overall mass balance of CO_2 in the chamber yields a box model:

$$\frac{dm_{CO2,Box}(t)}{dt} = \dot{m}_{CO2,OA}(t) - \dot{m}_{CO2,Box}(t) + \dot{G}_{m,CO2}\,(t) \qquad \text{Equation 2-1}$$

where $m_{CO2,Box}$ is the total mass of CO_2 in the chamber, $\dot{m}_{CO2,OA}$ is the mass flow rate of CO_2 in the outdoor air stream, $\dot{m}_{CO2,Box}$ is the mass flow rate of CO_2 in the chamber exhaust air stream, and $\dot{G}_{m,CO2}$ is the mass generation rate of CO_2 in the chamber.

Under the assumptions that the air density is constant and the outdoor airflow rate into the chamber is equal to the airflow rate leaving the chamber through the exhaust relief damper, Equation 2-1 simplifies to

$$V_{Box}\frac{dC_{CO2,Box}(t)}{dt} = \dot{V}_{OA}(t)\left(C_{CO2,OA}(t) - C_{CO2,Box}(t)\right)/10^6 + \dot{G}_{v,CO2}\,(t) \qquad \text{Equation 2-2}$$

where V_{Box} is the total volume of the chamber, $C_{CO_2,Box}$ is the chamber CO_2 concentration, $\dot{V}_{OA}$ is outdoor airflow rate, $C_{CO2,OA}$ is the outdoor air CO_2 concentration, and $\dot{G}_{v,CO2}$ is the volumetric generation rate of CO_2 in the chamber. Concentrations are expressed in terms of ppm and division by 10^6 converts the concentration to a unitless ratio of carbon dioxide to total air volume, so that the units of each term in Equation 2-2 are the change of the volume of CO_2 in the chamber in liters per second.

The ideal DCV controller was modeled as a feedforward controller, which utilizes perfect information of the CO_2 generation rate in the chamber to compute a ventilation rate that exactly rejects the effect of the disturbance. On the contrary, DCV controllers are feedback controllers (i.e., reactive instead of proactive) since measuring the generation rate is not practical. The ideal DCV strategy is to maintain the minimum ventilation rate if the expected CO_2 concentration is at or below the CO_2 setpoint. Otherwise, the ideal controller selects the ventilation rate that exactly maintains the CO_2 concentration at its setpoint. Determining the ventilation rate that maintains the chamber concentration at exactly its setpoint requires the solution of Equation 2-2.

A simultaneous solution strategy was employed to determine the ventilation rate for the ideal DCV controller and the solution of Equation 2-2. Provided the input data including the chamber air volume, the outdoor air CO_2 concentration profile, the CO_2 generation rate profile, and an initial chamber CO_2 concentration, Equation 2-2 may be numerically solved. For a fair comparison between the ideal DCV controller and each DCV controller tested, the outdoor air CO_2 concentration profile ($C_{CO2,OA}(t)$) and initial chamber concentration ($C_{CO2,Box}(t = 0)$) were taken to be equal to the recorded data from each DCV controller test. The explicit Euler method was employed to solve Equation 2-2 with a time step (Δt) of 10 s, which gives:

$$C_{CO2,Box}(t + \Delta t) = C_{CO2,Box}(t) + \frac{\Delta t}{V_{Box}}\left(\dot{V}_{OA}(t) * \left(C_{CO2,OA}(t) - C_{CO2,Box}(t)\right) + \dot{G}_{v,CO2}(t) \times 10^6\right) \quad \text{Equation 2-3}$$

When $C_{C02,Box}(t + \Delta t)$ was less than the setpoint ($C_{C02,Box,Set}$), $\dot{V}_{OA}(t)$ was set to the minimum ventilation rate. Otherwise, the ventilation rate that kept $C_{C02,Box}(t + \Delta t)$ at the setpoint was computed from:

$$\dot{V}_{OA}(t) = \frac{V_{Box} * \left(C_{CO2,Box,Set} - C_{CO2,Box}(t)\right)/10^6 - \Delta t * \dot{G}_{v,CO2}(t)}{\Delta t * \left(C_{CO2,OA}(t) - C_{CO2,Box}(t)\right)/10^6}$$ Equation 2-4

While the outdoor CO_2 concentration and the initial chamber concentration will minimally affect the ideal controller computations, an example result for the medium density step function where the initial chamber and outdoor CO_2 concentrations were set to 400 ppm is shown for illustrative purposes (Figure 2-4). The ventilation rate begins at the minimum (4 L/s). When the CO_2 injection begins at t = 0.5 hr the ventilation rate remains at the minimum until the CO_2 level reaches the setpoint. The ventilation rate then adjusts to 15 L/s to maintain the CO_2 concentration setpoint. When the CO_2 injection stops (t = 2 hr), the ventilation rate returns to the minimum and the CO_2 begins to decay.

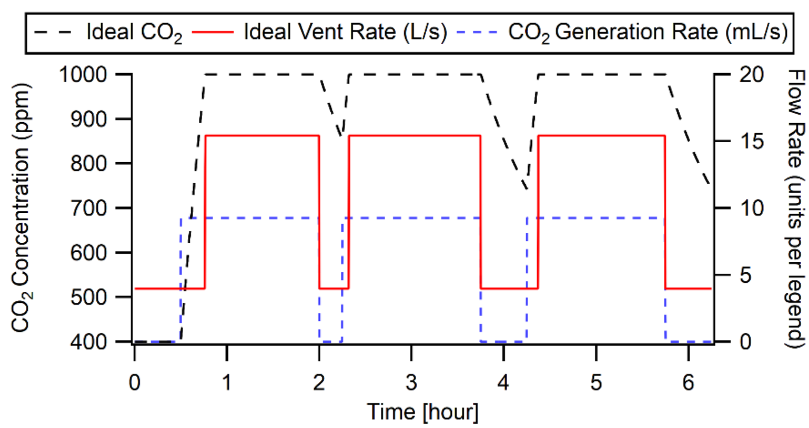

Figure 2-4: An example ideal controller calculation shown for an initial chamber CO_2 concentration and outdoor CO_2 concentration of 400 ppm.

Finally, the damper position that would achieve the ideal ventilation rate was calculated from a series of measurements correlating the damper position and the outdoor airflow rate measured with the calibrated orifice plate (Figure 2-5). This linearized relationship was used to calculate the damper position for the ideal controller:

$$D_{OA}(t) = a * \dot{V}_{OA}(t) + b$$ Equation 2-5

where $D_{OA}(t)$ is the damper position in volts for the AHU used to implement the test protocol and a and b are experimentally measured for the AHU. The commercially available controllers were tested in 2021 and the developed PI controller (Section 2.4) was tested in 2022; the AHU was altered to add a filter assembly in between these tests so the coefficients for Equation 2-5 were measured twice (Figure 2-5). The total damper movement over the test was found by summing the absolute value of the change in damper position over all time steps, where n is the length of the test.

$$D_{OA,total} = \sum_{t=0}^{n} |D_{OA}(t + \Delta t) - D_{OA}(t)| \qquad \text{Equation 2-6}$$

Since the ideal controller result was calculated for each test with the actual outdoor air CO_2 concentration, the result for the total ideal damper travel may vary depending on the outdoor CO_2 concentration seen over the course of the test.

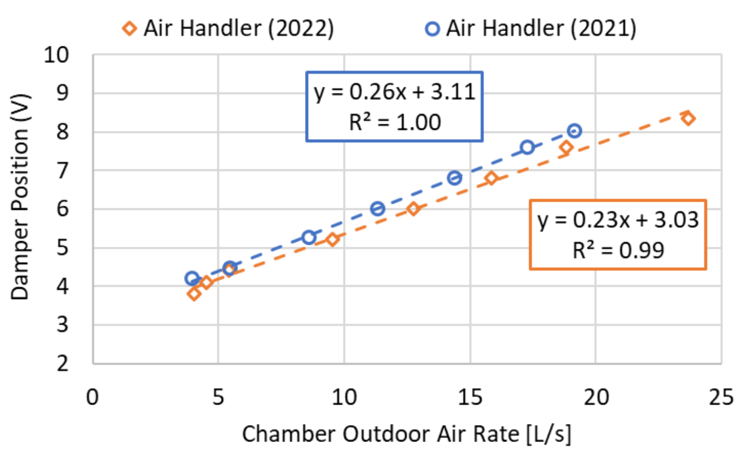

Figure 2-5: Relationship between chamber outdoor air rate and damper position used in ideal controller calculation. Each point represents an average result for several minutes of data collected at 0.1 Hz.

2.2.5 Control Performance Evaluation

For each controller, all six tests were analyzed to determine how closely the actual chamber CO_2 concentration matched the ideal chamber CO_2 concentration. For each time step, the actual CO_2 concentration was compared to the ideal chamber CO_2 concentration and binned into one of three categories:

1. Target ventilation rate – actual chamber CO_2 concentration within 75 ppm of ideal
2. Over-ventilated – actual chamber CO_2 concentration less than 75 ppm of ideal
3. Under-ventilated – actual chamber CO_2 concentration more than 75 ppm of ideal

The accuracy of the controller in tracking the CO_2 setpoint over time was used as the performance metric because CO_2 concentration is the control variable. A shortcoming of using CO_2 concentration as the control variable is that it only an indicator of ventilation rate [41]. The actual ventilation rate can only be calculated from CO_2 concentration when all other variables are known (change in CO_2 concentration over time, CO_2 generation rates, and space volume). Therefore, tracking deviation greater than 75 ppm from the CO_2 setpoint is used as an indicator of the ventilation performance. At steady state conditions for the CO_2 generation rates used in this test procedure, a difference of less than 75 ppm from the CO_2 setpoint equates to being with 15% of the target ventilation rate.

The number of time steps in groups 1 to 3 was converted to a percentage of the total time steps. The total movement of the outdoor air damper was also considered in evaluating the control performance. The total damper movement was summed for the controller tested (Equation 2-6). The ratio of the total damper travel to the ideal controller travel was calculated.

2.3 Commercially Available Controllers Tested

Six commercially available packaged system DCV controllers were evaluated with the test protocol and analyzed in comparison to the ideal controller (Table 2-1). In all cases, the exact algorithm pre-programmed into the controller was unknown, although in some cases the general method was described by the manufacturer (Table 2-1). None of the controllers tested allowed for manual tuning; the only setting available in all cases was a CO_2 setpoint or activation level. Additionally, the Honeywell Jade had a “slow” or “fast” damper setting that was accessible with a external configuration tool; both settings were tested.

In all cases, the controller was set to have a minimum damper position of 4.2 V (minimum flow rate of 4 L/s) and a maximum damper position of 10 V. In most cases, the control logic was stored on the device as firmware, except for the Pelican Pearl, which maintained the control logic in the cloud (See Section 2.6 for discussion for comparison of device firmware versus cloud-based computing). Review of manufacturer documentation and discussion with a few of the manufacturers revealed different operating control principles. For example, when the CO_2 concentration is over the setpoint, the Honeywell Jade opens the damper until the setpoint is met. When the CO_2 level drops below the setpoint minus the dead band (typically 100 ppm), the damper closes back to minimum. Manuals for the Johnson Control devices describe a PI-controller with a patented adaptative tuning method. The Pelican Pearl uses a response curve function where the CO_2 setting is the concentration at which the damper starts to open past the minimum setting. The manufacturer recommends using the default setting of 800 ppm as the activation CO_2 concentration; both 800 and 1,000 ppm were tested as activation levels. Pelican also has a setpoint-based feedback control method under development that was tested; the details of the operating mechanism were unknown. The control method for the XC Spec and Belimo Zip were unknown.

Table 2-3: Commercially available packaged system DCV controllers tested.

#	Manufacturer and Model	Config.	Configuration Parameters	Control Method per Manufacturer
1	Honeywell Jade W7220	a	CO_2 setpoint: 1,000 ppm Damper speed: slow	Damper opens at fixed rate (slow/fast) until setpoint met. When CO_2 value drops below setpoint minus dead band (100 ppm), damper closes to minimum.
		b	CO_2 setpoint: 1,000 ppm Damper speed: fast	
2	Johnson Controls TEC3000	-	CO_2 setpoint: 1,000 ppm	PI algorithm with patented pattern recognition adaptive control tuning [31].
3	Johnson Controls Peak PK-ECO1001-0	-	CO_2 setpoint: 1,020 ppm	
4	Pelican PEARL (Cloud-based)	a	Activation CO_2: 800 ppm	Response curve – damper position function of CO_2 value.
		b	Activation CO_2: 1,000 ppm	
		c	CO_2 setpoint: 1,000 ppm	Feedback algorithm
5	XC Spec Air Quality Display	-	CO_2 setpoint: 1,000 ppm	Unknown
6	Belimo Zip ECON-ZIP-BASE	-	CO_2 setpoint: 1,025 ppm	Unknown

2.4 PI Controller

2.4.1 PI Controller Development

A PI controller was modeled and tested to optimize selection of the proportional gain (K_p) and integral gain (K_i) tuning parameters for best controller performance across the range of occupancy patterns and densities in Figure 2-3. A PI controller with proportional gain (K_p) and integral gain (τ_i) tuning parameters that achieves good performance across a variety of building types without need for a proprietary and/or patented algorithms would be a useful tool for building operators and engineers. First, a base PI algorithm along with a box model of the chamber was programmed in software to simulate the total system. The PI algorithm used the current error between the measurement and the setpoint ($C_{C02,Box,Set}$), the time step (Δt), and the proportional (K_p) and integral gains (τ_i) to calculate the outdoor air rate $\dot{V}_{OA}(t)$. The chamber box model (Equation 2-3) and the outdoor air CO_2 concentration were then used to calculate the chamber CO_2 concentration in the next time step.

Two improvements were made to the base PI algorithm to improve ventilation control. First, the error of the difference between the setpoint and the chamber concentration (Equation 2-7) was calculated with respect to a dead band (db) (Equation 2-8). If the error was less the dead band (db), the error was set to zero. This prevented excessive damper movement. Second, anti-integral windup with back calculation was applied so that the outdoor air rate stayed within the bounds of the minimum and maximum for the physical system. This prevents windup during periods that the controller saturates (when the candidate ventilation rate $\dot{V}_{OA}^{*}$ is outside the bounds of the maximum or minimum rate) (Equation 2-9 to Equation 2-11) [42]. Finally, the outdoor air rate $\dot{V}_{OA}(t)$ was calculated with Equation 2-12. This extended PI algorithm was modeled with a 1 min time step and gains were constrained to $K_p > 0$ and $\tau_i > 0$. Note that while the outdoor air rate and K_p are expressed in units of L/s and L/s.ppm-CO_2, the control output (and associated K_p) can be damper position in instead of airflow rate by applying a conversion factor between damper position and airflow rate (using a linear approximation).

$e(t) = C_{CO2,Box,Set} - C_{CO2,Box}(t)$	Equation 2-7
$if\ C_{CO2,Box}(t) < C_{CO2,Box,Set} - db,\ then\ e_{db}(t) = e(t) - db$ $else\ if\ C_{CO2,Box}(t) > C_{CO2,Box,Set} + db,\ then\ e_{db}(t) = e(t) + db$ $else\ e_{db}(t) = 0$	Equation 2-8
$I(t) = I_B(t-1) + \frac{\Delta t}{60} * e_{db}(t), where\ I_B(0) = 0$	Equation 2-9
$\dot{V}_{OA}^{*} = -K_p\left[e_{db}(t) + \frac{I(t)}{\tau_i}\right]$	Equation 2-10
$if\ \dot{V}_{OA}^{*} < \dot{V}_{OA,min},\ then\ I_B(t) = -\tau_i\left[e_{db}(t) + \frac{\dot{V}_{OA,min}}{K_p}\right]$ $if\ \dot{V}_{OA}^{*} > \dot{V}_{OA,max},\ then\ I_B(t) = -\tau_i\left[e_{db}(t) + \frac{\dot{V}_{OA,max}}{K_p}\right]$ $else, I_B(t) = I(t)$	Equation 2-11
$\dot{V}_{OA}(t) = -K_p\left[e_{db}(t) + \frac{I_B(t)}{\tau_i}\right]$	Equation 2-12

2.4.2 PI Controller Testing

The extended PI algorithm (Equation 2-7to Equation 2-12) was implemented with a prototype controller using LabVIEW software, the chamber CO_2 sensor, and Pelican PEARL hardware to update the ventilation damper position. Pelican's application programming interface (API) was used to control the damper position setting for the PEARL; the proprietary control algorithms inside the PEARL described earlier were bypassed and not used for this test. The CO_2 setpoint ($C_{C02,Box,Set}$) was 1,000 ppm. Once a minute, the average value of the CO_2 sensor (rounded to 1 ppm to represent typical CO_2 sensor resolution) was passed to the PI algorithm which updated the outdoor air rate ($\dot{V}_{OA}(t)$). The outdoor air rate was converted to a damper position once per minute and sent to the PEARL controller over Pelican's application programming interface (API). Note that while a detailed correlation between damper position and outdoor airflow rate was available (Figure 2-5), only the minimum and maximum damper positions and flow rates were used to calculate the conversion factor (0.26 V/(L/s)) to be representative of the typical data available in field installation. The time delay to update the damper position command through the web service was a few seconds.

2.5 Results

2.5.1 Commercially Available Controllers

Results for the commercially available controllers (labeled C1 to C6) for the medium occupancy density step function are shown in Figure 2-6; results for the other occupancy density functions are included in the Supplementary Information. For C1, Honeywell Jade, the control algorithm opens the damper at a fixed rate once the setpoint is exceeded. Result C1a has the damper speed set to "slow" and C1b has the damper speed set to "fast". In both cases, the CO_2 concentration overshoots the setpoint which is when the damper starts to open. Damper opening continues until the CO_2 concentration drops to 100 ppm below the setpoint, which causes the damper to return to the minimum position, and the process repeats. The “slow” versus “fast” setting determines the frequency of this process. This control method results in continuous oscillations of the CO_2 concentration and excessive movement of the damper.

Controllers C2 and C3, two products from Johnson Controls International (JCI), appear to contain similar control algorithms since the results are similar (Figure 2-6). In both cases, the CO_2 concentration overshoots the setpoint by approximately 300 ppm before the damper begins to open. While the total damper movement was similar to the ideal controller, this delay in response results in poor CO_2 control.

Tests C4a and C4b, the Pelican Pearl, used the response curve method where the damper opened all the way at the upper CO_2 concentration limit of 1,600 ppm. In C4a it was programmed to start opening above the activation level at 1,000 ppm and in C4b this value was reduced to 800 ppm. The strategy resulted in stable CO_2 values that exceeded the setpoint by approximately 200 ppm (Figure 2-6). While the total damper movement was similar to the ideal controller, the response curve approach generally resulted in a steady-state offset from the CO_2 setpoint. In the tests with low occupancy density (Figure S2-1 and Figure S2-3), the settings in C4a achieved an excellent result; the increase in CO_2 deviation from the setpoint increased as the simulated occupancy density increased. Since Pelican operates over a cloud-based platform, it is possible for operators to adjust settings remotely based on CO_2 monitoring results, a feature that was not available for any of the other controllers tested. At our request, Pelican enabled a demonstration version of a feedback algorithm (C4c). The performance was similar to that observed with the JCI algorithm.

Controller C5 is the XC Spec Air Quality Display for which the details of the algorithm were unavailable. The results suggest a response curve strategy based on the steady-state offsets from the setpoint observed (Figure 2-6). However, the XC Spec settings (which we did not have access to) appear to be more aggressive such that the observed CO_2 concentrations were much lower than the setpoint, except in the case of the high occupancy density tests where the steady-state CO_2 concentration was within 100 ppm of the setpoint (Figure S2-2 and Figure S2-5). In all tests the damper moved constantly with small movements, resulting in the greatest total movement among controllers tested.

Controller 6, the Belimo Zip that uses a PI algorithm, had the best performance among all controllers tested (Figure 2-6). This controller had a small overshoot of less than 150 ppm at the beginning of each period of CO_2 generation but had otherwise excellent performance. Controller C-PI in Figure 2-6 is the test result for the PI controller developed by the research team; results are described further in Section 2.5.2.

The performance metrics for each controller averaged over all six tests are summarized in Figure 2-8. The stacked bars show the percent of time that the controller was under (red), over (yellow), or at (green) the target ventilation rate. The single bar shows the ratio of the actual damper travel compared to the ideal. While performance varied between controllers and between tests, on average the commercially available controllers demonstrated poor control of CO_2 and two controllers had damper movement more than three times that required by an ideal controller. The best performing Belimo Zip achieved good CO_2 control ~80% of the time with damper movement slightly less than the ideal controller. Note that it’s possible for the damper ratio value to be less than 1 if the controller reduces damper movement in exchange for reduced control of CO_2.

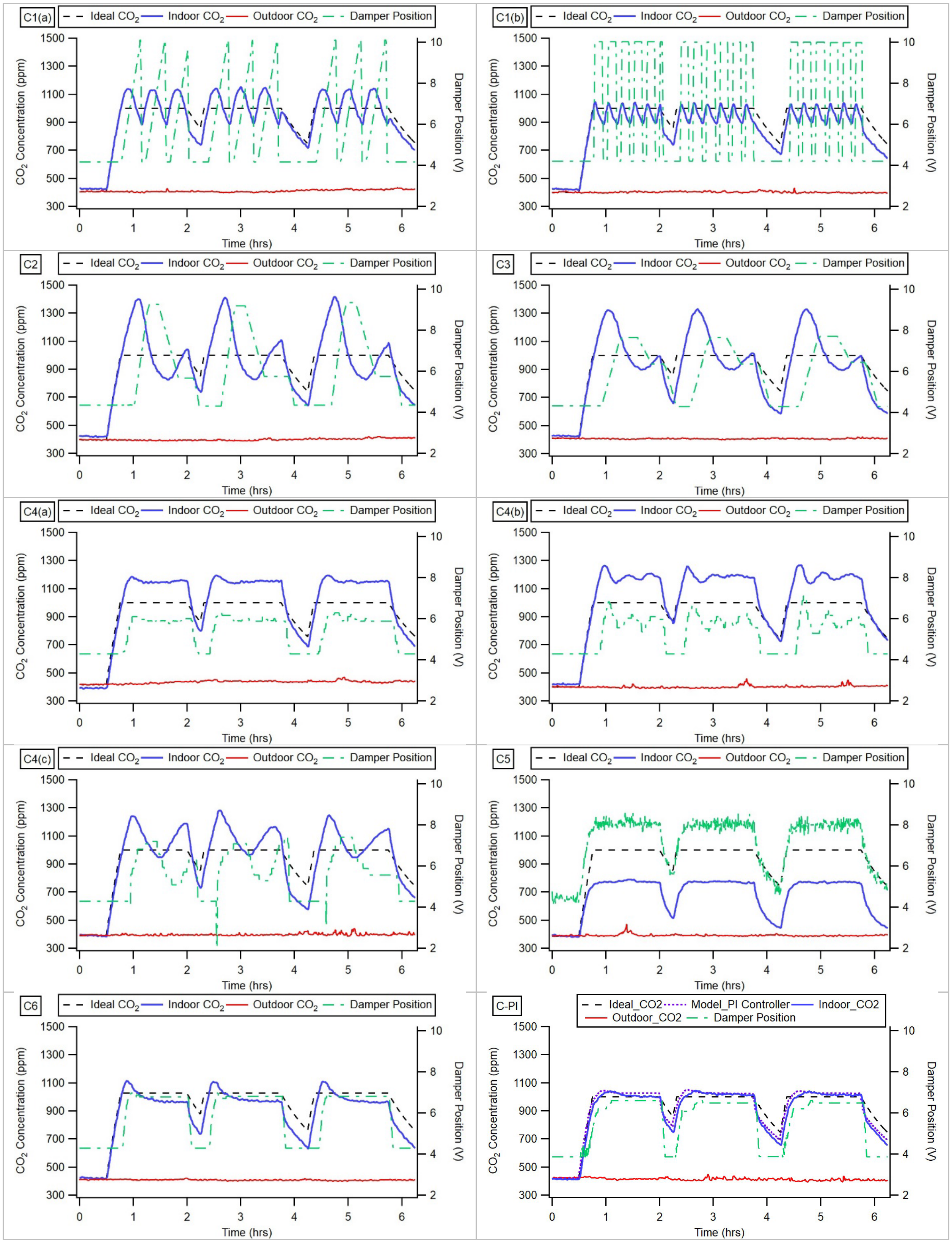

Figure 2-6: Controller performance results for the medium density step function

2.5.2 Test Conditions and Repeatability

We observed that tests often failed the criterion that required the absolute value of the five-minute moving-average difference of the indoor and exhaust CO_2 concentration to be less than 50 ppm (Table 2-2). An example of four repeat tests is shown for Controller 2 for the high-density step function (Figure 2-7). The high-density step function is shown because it has the highest CO_2 generation and outdoor airflow rates, which resulted in the greatest differences in the indoor and exhaust CO_2 concentrations. Although the test had to be run four times to achieve a passing result, the failed results (in terms of indoor CO_2 concentration and damper movement) are nearly identical to the passing result. This suggests the constraint on this criterion could be relaxed, perhaps to 75 ppm, to reduce the number of repeat tests. The repeat tests for Controller 2 are shown since JCI reports that the device contains a pattern recognition adaptive control algorithm to adjust gains [30]. As seen in Figure 2-7, there was no observed change in the response over the course of the testing and no evidence of impacts from the adaptive algorithm. The current test protocol would need to be modified to include longer testing sequences for controllers that demonstrate adaptive behavior, however, the need did not arise for the sample of controllers that was tested here.

2.5.3 PI controller

The model of the PI controller described in Section 2.4 was initially simulated and laboratory tested for all six tests with K_p = 0.076 L/s.ppm-CO_2 (equating to 20 mV/ppm-CO_2 for the OA damper) and τ_i = 8 min. Both the controller performance and the simulation agreement with the laboratory test data were excellent (Figure 2-6 and Figure S2-1 - Figure S2-5, C-PI). The PI controller achieved within 75 ppm of the CO_2 setpoint an average 92% of the time across all six tests while the remaining 8% time was in the overventilated region. The modeled performance (99% of time within 75 ppm) was better than the actual performance, likely due to small differences in the physical and modeled AHU and the modeled assumption of uniform CO_2 concentration in the chamber. The PI controller achieved this performance with a damper travel ratio of 1.5. It is notable that a PI algorithm configured with only a minimum and maximum damper position and without tuning exceeded the CO_2 control performance of the six commercially available controllers that were tested.

While a complete set of laboratory tests takes approximately a week to run, the simulation can be run in seconds and thus provides for a rapid pathway by which different control strategies and settings can be assessed. With the model validated by the laboratory test data, the PI controller was simulated for a range of proportional (K_p) and integral (τ_i) gains to determine the best settings for the PI algorithm applied to all six CO_2 generation profiles; the results across all six tests were averaged in Figure 2-9. Integral gains of 2 to 16 minutes all resulted in CO_2 concentration within the 75 ppm target more than 95% of the time. However, the proportional gain must be sufficiently low (20 to 100 mV/ppm) to avoid damper oscillations and excessive movement. Since outdoor airflow rates generally scale with floor area, the model was re-run with double the ceiling height (with all other inputs the same) to understand the impact of increasing the room air volume for the same floor area. In this case, the additional capacitance of the room air delayed outdoor air damper opening. However, once the CO_2 setpoint was reached, the steady-state outdoor air requirement was the same and the controller performance was similar. The doubled room air capacitance doubled the proportional gain value at which damper oscillations initiated.

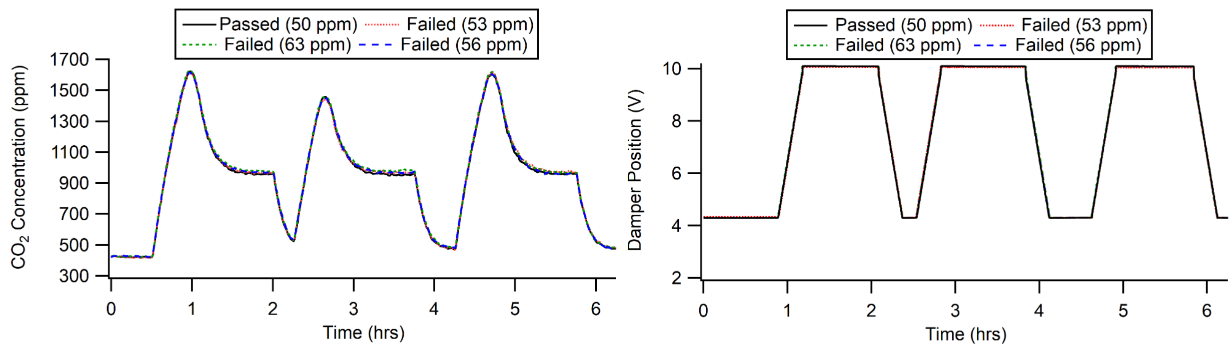

Figure 2-7: Four repeat tests for Controller 2 for the high density step function. Three tests failed the criterion that required the absolute value of the moving-average difference of the inlet and exhaust CO_2 concentrations to be less than 50 ppm (value of difference shown in legend).

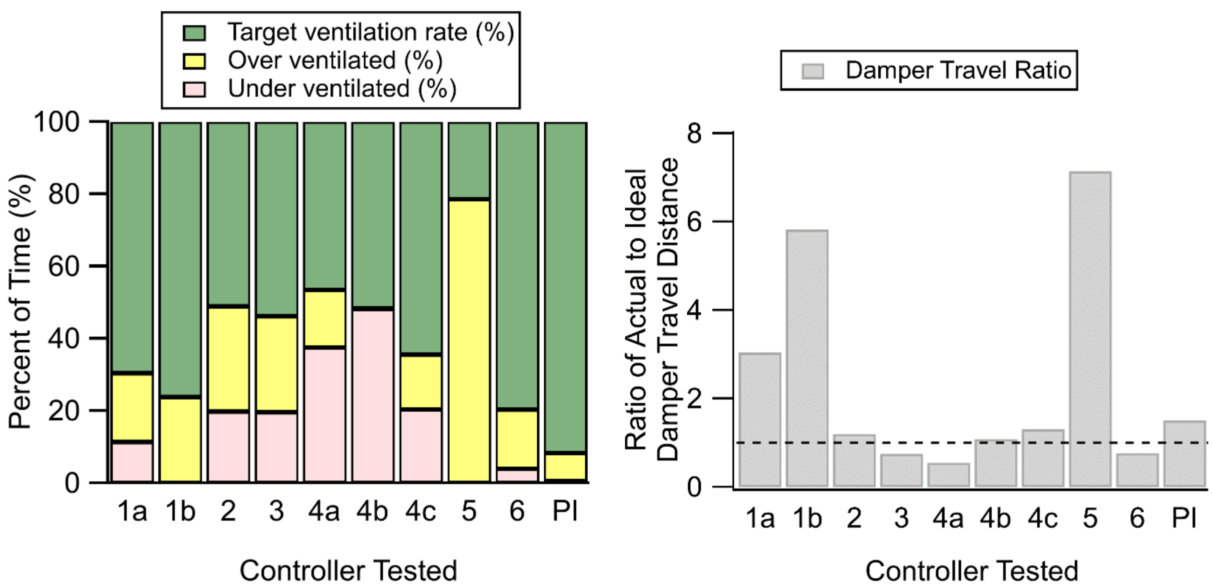

Figure 2-8: Results averaged for all six occupancy profiles for each controller and test condition. The stacked bar shows the percent of time that the controller was under, over, or at the target ventilation rate. The single bar shows the ratio of the actual damper travel compared to the ideal.

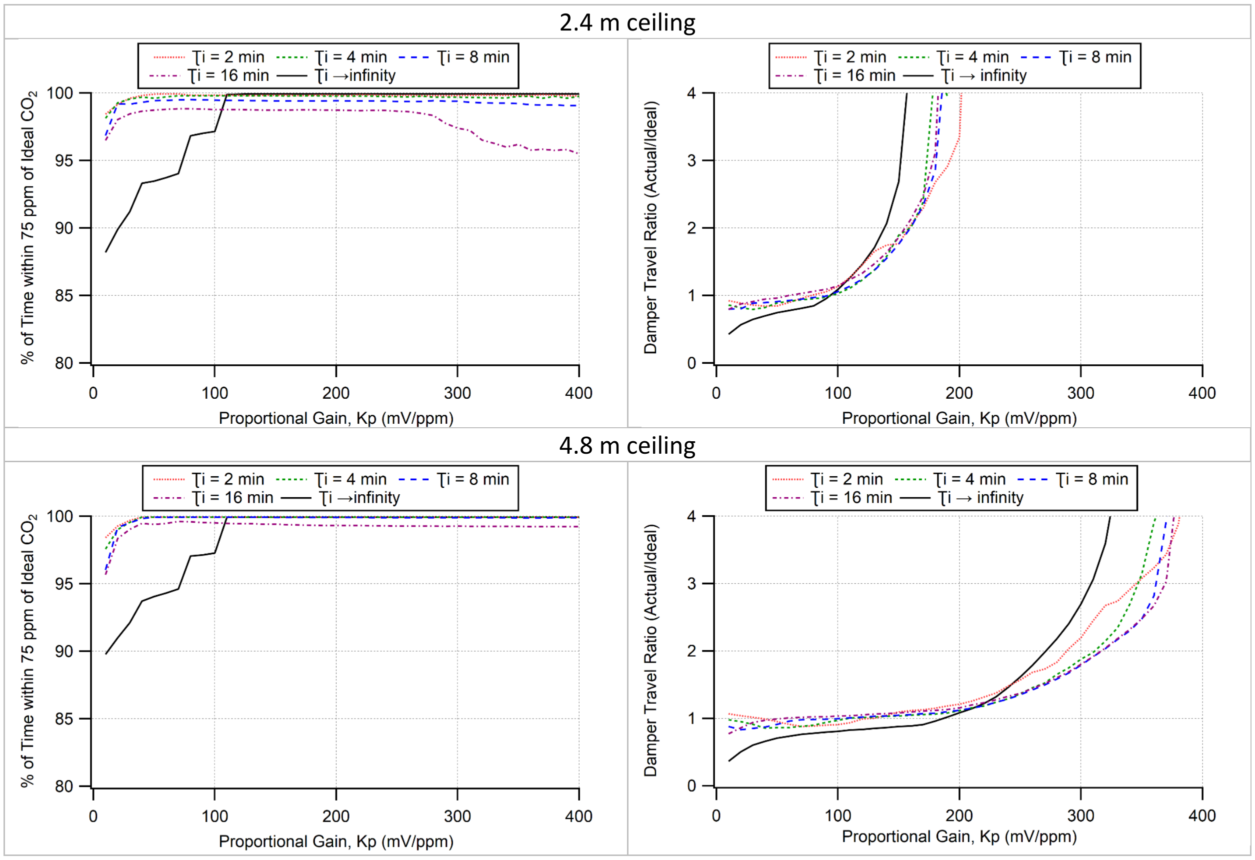

Figure 2-9: Impact of varying proportional (K_p) and integral (τ_i) gain on controller performance for maintaining the CO_2 concentration setpoint (left) and damper movement (right) relative to the performance of an ideal feedforward controller. A standard ceiling height (top) and two-story ceiling (bottom) were simulated.

2.6 Discussion and Conclusions

Six commercial DCV controllers tested under a range of typical occupancy patterns and densities generally had poor to marginal performance for CO_2 control. The best performing controller (Belimo Zip) achieved target CO_2 control 80% of the time with damper movement slightly less than an ideal controller. Two controllers had damper movement more than three times required by the ideal controller. Notably, a PI algorithm we applied and configured with minimum and maximum damper position and preset, non-adaptable gains, achieved superior performance with target CO_2 control 92% of the time. The PI algorithm achieved excellent CO_2 control performance under a wide range of simulated occupancy patterns and densities without tuning specific to the CO_2 generation profile or building volume (i.e. building-specific tuning). This indicates that more complicated DCV control approaches (model-based and learning-based) summarized by Lu et al. (2022) are unnecessary for the range of DCV use cases evaluated in this study [32]. An important limitation of this study is the focus on single-zone constant volume DCV controllers, which are prevalent in light commercial buildings and schools and is the most straightforward application of DCV [5]. Multi-zone and variable air volume systems require additional control sequences to consider CO_2 sensors in each zone, mixing between zones, and variable supply airflow rates [43] [44] [45]. The test methodology presented here could be expanded to evaluate multi-zone and/or variable air volume DCV controllers.

The results from the study clearly demonstrate that the control algorithms pre-programmed into single-zone DCV controllers are a substantial contributor to poor CO_2 control. While the goal of this study was to isolate the deviation from the CO_2 setpoint that was attributable to the control algorithm, it is important to consider that the CO_2 concentration in a space controlled by a DCV system may also be affected by errors in CO_2 sensor accuracy and placement as well as configuration and installation errors [26, 46]. Improving DCV control algorithms for single-zone CAV HVAC systems will have positive impacts in improving control of outdoor air dampers and resulting CO_2 concentrations. This is expected to reduce the transmission of airborne infectious diseases, optimize HVAC energy use, and reduce damper actuator failures. Manufacturers can improve their control algorithms using the PI control approach demonstrated here, or with alternate approaches, so long as they are laboratory tested and demonstrate good CO_2 tracking and damper movement performance.

This research is the first to demonstrate the importance of testing DCV controllers and to propose a test method, which is straightforward and can be executed by a laboratory with an environmental chamber modified to the test protocol with a scaled AHU. Although execution of all six tests provides the most information, controller problems are most evident when tested with the step function. Without an accepted test procedure and subsequent codified performance requirements and/or demand from building owners and operators, manufacturers are unlikely to be motivated to improve their products.

Unfortunately, even if manufacturers develop and deploy improved algorithms, change is likely to be slow given that HVAC systems are infrequently replaced. Possibilities to achieve scalable improvements on a faster timescale are either updating firmware on existing controllers or replacing controllers. Either option requires a technician to access each packaged system to complete this work, increasing the cost of the upgrade. The exception is cloud-based control systems where the control logic either exists on the cloud and/or can be updated remotely to a local device with an edge computing strategy [47]. An additional benefit of cloud-based systems is the ability to track system performance and detect faults. Potential draw backs are maintenance fees for device communication and data storage, cybersecurity and privacy concerns, and performance impacts from connectivity losses (which may be mitigated with edge computing that integrates local devices with cloud computing). Regardless of the method for which DCV control is implemented, this work clearly demonstrates the need to improve embedded control algorithms and deploy those improvements across the industry.

2.7 Supplementary Information

The figures below contain the complete results for all controllers tested with the low density step function (Figure S2-1), high density step function (Figure S2-2), low density gradual function (Figure S2-3), medium density gradual function (Figure S2-4), and high density gradual function (Figure S2-5).

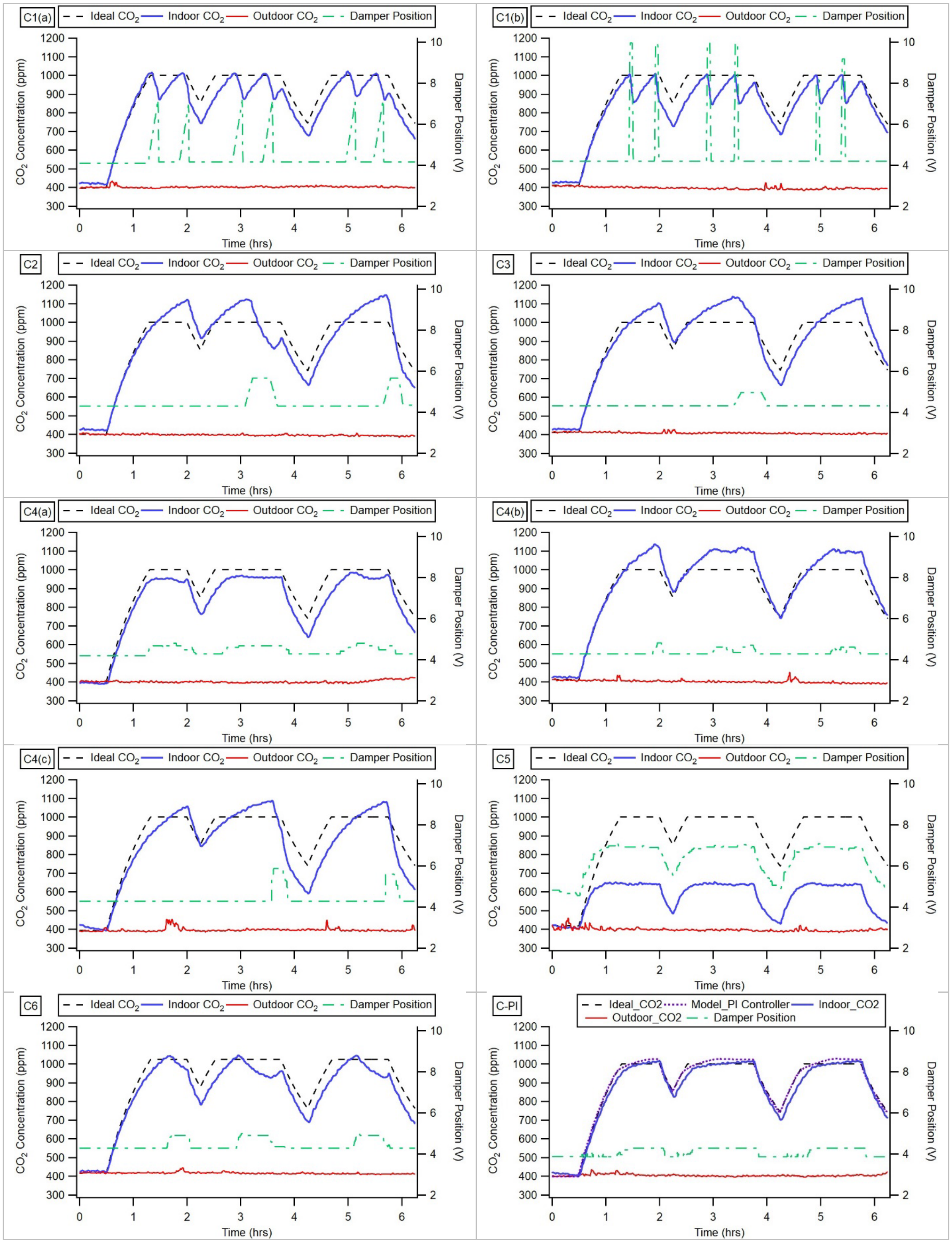

Figure S2-1: Controller performance results for the low density step function

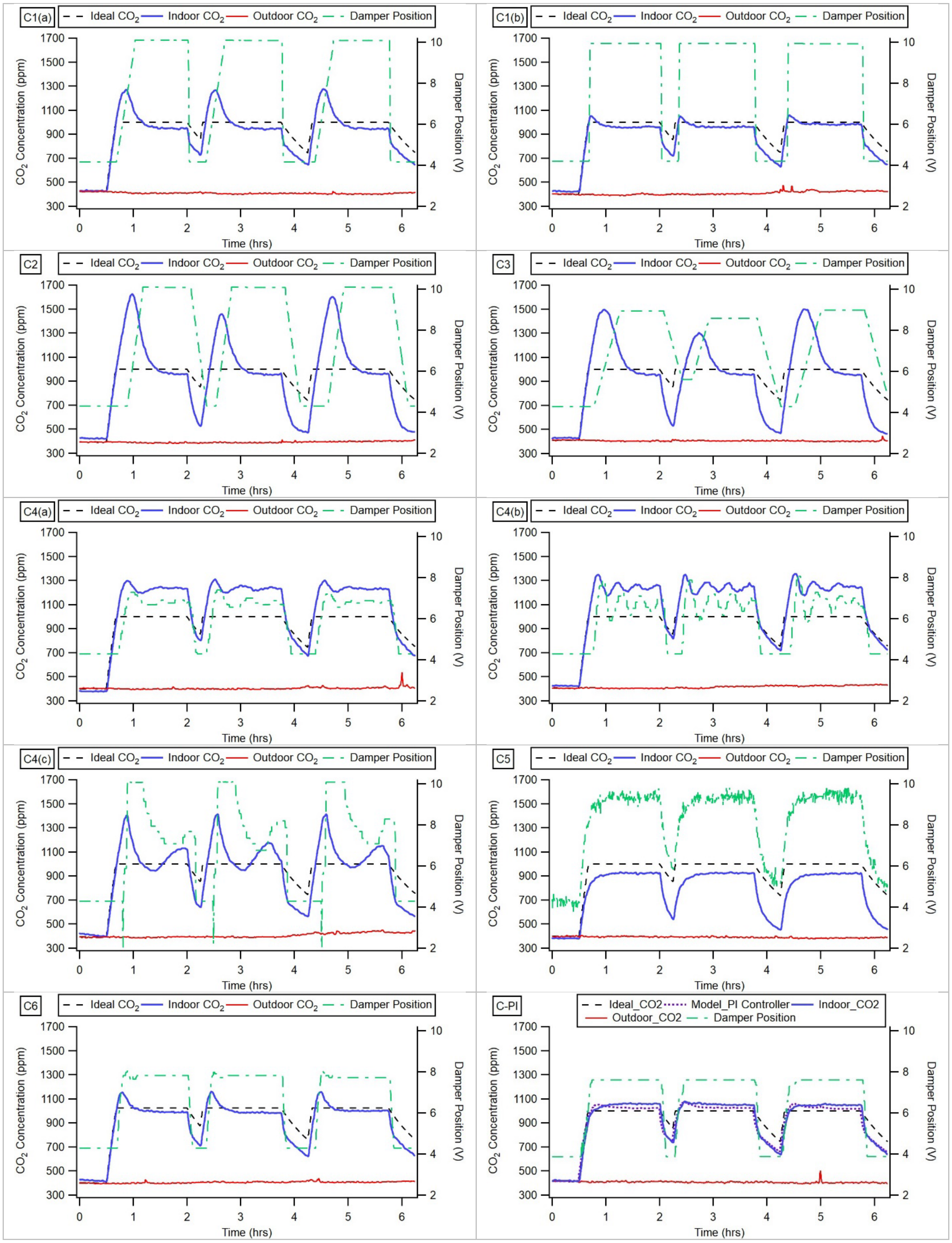

Figure S2-2: Controller performance results for the high density step function

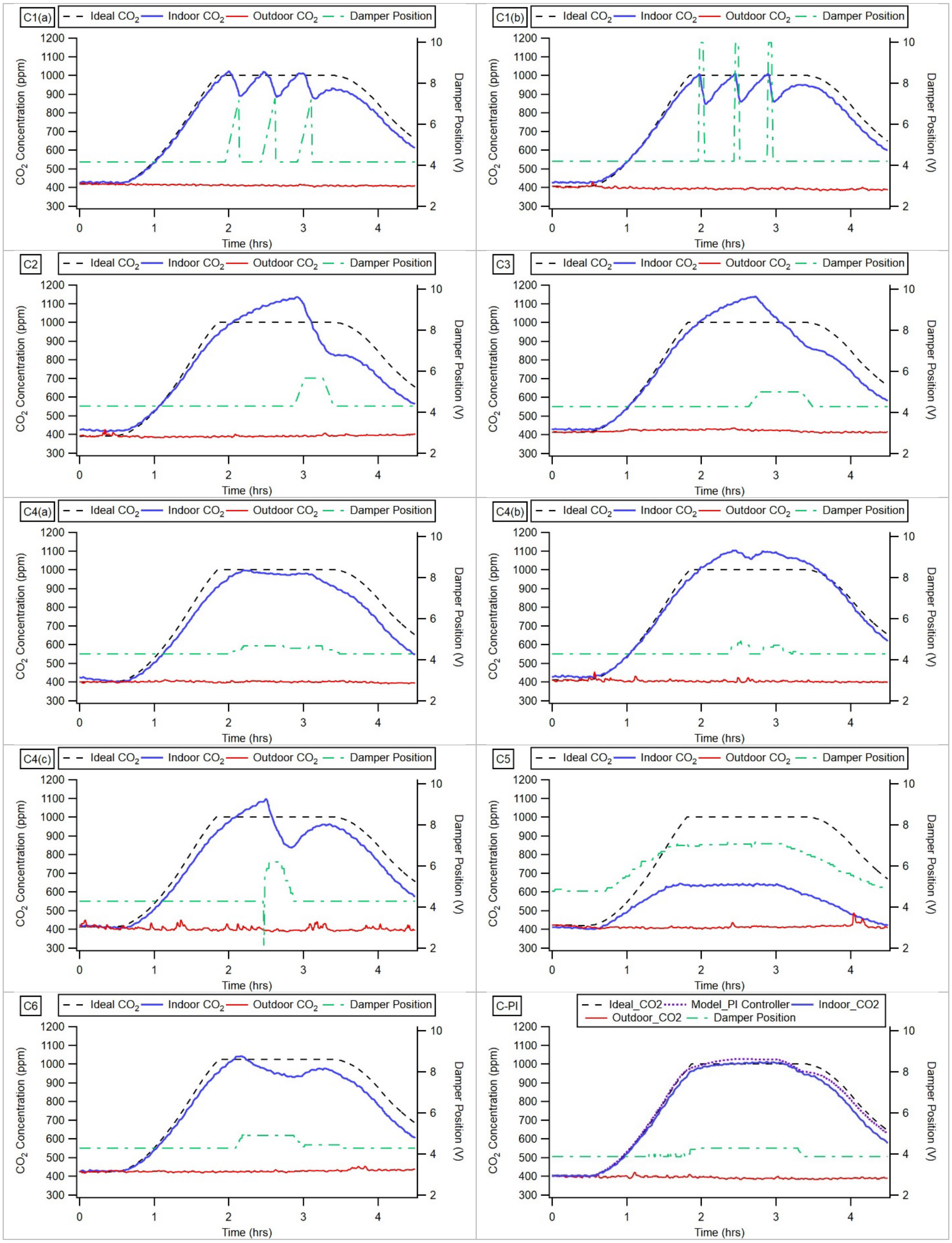

Figure S2-3: Controller performance results for the low density gradual function

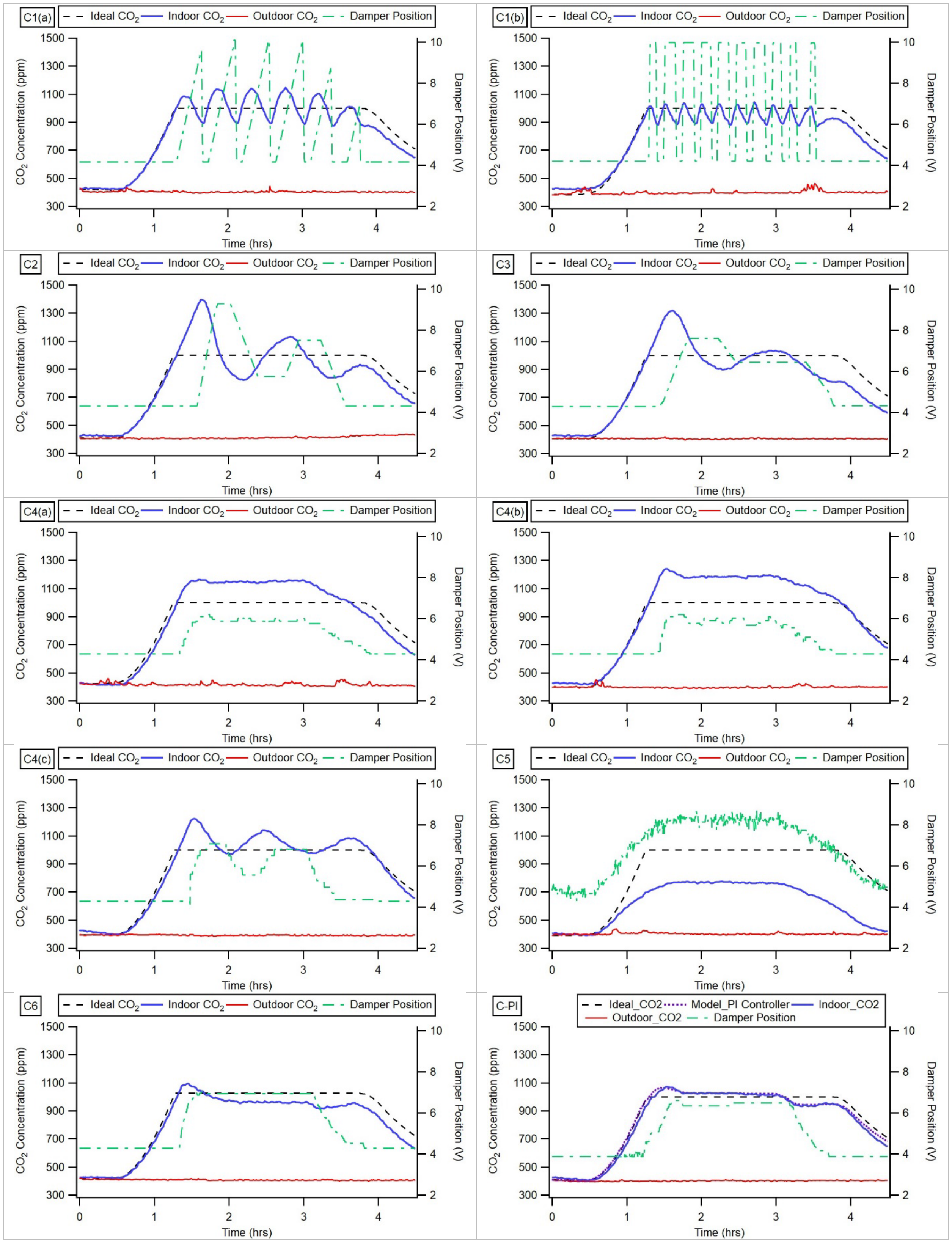

Figure S2-4: Controller performance results for the medium density gradual function

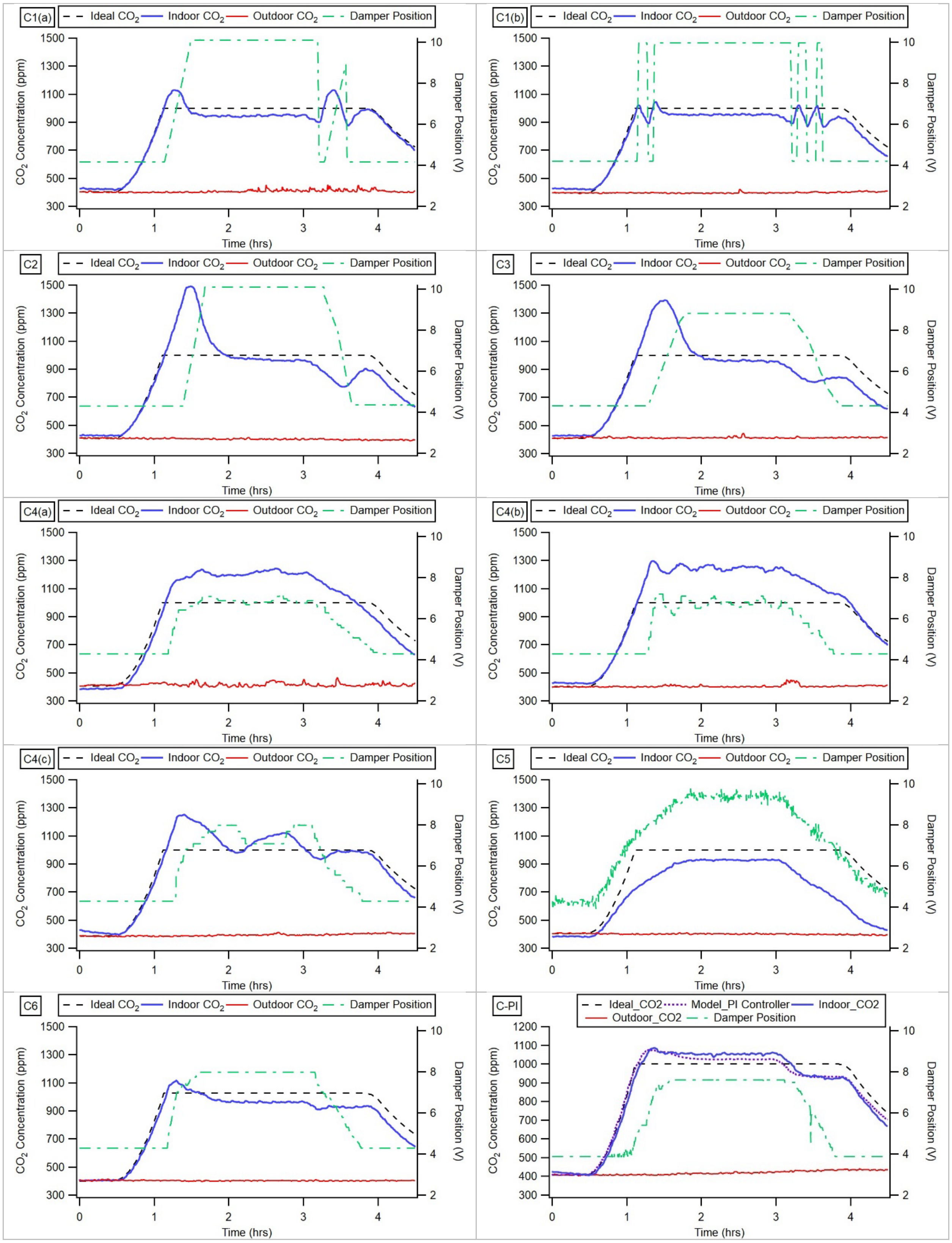

Figure S2-5 - Controller performance results for the high density gradual function

Chapter 3 Optimization of ventilation and filtration system operation in classrooms to minimize airborne infectious disease transmission, particulate matter exposure, and energy consumption

3.1 Introduction

In a Chapter 2, we designed a test method to evaluate the performance of CO_2-based DCV algorithms and tested six commercially available packaged controllers [48]. We also developed a straightforward proportional-integral (PI) feedback DCV controller that achieved superior performance compared to the commercially available controllers tested. This improved DCV controller serves as the first building block for the IAQ-Energy Controller, which is designed to minimize airborne infectious disease transmission, particulate matter exposure, and energy consumption (Figure 3-1).

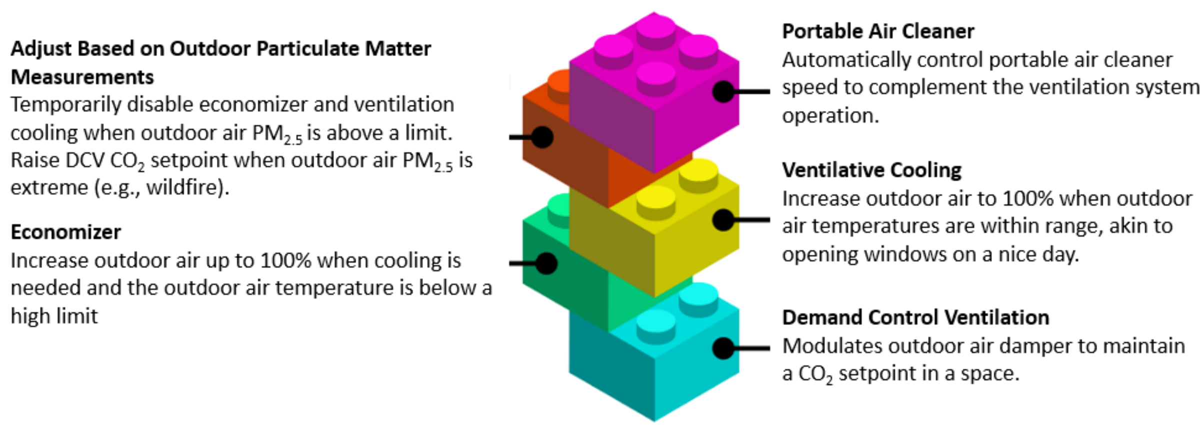

Figure 3-1: Building blocks of the rule-based IAQ-Energy Controller

The second building block of the IAQ-Energy Controller adds an economizer function (Figure 3-1). An economizer increases outdoor air when the thermostat calls for cooling and when the outdoor air is within temperature and/or enthalpy conditions set by the controller. In theory, a combined differential dry bulb and enthalpy economizer that ensures extra outdoor air used for cooling is always at a lower temperature and enthalpy than indoors would deliver the best performance [49]. However, this requires four sensors (outdoor and return air temperature and humidity) and calculation of enthalpy. Taylor et al.

(2010) demonstrated that uncertainties associated with temperature (±1°C) and relative humidity (±4 %) measurements using HVAC-grade sensors result in large uncertainties in differential enthalpy calculations and that a simple fixed dry bulb control delivers similar or better performance than differential enthalpy control in almost all climates modeled provided that the fixed dry bulb high limit is adjusted for the environment (e.g., reduced in higher humidity regions) [49]. This approach has the advantage of only requiring one outdoor air temperature sensor to determine economizer status. A supply air temperature sensor may also be used to limit the outdoor airflow rate and compressor operation to ensure the supply air temperature is not too cold (i.e., stays above a low limit). Economizer cooling is commonly used in combination with DCV. In this case, a call for economizer cooling temporarily overrides DCV until the call for cooling is satisfied. A fixed dry-bulb temperature control based on the work of Taylor et al. (2010) serves as the second building block for the IAQ-Energy Controller (Figure 3-1).

A shortcoming of economizer cooling is it does not open the outdoor damper to 100% until the indoor space warms to the cooling setpoint and the thermostat calls for cooling. This misses the opportunity to bring in as much outdoor air as possible when outdoor air temperatures allow, akin to opening windows on a nice day. Strategies to use additional ventilation for cooling are referred to as "ventilative cooling," which serves as the third building block for the IAQ-Energy Controller (Figure 3-1). While economizer controllers are widely commercially available, using additional ventilation to cool below the cooling setpoint is rarely applied, and the approach is not described in US building codes and standards (e.g., ASHRAE Standard 90.1 [50] or California's Building Energy Efficiency Standards [23]). Sophisticated modeling is needed to predict energy savings for ventilative cooling strategies and additional control logic is needed to implement the approach. The International Energy Agency has been researching and publishing case studies on ventilative cooling strategies, with the greatest activity occurring in Europe

[51]. However, the case studies describe custom-engineered, building-specific solutions that are difficult to scale. Ventilative cooling is possible when the outdoor air temperature is above the building's heating balance point, which is the outdoor air temperature where heating must be provided to maintain thermal comfort [52]. The balance point is specific to a building and depends on internal gains, envelope heat transfer, and air exchange rate with outdoors. Buildings with high internal gains (which include densely occupied classrooms), adequate insulation, and tight envelopes (as seen in newer buildings), and those located in hot/dry climates with large diurnal temperature swings, have the greatest potential to save energy with ventilative cooling. In addition to the heating balance point, humidity levels must be considered in ventilative cooling controls.

A problem with economizers and ventilative cooling is that increased particulate matter (PM) from outdoors is introduced indoors. Additionally, filters will load more quickly, increasing filter maintenance. Therefore, it follows that economizer use and ventilative cooling should be avoided when outdoor PM is high. A PM sensing strategy, as well as determination of the value of the high limit, is needed to add this functionality, which is not generally included in commercially available economizer controllers.

The approach should consider removal efficiencies of HVAC system filters, which are rated by their minimum efficiency reporting value (MERV) [53]. Filters used in HVAC systems are generally MERV 8, 11, or 13 (and occasionally MERV 14), which all have good removal efficiencies for particles above 3 μm (Figure 3-2). However, particles below 3 μm are harder to remove and filter efficiency varies dramatically based on the MERV rating and even within a MERV class [54]. This supports that controls to limit ventilation should primarily be based on sensing particles smaller than 3 μm since they are hardest to remove by filtration.

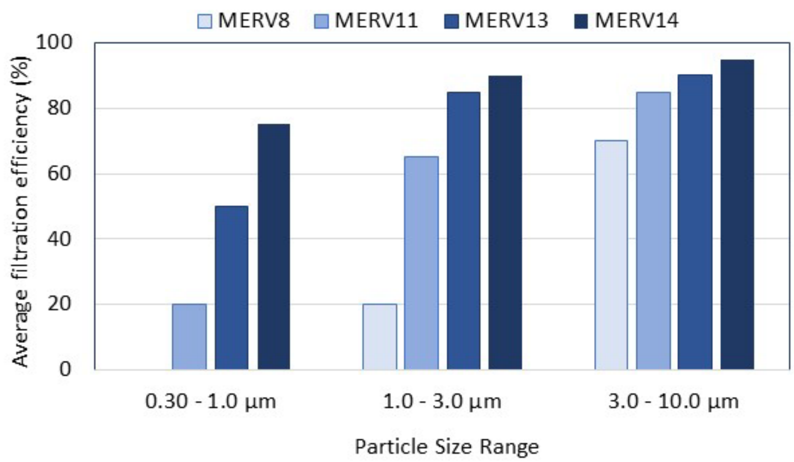

Figure 3-2: Minimum performance required for a filter by MERV rating from ASHRAE Standard 52.2-2017

The largest health impacts from PM are attributed to $PM_{2.5}$, which is integrated mass of PM with an aerodynamic diameter less than or equal to 2.5 µm, as these particles travel deeper into the respiratory system and can harm respiratory and cardiovascular systems [55, 56]. An analysis of data from the 2015 Global Burden of Diseases Study by Cohen et al. (2018) found that ambient $PM_{2.5}$ was the fifth-ranking mortality risk factor and that the number of deaths attributable to $PM_{2.5}$ exposure increased from 3.5 million in 1990 to 4.2 million in 2015 [57]. There is evidence that increased mortality risk persists at long-term ambient $PM_{2.5}$ exposure levels below the current US regulatory level of 12 µg/m^3 for annual average exposure [58, 59]. Thus, filtration of $PM_{2.5}$ is critical and controlling the ventilation strategy based on outdoor $PM_{2.5}$ is necessary to limit exposure. In cases where outdoor air $PM_{2.5}$ is very high (e.g., during a wildfire event or near roadways during heavy traffic), a decision could be made to further limit outdoor air, for example by raising the CO_2 setpoint on the DCV system.

Finally, for classrooms that generally have minimal indoor sources of $PM_{2.5}$ generation, any increase in outdoor air for economizer use or ventilative cooling will result in some increase in indoor $PM_{2.5}$ exposure. Adding a portable air cleaner to a room is a robust and energy-efficient method to reduce exposure to all particles, including $PM_{2.5}$ from outdoors and infectious respiratory aerosols [10, 60]. The drawbacks to portable air cleaners are noise, replacement costs of the included filter, control of the air cleaner (which is generally manual), and energy use. The final building block of the IAQ-Energy Controller is an internet-connected portable air cleaner that is automatically controlled to modulate speed to complement the ventilation system operation.

In this study, we propose a rule-based control logic to implement the IAQ-Energy Controller concept. For a classroom application, we then model the IAQ-Energy Controller compared to a fixed rate ventilation system and a state-of-the-art Economizer + DCV system and consider how energy use, indoor exposure to $PM_{2.5}$, and removal rates of infectious respiratory aerosols vary across 14 cities in the US.

3.2 Methods

3.2.1 IAQ-Energy Controller: Framework and Modes

The controller logic contains five modes represented in Table 3-2 and the control logic flow diagram shown in Figure 3-3. The modes are designed to limit exposure to $PM_{2.5}$ from outdoors, reduce energy use, and meet or exceed ASHRAE Standard 241-2023 for control of infectious aerosols by providing an equivalent clean (i.e. respiratory particle free) airflow (ECA) of 20 L/s-person, or 540 L/s for the modeled classroom with 27 occupants [61]. This is done by modulating the fraction of outdoor air and return air for the central HVAC system and the speed of a PAC that uses a HEPA filter.

The controller logic consists of a series of “if” and “else if” statements to determine controller mode as described below.

1. First, when outdoor $PM_{2.5}$ is above a maximum concentration limit (set to 35 μg/m^3, the EPA threshold for unhealthy for sensitive groups), the controller raises the indoor CO_2-based DCV setpoint to 1700 ppm (from 1000 ppm) to reduce outdoor air and, where needed, operates a PAC to provide the ECA needed to meet Standard 241.

2. Else, when outdoor $PM_{2.5}$ is above a moderate concentration limit (set to 12 μg/m^3, the EPA threshold for moderate prior to May 2024 [62]), the CO_2-based DCV setpoint is set to 1000 ppm, which historically has been an accepted standard for balancing indoor air quality and energy use [48]. A PAC may still be needed to provide the ECA needed to meet Standard 241, but at lower speed to reduce noise and save energy.
3. Else, when outdoor $PM_{2.5}$ is below the moderate concentration limit, outdoor and indoor temperatures are compared to determine if ventilative cooling is available. This occurs when the outdoor dry bulb temperature is below the economizer high limit and above the balance point of the building and when the indoor temperature is above the heating setpoint. The balance point can be estimated from historical heating and cooling data for a specific building, modeling data for buildings of the same type, or can be learned over time by the controller based on the relationship between heating and cooling demand and outdoor temperature. When ventilative cooling is active, the DCV function is overridden, and the HVAC system supplies 100% outdoor air. In classrooms with smaller central HVAC systems, a PAC may still be needed to provide the ECA necessary to meet Standard 241, but at lower speed to reduce noise and save energy.
4. Else, when conditions are not in the range for ventilative cooling, the economizer is used if the outdoor temperature is below the dry bulb high limit and the thermostat calls for cooling. This occurs in limited cases where cooling is needed at outdoor temperatures that are below the balance point. In this mode, the setpoints are the same as the ventilative cooling mode.
5. Else, default operating mode is used, which has the same setpoints as Mode 2. This occurs when $PM_{2.5}$ is low, but outdoor temperatures are not suitable for ventilative or economizer cooling.

Table 3-1: Rules-based control logic for IAQ-Energy Controller.

Mode	Logic		Variable		Value	Logic	Setpoints
1. PM High	IF		Outdoor $PM_{2.5}$	≥	$PM_{2.5}$ High Limit = 35 μg/m^3	THEN	Indoor CO_2 = 1700 ppm PAC to meet ASHRAE 241
2. PM Moderate	Else IF		Outdoor $PM_{2.5}$	≥	$PM_{2.5}$ Moderate Limit = 12 μg/m^3	THEN	Indoor CO_2 = 1000 ppm PAC to meet ASHRAE 241
3. Ventilative Cooling	Else IF	AND	Outdoor (OA) Temp	<	Dry Bulb High Limit	THEN	100% Outdoor Air PAC to meet ASHRAE 241
				>	Balance Point (BP)		
			Room (RM) Temp	>	Heating Setpoint (HS)		
4. Economizer Cooling	Else IF	AND	Outdoor Temp	<	Dry Bulb High Limit (HL)	THEN	Same as Mode 3.
			Call for Cooling	=	On		
5. Default	Else						Same as Mode 2.

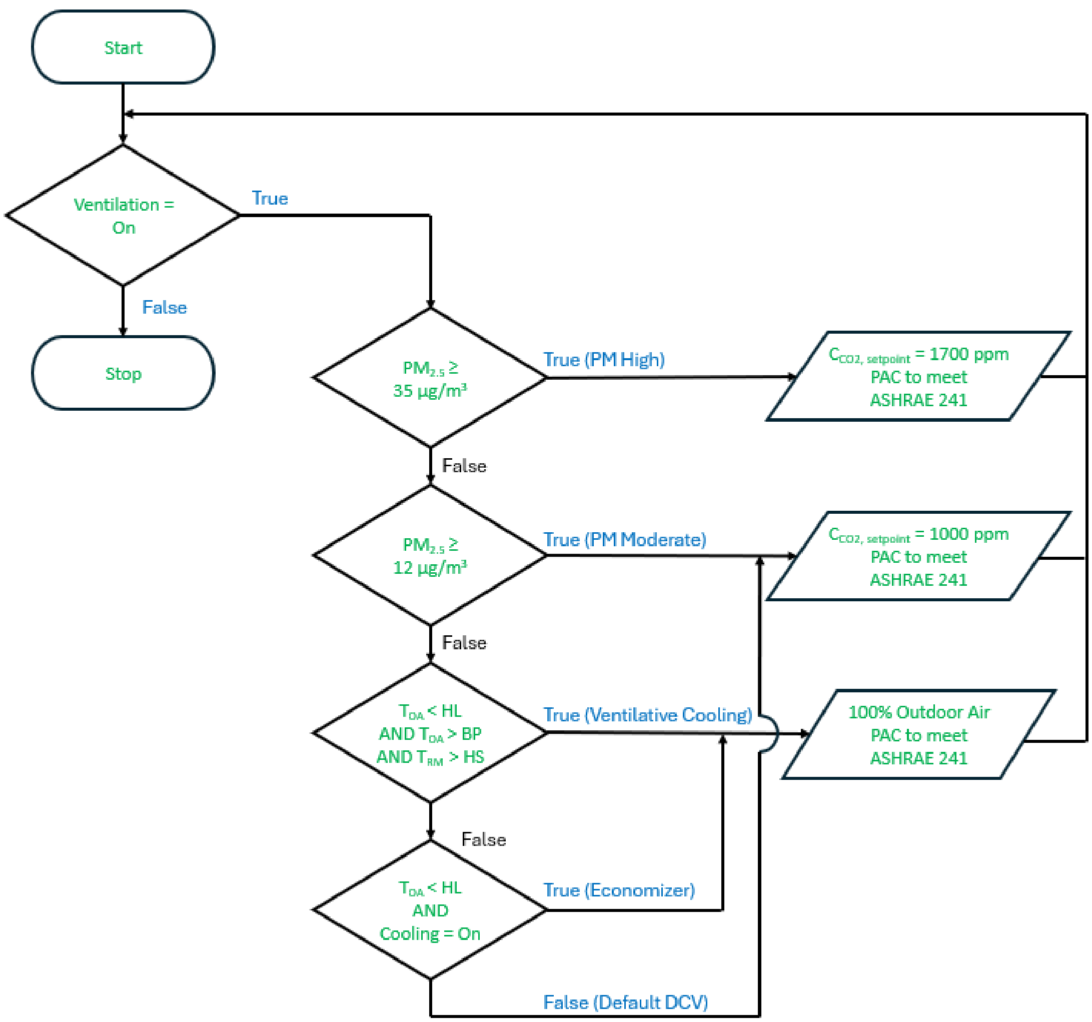

Figure 3-3: Rules-based control logic flow diagram for IAQ-Energy Controller.

3.2.2 IAQ-Energy Controller: HVAC System and Portable Air Cleaner Sizing

A box model was used to estimate the steady-state infectious aerosol removal by the central HVAC system to determine the minimum PAC filtration rate required to meet Standard 241. For DCV modes (Mode 1 and Mode 2), a box model was used to estimate the steady-state flow rate for outdoor air ($\dot{V}_{OA,SS}$) as a function of the CO_2 setpoint ($C_{CO2,setpoint}$) (Equation 3-1). Note that the steady-state model was used only to size the PAC; a dynamic model was used to evaluate time-varying flow rates as described in Section 3.2.8.

$$\dot{V}_{OA,SS} = \frac{\dot{G}_{v,CO2} \times n_{people}}{(C_{CO2,setpoint} - C_{CO2,OA}) \times 10^{-6}} \qquad \text{Equation 3-1}$$

$\dot{V}_{OA,SS}$ was calculated for the following parameters: Outdoor air CO_2 concentration of 425 ppm ($C_{CO2,OA}$), 27 people (n_{people}), and a CO_2 generation rate of 5 x 10^{-3} L/s-person ($\dot{G}_{v,CO2}$) [63]. The controller has a standard operation CO_2 setpoint of 1,000 ppm for Mode 2 and a raised CO_2 setpoint of 1,700 ppm for Mode 1, which resulted in $\dot{V}_{OA,SS}$ of 235 L/s for Mode 2 and 106 L/s for Mode 1.

The total supply air rate, which is a combination of outdoor air and recirculation air, varies depending on the cooling and dehumidification requirements for the HVAC system. In our previous work, we configured, sized, and simulated a packaged HVAC unit in 13 cities to determine the impact of five ventilation flow rates and three filtration systems on HVAC energy use and peak electricity demand, thermal comfort, and probability of airborne infectious disease transmission [6]. In the present work, we used the same HVAC system model and classroom model, modifying the controls to implement and simulate the IAQ-Energy Controller. We simulated the same cities and added Stockton, California, to better understand the potential of the IAQ-Energy Controller in California’s Central Valley, which contains eight out of ten of the US cities with the highest average outdoor $PM_{2.5}$ concentrations from

2018-2022 [64]. The supply airflow, $\dot{V}_{SA}$, for the classroom HVAC system varied by city between 283 to 826 L/s owing to differences in the size of the HVAC system necessary to meet heating and cooling needs (Table 3-2).

The ECA for the filtered recirculation air (ECA_{RA}) was determined from Equation 3-2 as the difference between the supply flow rate ($\dot{V}_{SA}$) and $\dot{V}_{OA,SS}$ multiplied by the filtration efficiency for infectious aerosols (f_{IA}), estimated from Standard 241 to be 0.77 for a MERV 13 filter [61].

$$ECA_{RA} = (\dot{V}_{SA} - \dot{V}_{OA,SS}) \times f_{\mathrm{IA}} \qquad \text{Equation 3-2}$$

The resulting value for ECA_{RA} varies by city (due to cities with higher cooling and dehumidification needs having a greater supply airflow) and by controller mode (Table 3-2). ECA_{RA} is highest in Mode 1 when outdoor airflow is lowest, lower in Mode 2 and 5 when outdoor airflow is moderate, and zero when outdoor airflow is 100% of the supply airflow.

The ECA needed for the portable air cleaner (ECA_{PAC}) was calculated by subtracting $\dot{V}_{OA,SS}$ and ECA_{RA} (both delivered by central HVAC system) from the target ECA of 540 L/s (Equation 3-3). In some cases, the ECA available from the central HVAC system exceeded the target, and in this case ECA_{PAC} was set to zero (Table 3-2).

$$ECA_{PAC} = ECA - \dot{V}_{OA,SS} - ECA_{RA} \ \ where\ ECA_{PAC} \ \geq 0 \qquad \text{Equation 3-3}$$

The highest rates for ECA_{PAC} (0 to 298 L/s) are required in Mode 1 when outdoor air rates are the lowest. Consumer-grade PACs certified by Energy Star have an ECA on the highest speed up to 283 L/s (mean = 95 L/s, median = 78 L/s, SD = 58 L/s), and multiple PACs can be used in a space to meet an ECA target [65]. In classrooms with high cooling loads and thus large supply airflows in the central HVAC, the modeling predicts that no PAC is needed to meet Standard 241. Conversely, classrooms in mild climates like Seattle and San Francisco will require 225 and 283 L/s respectively in PAC capacity, which can be accomplished with two consumer-grade PACs. While many PACs are designed to be manually controlled with discrete speed options (e.g. low, medium, high), internet-connect models are available that enable remote control of the entire fleet through an application programming interface (API). For example, we have tested the API for the Wynd Max PAC in our laboratory and confirmed it can turn the air cleaner on and off, set the fan to any speed from 0 to 100, and change the color of an indicator light to communicate information to the building occupants.

Table 3-2: HVAC system sizing and supply airflow ($\dot{V}_{SA}$), as well as steady-state estimates for outdoor airflow ($\dot{V}_{OA,SS}$), recirculation airflow (ECA_{RA}) and minimum ECA needed for the portable air cleaner (ECA_{PAC}) to satisfy ASHRAE Standard 241 for each mode of the IAQ-Energy Controller.

IECC Climate Zone	City	Heat Pump Capacity (Cool/Heat) (kW)	Heat Strips (kW)	ECA Target (L/s)	$\dot{V}_{SA}$ (L/s)	Mode 1			Mode 2 and 5			Mode 3 and 4		
						$\dot{V}_{OA,SS}$ (L/s)	ECA_{RA} (L/s)	ECA_{PAC} (L/s)	$\dot{V}_{OA,SS}$ (L/s)	ECA_{RA} (L/s)	ECA_{PAC} (L/s)	$\dot{V}_{OA,SS}$ (L/s)	ECA_{RA} (L/s)	ECA_{PAC} (L/s)
1A	Miami	16.0/15.0	0	540	826	106	554	0	235	455	0	826	0	0
2A	Houston	16.0/15.0	0	540	826	106	554	0	235	455	0	826	0	0
2B	Phoenix	16.0/15.0	0	540	826	106	554	0	235	455	0	826	0	0
3B	Las Vegas	16.0/15.0	0	540	826	106	554	0	235	455	0	826	0	0
3B	Stockton	13.9/12.1	0	540	732	106	482	0	235	382	0	732	0	0
3A	Atlanta	13.9/12.1	0	540	732	106	482	0	235	382	0	732	0	0
4A	Baltimore	10.6/9.3	4	540	543	106	336	98	235	237	68	543	0	0
4B	Albuquerque	10.6/9.3	0	540	543	106	336	98	235	237	68	543	0	0
5B	Denver	10.6/9.3	4	540	543	106	336	98	235	237	68	543	0	0
6A	Minneapolis	10.6/9.3	10	540	543	106	336	98	235	237	68	543	0	0
3B-AC	Los Angeles	10.6/9.4	0	540	543	106	336	98	235	237	68	543	0	0
5A	Chicago	10.6/9.5	8	540	543	106	336	98	235	237	68	543	0	0
3C	San Francisco	6.9/6.6	0	540	378	106	209	225	235	110	195	378	0	162
4C	Seattle	5.1/4.9	4	540	283	106	136	298	235	37	268	283	0	257

3.2.3 Modeling Overview

A simulation was built to evaluate three methods for ventilation control of an HVAC system (Figure 3-4):

1. Fixed ventilation rate

2. State-of-the-art controller with CO_2-based DCV and economizer

3. IAQ-Energy Controller as described in 3.2.1 and 3.2.2

In each city simulated, five years of historical weather and outdoor $PM_{2.5}$ data were applied to an EnergyPlus simulation and a box model simulation for indoor $PM_{2.5}$ exposure, as shown in an overview in Figure 3-4 and described in detail in the subsequent sections. The outputs analyzed from the models are:

1. Total annual energy use for the HVAC system combined with the PAC (where applicable)

2. Average and maximum daily indoor exposure to outdoor-source $PM_{2.5}$

3. Total annual $PM_{2.5}$ deposited on the HVAC system filter

4. Average ECA for respiratory aerosol removal as defined by ASHRAE Standard 241

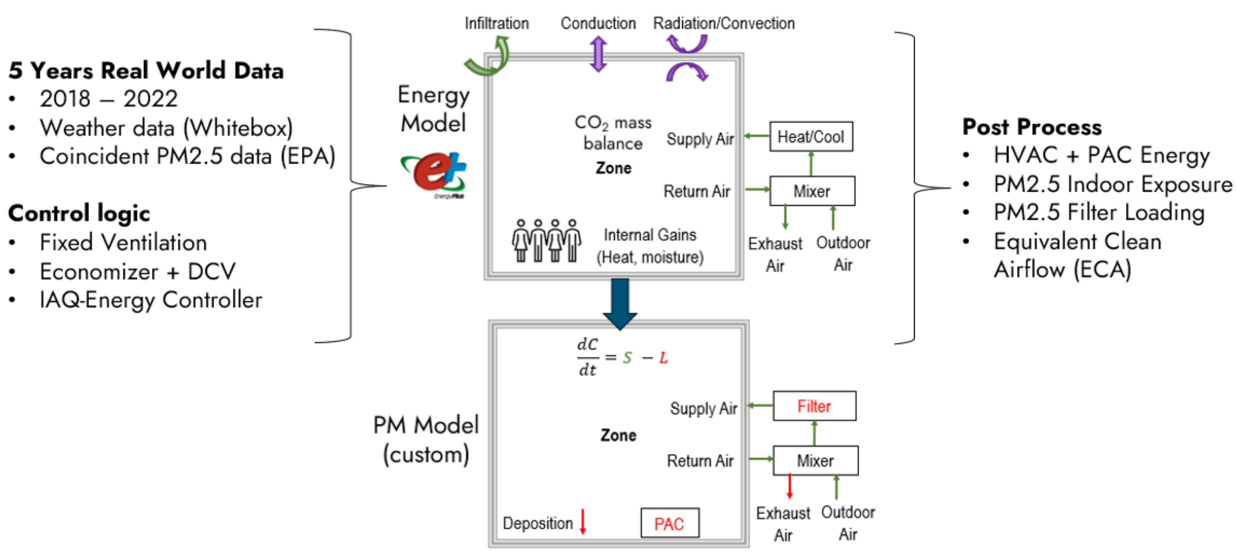

Figure 3-4: Overview of inputs to EnergyPlus Model and custom $PM_{2.5}$ model and post-processed data

3.2.4 Weather and $PM_{2.5}$ Data

EnergyPlus simulations generally use widely available and typical metrological year (TMY) weather files that have been built to represent the climate in a specific location. This study required weather files for EnergyPlus simulation along with accompanying hourly outdoor $PM_{2.5}$ data for the $PM_{2.5}$ simulation, for which no "typical" files exist. Because weather and $PM_{2.5}$ are correlated [66], we obtained historical data for 2018-2022 to simulate five years of weather and $PM_{2.5}$ for each city to account for year-to-year variability. EnergyPlus weather files for the 14 cities in Table 3-2 from 2018 to 2022 were purchased from weather data aggregator White Box Technologies [67]. $PM_{2.5}$ data files for the same locations and time periods were built from a database maintained by the Environmental Protection Agency (EPA) using a tool developed in Python by Green [68]. The tool addressed missing data as well as negative $PM_{2.5}$ concentrations, which are physically impossible and may represent a bias with the measurement equipment or other issues that were not captured during the QA/QC process. Frequent values less than -1 µg/m^3 raise concerns about the data quality for that monitoring station or may simply reflect that the $PM_{2.5}$ concentrations were very low much of the time. $PM_{2.5}$ monitoring stations that had 1) more than 10% missing data or 2) recorded $PM_{2.5}$ values less than or equal to -2 µg/m^3 for more than 2% of the data for the period from 2018 to 2022 were excluded. For the remaining EPA stations, the closest to the weather station used by Whitebox Box Technologies was selected as the primary data source (Table 3-3). In the case of Miami, the original exclusion criteria resulted in no viable EPA station within 50 miles. Therefore, the second criterion for Miami was relaxed to exclude stations with $PM_{2.5}$ values less than or equal to -3 µg/m^3 for more than 3% of the data, which resulted in a viable EPA station 18 miles away.

After the primary EPA station was selected, any gaps in data of four hours or less were filled by linear interpolation using the two nearest points. This occurred between 0.2 to 1.7% of the time, depending on location (Table 3-4). Finally, any gaps in data of 5 hours of more were filled by splicing the values from the closest $PM_{2.5}$ monitoring station with available data. This occurred between 0.8 to 6.8% of the time (Table 3-4). Finally, negative $PM_{2.5}$ values were set to zero, which occurred between 0 and 4.3% of the time (Table 3-4). As the $PM_{2.5}$ threshold for moderate was 12 μg/m^3, setting negative values to zero had no material impact on the operation of the simulated impact of IAQ-Energy controller.

Table 3-3: Location of weather stations used for energy modeling and EPA monitoring stations used for $PM_{2.5}$ modeling for each city simulated

	Weather Stations		EPA $PM_{2.5}$ Sites			
City	Latitude	Longitude	Site ID	Latitude	Longitude	Distance between stations (km)
Albuquerque	35.042	-106.616	35-1-29	35.017	-106.657	5
Atlanta	33.630	-84.442	13-89-2	33.688	-84.291	14
Baltimore	39.173	-76.684	24-27-6	39.143	-76.846	16
Chicago	41.786	-87.752	18-127-24	41.618	-87.199	49
Denver	39.833	-104.658	8-31-28	39.786	-104.989	29
Houston	29.980	-95.360	48-201-1034	29.768	-95.221	26
Las Vegas	36.072	-115.163	32-3-1501	36.140	-115.176	7
Los Angeles	33.938	-118.389	6-111-2002	34.276	-118.684	45
Miami	25.791	-80.316	12-11-34	26.054	-80.257	29
Minneapolis	44.880	-93.230	27-53-962	44.965	-93.255	10
Phoenix	33.428	-112.004	4-13-4003	33.403	-112.075	7
San Francisco	37.620	-122.365	6-1-12	37.794	-122.263	22
Seattle	47.444	-122.314	53-33-2004	47.386	-122.230	9
Stockton	37.889	-121.226	6-99-5	37.642	-120.994	36

Table 3-4: Percent of $PM_{2.5}$ data from 2018 to 2022 by city that was filled in or adjusted with each method

	Missing values interpolated	Missing values filled in from nearest station	Negative values set to zero
Albuquerque	0.8%	2.5%	0.0%
Atlanta	0.5%	2.4%	0.1%
Baltimore	0.7%	2.4%	1.5%
Chicago	0.9%	6.8%	1.8%
Denver	0.7%	3.3%	0.0%
Houston	0.5%	4.0%	1.1%
Las Vegas	0.2%	0.9%	0.0%
Los Angeles	0.3%	2.5%	4.3%
Miami	0.5%	1.7%	2.9%
Minneapolis	0.3%	2.3%	2.5%
Phoenix	1.7%	2.6%	1.1%
San Francisco	0.6%	0.8%	1.3%
Seattle	0.4%	3.2%	3.4%
Stockton	0.4%	2.2%	1.1%

3.2.5 EnergyPlus Modeling

This work builds upon a previous study where we used EnergyPlus to simulate a classroom and analyzed energy use as a function of outdoor air ventilation rates (3.5, 7.0, 10.5 L/s-person, 100% outdoor air, and 7.0 L/s-person with an economizer) and HVAC system filter MERV rating (MERV 8 and 13) [6]. The study included simulation in 13 cities (Table 3-2, not including Stockton, CA). The building model represented a single classroom with floor area 89 m^2 and 27 occupants. The design of the building envelope varied by city simulated and was based on properties from the Department of Energy's commercial building reference models. The HVAC model was a single zone packaged heat pump model with an outdoor air controller that was configured to operate between 07:30 to 16:00 on school days. As is standard practice in industry, the heat pump was sized to meet the design day cooling load and electric resistance back up heat strips were sized to meet the design day heating load. Compared to the TMY weather files used in the previous work, sizing the HVAC equipment based on 2018 to 2022 observed weather increased the cooling capacity required in Los Angeles, Chicago, and San Francisco and reduced or eliminated the need for backup electric resistance heat strips in most cities (Table 3-2). Complete details of the building model, the HVAC system model, and the filtration model are described in the previous work [6].

The current work modified the previously published model to simulate energy impacts of the IAQ-Energy Controller. Two updates were made to the classroom model. First, the CO_2 generation rate was updated to 5 x 10^{-3} L/s-person to reflect average generation rate estimates for 12- to 13-year-old children in the US [69]. The outdoor CO_2 concentration was set to a constant 425 ppm. Second, infiltration rate was set to a constant 0.21 1/hr (based on a field study in 37 schools across the US [70]) when the ventilation system was off to simulate uncontrolled air exchange between indoors and outdoors. Infiltration when the mechanical ventilation system was on was set to 0 because the ventilation system positively pressurizes the classroom relative to outdoors.

Three versions of the EnergyPlus simulation were then created to simulate three versions of the ventilation system:

Fixed Rate Ventilation: The EnergyPlus “Controller:OutdoorAir” object was configured to provide a constant rate ventilation during scheduled occupied hours of 189 L/s for the 27 occupant classroom to meet the requirements of ASHRAE Standard 62.1 “Ventilation and Acceptable Indoor Air Quality” [22].

Economizer with DCV: The “Controller:OutdoorAir” object was modified to have a “FixedDryBulb” economizer with temperature setpoint varying by city, as described in our previous work [6]. The “Controller:MechanicalVentilation” object was modified to use the “IndoorAirQualityProcedure” with a CO_2 setpoint of 1,000 ppm. The minimum ventilation rate was set to 54 L/s to reflect the reduced minimum ventilation requirement needed for DCV per ASHRAE Standard 62.1 [22].

IAQ-Energy Controller: For each year in each city, the outdoor $PM_{2.5}$ and outdoor temperature were used to determine the IAQ-Energy Controller mode (as described in Table 3-2) for each hour of the year. An hourly CO_2 CSV setpoint file was constructed with 1700 ppm for mode 1 (PM high) and 1000 ppm for mode 2 (PM moderate) and mode 5 (default). The CO_2 setpoint was not relevant for mode 3 and 4 (ventilative and economizer cooling) since 100% outdoor air overrides the economizer control. The CO_2 setpoint schedule was implemented in EnergyPlus using the “Controller:MechanicalVentilation” object and the “IndoorAirQualityProcedure” with the CO_2 setpoint specified as the input file for that city for that year. Next, an hourly minimum ventilation rate setpoint file was constructed to set the minimum ventilation set to the full supply airflow rate when conditions were met for mode 3 (ventilative cooling). Otherwise, the minimum ventilation rate was set to 54 L/s for the classroom. The actual ventilation rate needed to maintain CO_2 at the setpoint was determined from the simulation.

We were unable to directly simulate the economizer function in EnergyPlus because EnergyPlus does not allow the economizer to be disabled on a schedule with the “Controller:OutdoorAir” object. Enabling the economizer in EnergyPlus allowed the economizer to run even in modes 1 and 2 when $PM_{2.5}$ was above the limit. Therefore, the simulations were first run without the economizer and then the outdoor air rate that would result from the economizer function was determined via post-processing. For each time step, the maximum economizer sensible cooling availability was calculated from Equation 3-4 when outdoor $PM_{2.5}$ < 12 μg/m³.

$$E_{econ,max} = \left(\dot{V}_{SA} - \dot{V}_{OA}\right) \times (T_{RM} - T_{OA}) \times \rho_{OA} \times c_p \times \Delta t \qquad \text{Equation 3-4}$$

In Equation 3-4, the following parameters were determined by the EnergyPlus simulation at each time step: outdoor air rate ($\dot{V}_{OA}$), room temperature (T_{RM}), outdoor air temperature (T_{OA}) and outdoor air density (ρ_{OA}). Specific heat (c_p) was assumed to be constant at 1,006 J/(kg.K) and the simulation time step (Δt) was constant at 300 s.

Next, the mechanical sensible cooling energy (E_{cool}) delivered in the time step (as calculated by EnergyPlus) was compared to the economizer cooling energy ($E_{econ,max}$) available. Sensible cooling was used as the metric because the modeled thermostat controlled the cooling signal based on room temperature. When E_{cool} and $E_{econ,max}$ were both greater than 0, the applied economizer cooling energy ($E_{econ,applied}$) was determined as the lesser of E_{cool} and $E_{econ,max}$ per Equation 3-5 (i.e. the economizer will not cool the room below the setpoint, regardless of how much cooling is available).

$$E_{econ,applied} = E_{econ,max} \qquad when\ E_{econ,max} < E_{cool}$$
$$E_{econ,applied} = E_{cool} \qquad when\ E_{econ,max} \geq E_{cool}$$

Equation 3-5

Finally, for time steps where the economizer was applied, the new adjusted outdoor air ventilation rate ($\dot{V}_{OA,adj}$) was calculated with Equation 3-6:

$$\dot{V}_{OA,adj} = \frac{E_{econ,applied}}{(T_{RM}-T_{OA}) \times \rho_{OA} \times c_p \times \Delta t} + \dot{V}_{OA}$$

Equation 3-6

Then, the hourly minimum ventilation rate setpoint file was updated. For hours when $E_{econ,applied}$ > 0, the minimum ventilation rate was set to the adjusted ventilation rate. Otherwise, the setpoint file remained unchanged. Finally, the EnergyPlus simulation was re-run with the updated minimum ventilation rate setpoint file. This workaround method produced similar results to what would have been calculated if EnergyPlus had the functionality to simulate the entire control sequence. Comparing the results of the economizer workaround to EnergyPlus economizer calculations showed that the workaround sometimes resulted in additional economizer cooling in a timestep. The resulting indoor temperatures from the extra economizer cooling were always above the heating setpoint and were generally within 0.5°C of the cooling setpoint. The differences are attributed to the limited functionality of EnergyPlus that only allowed specification of the ventilation rate on an hourly schedule, whereas EnergyPlus simulated the integrated economizer with a 5-minute timestep. Since the IAQ-Energy Controller economizer mode is limited to times when cooling is required at outdoor temperatures less than 16°C, calculation differences impact relatively few hours annually, as seen in Section 3.3.2.

For all three simulations, the annual energy used for cooling, heating, and the air handler fan was summed from the time series output from EnergyPlus. For the IAQ-Energy Controller, the annual PAC energy was calculated from the air cleaner airflow (ECA_{PAC}) at each time step and the air cleaner efficiency. The air cleaner was assumed to meet the minimum efficiency for EnergyStar, which is 1.4 L/s.W for air cleaners with a ECA of 71 L/s or greater [71].

3.2.6 Indoor $PM_{2.5}$ Model

A box model was constructed to simulate the indoor room $PM_{2.5}$ concentration as a function of time. First, the model was initialized so that the room $PM_{2.5}$ concentration ($PM25_{RM}$) was equal to the outdoor $PM_{2.5}$ concentration ($PM25_{OA}$) at time zero. While this initial condition is an overestimate of the initial room $PM_{2.5}$ concentration, testing the other boundary (initial indoor concentration equal to zero) determined that the two solutions converged within the first day of the simulation, which was an unoccupied school holiday. Therefore, any error associated with the initial condition assumption does not impact the exposure results which were calculated for occupied school days only.

For each subsequent time step (Δt) of 300 s, the change in $PM_{2.5}$ in the room due to sources and sinks was calculated. The only source of $PM_{2.5}$ considered in the model is from outdoor air. When the HVAC system is on, $PM_{2.5}$ in the outdoor air enters the room through the filtered outdoor air intake. During these times, the infiltration through the envelope is assumed to be zero because the room is positively pressurized by the mechanical ventilation system. When the HVAC system is off, pressure across the building envelope is driven by wind and the stack effect. During these times, $PM_{2.5}$ in the outdoor air enters the room through unfiltered infiltration.

During occupied hours when the HVAC system was on ($\dot{V}_{SA}[t] > 0$), the $PM_{2.5}$ concentration from outdoor air ($PM25_{RM\_OA}$) added to the room by the mechanical ventilation system was calculated from Equation 3-7, where V is the room volume and f_{PM25} is filtration efficiency for $PM_{2.5}$, which is the average mass fraction of $PM_{2.5}$ removed from the MERV 13 filter on a single pass of the air stream. ASHRAE Standard 52.2-2017 specifies that MERV 13 filters must have a minimum removal efficiency of 0.50 for particle diameters 0.3 to 1.0 µm and 0.85 for particle diameters 1.0 to 3.0 µm [54]. Studies in Europe and United States estimate that the fraction of $PM_{2.5}$ mass less than 1.0 µm diameter($PM_{1.0}$) ranges from 52 to 84%, with variation attributed to the PM source (which is affected by location and time of year) [72-77]. For this model, we assumed 70% of the outdoor $PM_{2.5}$ mass was $PM_{1.0}$ and the remaining 30% of the mass was $PM_{1.0\text{-}2.5}$. This yielded a weighted average removal efficiency (f_{PM25}) for MERV 13 filtration of 0.61.

$$PM25_{RM\_OA}[t] = (\dot{V}_{OA}[t] \times \Delta t \ \times (PM25_{OA}[t] \times (1 - f_{PM25}) - (1(\ PM25_{RM}[t-1])/V \ \ when\ \dot{V}_{SA}[t] > 0 \qquad \text{Equation 3-7}$$

During unoccupied hours when the ventilation system was off ($\dot{V}_{SA}[t] = 0$), the $PM_{2.5}$ concentration from outdoor air added to the room due to infiltration (λ_{inf} = 0.21 1/hr) was calculated from Equation 3-8, where p_{e_PM25} is the penetration efficiency for $PM_{2.5}$. A review by Diapouli et al. (2013) showed that penetration efficiency for $PM_{2.5}$ ranges from 0.5 to 1.0; a mid-range value of 0.8 was used for this model [78].

$$PM25_{RM\_OA}[t] = \lambda_{inf} \times \Delta t \times (PM25_{OA}[t] \times p_{e\_PM25} - PM25_{RM}[t-1])$$
$$when\ \dot{V}_{SA}[t] = 0 \quad \text{Equation 3-8}$$

Next, the $PM_{2.5}$ concentration removed by recirculated air ($PM25_{RM\_RA}$), the portable air cleaning system ($PM25_{RM\_PAC}$), and deposition ($PM25_{RM\_DEP}$) were calculated from Equation 3-9 to Equation 3-11. ECA_{PAC} is the volumetric flow rate of the PAC and λ_{dep} is the $PM_{2.5}$ loss rate to deposition, which ranges from 0.1 1/h to 0.4 1/h and was taken to be 0.2 1/h [78]. Note that since the PAC is modeled as a HEPA filter, the ECA is assumed to be the same for both $PM_{2.5}$ and infectious aerosol removal.

$$PM25_{RM\_RA}[t] = -(\dot{V}_{SA}[t] - \dot{V}_{OA}[t]) \times \Delta t \times PM25_{RM}[t-1] \times (f_{PM25})/V \quad \text{Equation 3-9}$$

$$PM25_{RM\_PAC}[t] = -ECA_{PAC}[t] \times \Delta t \times PM25_{RM}[t-1]/V \quad \text{Equation 3-10}$$

$$PM25_{RM\_DEP}[t] = -PM25_{RM}[t-1] \times \Delta t \times \lambda_{dep} \quad \text{Equation 3-11}$$

Finally, the $PM_{2.5}$ concentration at each subsequent time step was determined from Equation 3-12:

$$PM25_{RM}[t] = PM25_{RM}[t-1] + PM25_{RM\_OA}[t] + PM25_{RM\_RA}[t] + PM25_{RM\_PAC}[t] + PM25_{RM\_DEP}[t] \quad \text{Equation 3-12}$$

The average annual indoor $PM_{2.5}$ exposure during occupied hours as well as the highest average daily indoor exposure was calculated for each year.

3.2.7 $PM_{2.5}$ mass deposited on the filter

Applying the $PM_{2.5}$ from Section 3.2.6, the $PM_{2.5}$ deposited on the HVAC system filter as a function of time was calculated from Equation 3-13:

$$PM25_{filter}[t] = (PM25_{OA}[t] \times \dot{V}_{OA}[t] + PM25_{RM}[t-1] \times (\dot{V}_{SA}[t] - \dot{V}_{OA}[t])) \times f_{PM25} \times \Delta t \quad \text{Equation 3-13}$$

The total annual $PM_{2.5}$ deposited on the ventilation system filter was calculated for each year. While filter loading will also be impacted by PM_{10}, which is not considered here, the relative comparison of $PM_{2.5}$ loading is useful to understand how changes in ventilation approaches will impact filter lifetime.

3.2.8 Equivalent Clean Airflow Model

A simple model was constructed to calculate the ECA for respiratory aerosol removal as a function of time. The principles of the model are the same as described in Section 3.2.2 which calculated steady-state (as opposed to time-varying) ECA. The ECA at every time step was calculated from Equation 3-14. As a reminder, f_{IA} is the filtration efficiency for infectious aerosol removal and was taken to be 0.77 as described in Section 3.2.2.

$$ECA[t] = \dot{V}_{OA}[t] + \left(\dot{V}_{SA}[t] - \dot{V}_{OA}[t]\right) \times f_{\mathrm{IA}} + ECA_{PAC}[t] \quad \text{Equation 3-14}$$

The annual average ECA during occupied hours was calculated for each year. Additionally, the ECA was converted to an air exchange rate by dividing by the building volume. Recall that ECA considers only exposure to respiratory aerosols and not to pollutants such as $PM_{2.5}$.

3.2.9 Simulation Execution and Data Processing

For the IAQ-Energy Controller, weather and $PM_{2.5}$ data files were processed to determine HVAC mode and to create CO_2 and ventilation rate schedules for EnergyPlus using data analysis software IgorPro v8. A Python script was written to produce each input data file (IDF) that defined each EnergyPlus simulation. This IDF was built from a set of objects that was the same for all simulations and then added customized objects that varied for the ventilation system configuration or for the location, which included envelope properties, cooling and heating capacity, economizer high limit (for economizer with DCV simulations), and CO_2 and ventilation schedules (for the IAQ-Energy Controller). In total, 210 IDFs were constructed, which included 70 weather files (5 years of weather for 14 cities) for each of the three versions of the ventilation system. A Python script then executed all 210 simulations and the timeseries data from each one was output as a CSV file. IgorPro v8 was used to import the data from all 210 simulations and post-process the calculations described in Sections 3.2.5 to 3.2.9.

3.3 Results and Discussion

3.3.1 Example Time Series Data

An example including five consecutive days of data from a simulation is shown to illustrate how the differences in ventilation control impact the indoor temperature, ventilation rate, heating and cooling energy, indoor CO_2 concentration, ECA, indoor $PM_{2.5}$ and $PM_{2.5}$ mass deposited on the HVAC filter (Figure 3-5). A mid-February week from 2022 in Stockton, California was selected for illustration due to a wide range of outdoor temperatures (2 to 24°C) and outdoor $PM_{2.5}$ concentrations (1 to 57 µg/m^3) experienced. As a reminder, As described in section 3.2.2, no portable air cleaner was included in this city for the IAQ-Energy Controller since the HVAC system was large enough to meet the ASHRAE Standard 241 for mitigation of respiratory aerosols in all control modes.

Fixed Rate Ventilation: The results for the fixed ventilation rate system are shown in each plot in Figure 3-5 with the solid blue line. As expected, the ventilation rate was 0.19 m^3/s when the room was occupied during the day (Figure 3-5 A). During occupied hours, the room temperature was maintained between the setpoints of 18.9 and 24.4°C (Figure 3-5 B). When the HVAC system turned off at the end of the day, the temperature of the room increased temporarily due to solar radiation and warm outdoor air temperatures. Minimal heating was used to condition the space first thing in the morning (as the building insulation maintains heat well overnight in the relatively mild central California climate) (Figure

3-5 C). Cooling demand during occupied hours was substantial, even in the winter, to offset the heat gain from the students, lighting and equipment, and solar radiation (Figure 3-5 D). As expected, cooling demand increased with daily peak outdoor air temperature. Indoor CO_2 concentration rose daily when students entered the room (both in the morning and after lunch) and plateaued around 1,100 ppm (Figure 3-5 E). Carbon dioxide concentration dropped quickly when students left for lunch as the constant ventilation rate was set based on the maximum occupancy. The ECA was divided by the room volume to convert the result to equivalent air changes per hour (ACH). Converting the ASHRAE Standard 241 target of 540 L/s yields an equivalent ACH target of 6.0 for the classroom. The equivalent ACH was constant at 6.7 when the ventilation system was running at a fixed rate (Figure 3-5 F). Indoor $PM_{2.5}$ concentration generally tracked the outdoor $PM_{2.5}$ concentration because of the constant ventilation rate (Figure 3-5 G). The indoor to outdoor $PM_{2.5}$ concentration ratio during occupied hours was consistently 0.14 at steady state. For the week shown, the peak indoor concentration during occupied hours was 7.8 $\mu g/m^3$ and the average was 3.4 $\mu g/m^3$. Particle accumulation rate on the filter was proportional to the outdoor $PM_{2.5}$ concentration with a maximum value of 41 mg/hr.

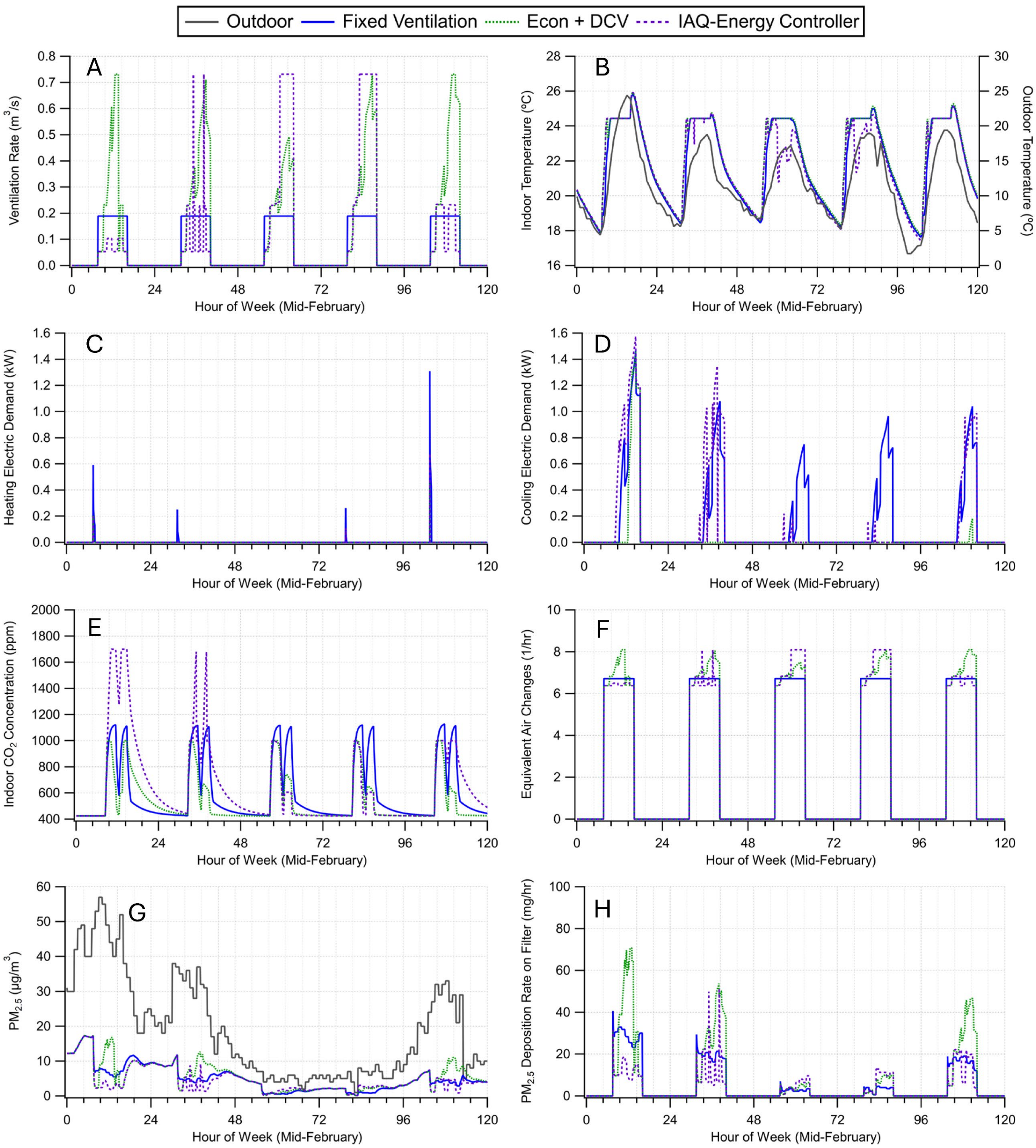

Figure 3-5: Example week of data for Stockton for all three ventilation systems simulated, mid-February 2022. Hour 0 corresponds to midnight.

Economizer + DCV: The results for the Economizer + DCV system are shown in each plot in Figure 3-5 with the dashed green line. When outdoor air temperatures were below the economizer high limit of 22.8°C, the ventilation increased up to the maximum of 0.73 m^3/s to provide cooling (Figure 3-5 A). As expected, when the amount of available economizer cooling available exceeded the cooling demand, the economizer modulated to provide the exact amount of ventilation needed to meet the cooling setpoint. This resulted in an indoor temperature profile that was the same as the fixed ventilation system (Figure 3-5 B). When the economizer was not active, the ventilation rate was reduced to meet the indoor CO_2 setpoint of 1,000 ppm. Although difficult to see in the plot, the heating demand compared to the fixed ventilation scenario was reduced (Figure 3-5 C). This is because the DCV system reduced the ventilation rate in the early morning before the students entered the classroom (since ventilation is required one hour prior to occupancy). Regardless, the magnitude of heating energy was small compared to cooling energy. For the week shown, the heating electricity required for the fixed ventilation system was 0.52 kWh compared to 0.06 kWh for the Economizer + DCV system. Cooling energy was drastically reduced for the Economizer + DCV system (Figure 3-5 D). For the week shown, the cooling electricity required for the fixed ventilation system was 18.2 kwh compared to 4.0 kwh for the Economizer + DCV system. For this system, compressor-based cooling is used only when economizer cooling cannot meet the load alone. Use of compressor-based cooling was delayed on day 1, eliminated on day 2 to 4, and drastically reduced on day 5. The increased ventilation for cooling substantially reduced CO_2 concentration relative to the fixed ventilation system (Figure 3-5 E). For the week shown, the average CO_2 concentration during occupied hours (e.g. excluding lunch and recess) was 859 ppm for the fixed ventilation system and 697 ppm for the Economizer + DCV system. Likewise, the increased ventilation for cooling increased the equivalent ACH (Figure 3-5 F). For the week shown, the average equivalent ACH during occupied hours was 7.1 for the Economizer + DCV system compared to 6.7 for the fixed ventilation system. This highlights the benefits of economizers for both saving energy and reducing the potential for respiratory aerosol transmission.

The major issue with economizers becomes clear when considering the indoor $PM_{2.5}$ concentration results (Figure 3-5 G). Since the economizer increases outdoor air for cooling without consideration of outdoor $PM_{2.5}$ concentration, the indoor $PM_{2.5}$ concentrations peak much higher than the fixed ventilation system. The EPA classification for $PM_{2.5}$ in the outdoor air for the week shown was "unhealthy" for day 1, "unhealthy for sensitive groups" for day 2, "good" for days 3 and 4, and "moderate" for day 5. Indoor $PM_{2.5}$ concentrations for the Economizer + DCV system substantially exceeded the fixed ventilation rate system on days 1, 2, and 5, peaking at 16.7 $\mu g/m^3$ (indoor/outdoor = 0.39), 12.7 $\mu g/m^3$ (indoor/outdoor = 0.35), and 11 $\mu g/m^3$ (indoor/outdoor = 0.38) respectively. Note that these indoor to outdoor ratios are much higher than the 0.14 steady state result for the fixed ventilation system. This model illustrates that, even with MERV 13 filters in place, there is increased $PM_{2.5}$ exposure for students and teachers due to the economizer use. For the week shown, the average $PM_{2.5}$ exposure was 5.3 $\mu g/m^3$ (1.6 times the fixed ventilation system) and the peak $PM_{2.5}$ exposure was 16.7 $\mu g/m^3$ (2.1 times the fixed ventilation system). Additionally, the increased outdoor air during high $PM_{2.5}$ conditions increased filter loading from 0.6 g to 0.9 g during the week shown (Figure 3-5 H).

IAQ-Energy Controller: To aid in interpretation of the results, a plot of the IAQ-Energy Controller mode for each hour of the example week is shown in Figure 3-6 (where the mode numbers correspond to the controller function described in Section 3.2.1). On the first day, the outdoor $PM_{2.5}$ concentration exceeded the high limit for all occupied hours and thus the controller was continuously in Mode 1 (high $PM_{2.5}$), which ran DCV with a 1,700 ppm setpoint to reduce outdoor air. Economizer cooling was not used because of the poor outdoor air quality. On day 2, the outdoor $PM_{2.5}$ concentration crossed between the moderate and high limits several times, resulting in the controller switching between Mode

1 and Mode 2 and DCV with 1,700 and 1,000 ppm setpoints, respectively. Again, the economizer was not used because of the poor outdoor air quality. On days 3 and 4, the outdoor air quality was good. In the morning, there was no cooling demand, and the controller operated in Mode 5, which is DCV with a 1,000 ppm setpoint. Once cooling was required, the controller switched to Mode 4 for economizer cooling. Once the outdoor temperature reached 16°C, the controller switched to Mode 3, with 100% outdoor air for ventilative cooling. On day 5, the $PM_{2.5}$ was above the moderate limit all day, resulting in continuous operation of Mode 2 (DCV with setpoint of 1,000 ppm).

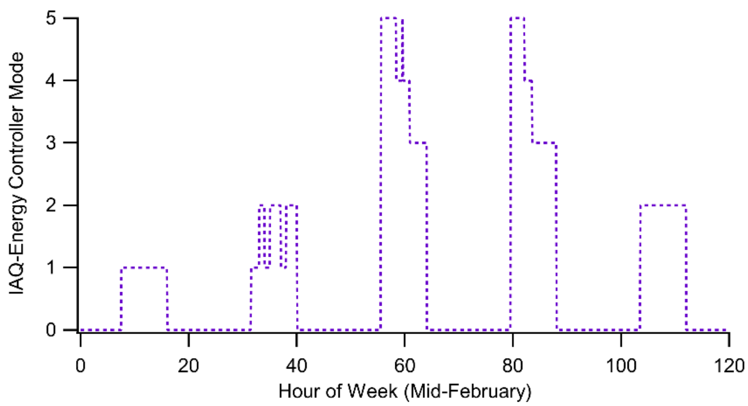

Figure 3-6: Example week of data for Stockton showing the controller mode for each time step, mid-February 2022. Modes correspond to the description in Section 3.2.1

The results for the IAQ-Energy Controller are shown in each plot in Figure 3-5 with the purple dotted line. The ventilation rate varied by day and by mode (Figure 3-5 A). On day 1, continuous use of Mode 1 kept maximum ventilation rates at 0.10 m^3/s, which was about half of the fixed ventilation system. On day 2, switching between Mode 1 and Mode 2 resulted in variations in ventilation rate. Short-term spikes in ventilation rate are attributed to the abrupt lowering of the CO_2 setpoint from 1,700 to 1,000 ppm. On days 3 and 4, the ventilation rate was initially low while the indoor CO_2 concentration was below the 1,000 ppm DCV setpoint. Before the CO_2 concentration reached the setpoint, the economizer activated and increased ventilation to provide cooling. Once the outdoor air temperature exceeded the balance point of 16°C, the ventilation increased to the maximum of 0.73 m^3/s. On day 5, the controller was continuously in Mode 2 due to moderate $PM_{2.5}$ and controlled the ventilation rate to meet the 1,000 ppm setpoint. The indoor temperature with the IAQ-Energy Controller was the same as the fixed rate ventilation system, except when ventilative cooling (Mode 3) was in use (Figure 3-5 B). When ventilative cooling was active, the delivery of 100% outdoor air decreased the indoor temperature below the cooling setpoint (yet it remained above the heating setpoint as designed).

Although difficult to see in the plot, the heating demand for the IAQ-Energy Controller was reduced compared to the fixed ventilation scenario (although the difference was small). Heating demand for the IAQ-Energy Controller and the DCV + Economizer were approximately equal, which is expected since both controllers use DCV when the heating mode is active (Figure 3-5 C). The cooling demand for the IAQ-Energy Controller was similar to the fixed ventilation system when $PM_{2.5}$ was above the moderate limit (Modes 1 and 2, which occurred on days 1, 2, and 5) and similar to the Economizer + DCV system during other times (days 3 and 4) (Figure 3-5 D). During this example week, both the Economizer + DCV system and the IAQ-Energy Controller effectively eliminated the cooling load on days 3 and 4 when air quality was good. The cooling energy use was higher for the IAQ-Energy Controller than for the Economizer + DCV system on days 1, 2, and 5 because the outdoor air $PM_{2.5}$ concentration was too high to use outdoor air for cooling. Over this week, cooling energy use was 16.4 kWh for the IAQ-Energy controller compared to 18.3 kwh for the fixed ventilation system and 4.0 kWh for the Economizer + DCV system. This model illustrates that, in locations where outdoor air is favorable for cooling and $PM_{2.5}$ is elevated outdoors, there is a potential tradeoff to be made between using an economizer to save energy for cooling and increased indoor $PM_{2.5}$ exposure.

As expected, the CO_2 concentration was elevated to 1700 ppm for the IAQ-Energy Controller on days 1 and 2 as it limited ventilation to reduce $PM_{2.5}$ introduced indoors (Figure 3-5 E). When the ventilative cooling function was in use on days 3 and 4, the occupied CO_2 concentration was the lowest of the three systems at around 600 ppm. For equivalent ACH, the IAQ-Controller was always greater than 6 and increased to 8 when ventilative cooling was in use on days 3 and 4 (Figure 3-5 F). Over the course of week shown here, the average equivalent ACH during occupied hours was 6.9 1/hr (compared to 6.7 1/hr for the fixed ventilation and 7.1 1/hr for the Economizer + DCV system).

The benefit of the IAQ-Energy Controller in balancing energy and occupant health is clearly seen in the indoor $PM_{2.5}$ exposure results. For the example week shown, the average occupied indoor $PM_{2.5}$ exposure was 2.7 μg/m^3, which was below the fixed ventilation system result of 3.4 μg/m^3 and about half of the Economizer + DCV system result of 5.3 μg/m^3 (Figure 3-5 G). Additionally, peak indoor $PM_{2.5}$ exposure of 9.2 μg/m^3 was 55% of the 16.7 μg/m^3 observed with the Economizer + DCV system. However, the peak $PM_{2.5}$ exposure of 9.2 μg/m^3 was above the fixed ventilation result of 7.8 μg/m^3, which was attributed to when the controller switched from Mode 1 to Mode 2 during moderate $PM_{2.5}$ conditions. The mode switch reduced the CO_2 setpoint from 1,700 to 1,000, which resulted in a short spike in ventilation rate to reduce the CO_2 quickly and a temporary increase in $PM_{2.5}$ exposure. This could be mitigated by reducing the CO_2 setpoint over several timesteps (e.g. 15-minutes) to avoid ventilation rate spikes. The limitation of ventilation during high $PM_{2.5}$ conditions also reduced the $PM_{2.5}$ deposition rate onto the filter for a total of 0.4 g over the week shown (Figure 3-5 H).

3.3.2 Frequency of Controller Mode

In the previous section we showed results for a five-day period for one city to illustrate how the choice of ventilation controls influenced the room conditions. Here, and in the sections that follow, we consider average results over a five-year period for each city, assuming operation only during the school year (excluding summers). The frequency of each mode used over five years for the simulated Economizer + DCV system is shown in Figure 3-7. As expected, the mild coastal climates of Los Angeles and San Francisco had the greatest economizer use, followed by the dry western climates of Phoenix, Las Vegas, Stockton, and Albuquerque. Dry climates generally have more potential for economizer cooling because of the high cooling loads and the large diurnal temperature swings that result in cool mornings [6]. Additionally, the outdoor air temperatures at which the economizer can be used are higher due to lower humidity levels in the air in dry climates.

The frequency of each mode used over five years for the simulated IAQ-Energy Controller is shown in Figure 3-8. Mode 1 ($PM_{2.5}$ above 35 μg/m^3) was used infrequently, with the most prevalent use in Stockton, California during 7% of the occupied hours. Most of the cities in which Mode 1 operation occurred were impacted by wildfire smoke at various points during the five year period. Mode 2 ($PM_{2.5}$ above 12 μg/m^3) was used between 6 to 32% of the time depending on location. Cities where Mode 1 or Mode 2 was used more than 25% of the time included Houston, Phoenix, Stockton, Atlanta, Albuquerque, and Denver. It is notable that these modes disable ventilative cooling and economizer use a substantial portion of the time (although not all this time was within the temperature range for economizing). Modes 3 and 4, ventilative and economizer cooling, were used between 4 to 49% of the time. For these modes, the main difference between the IAQ-Energy Controller and the Economizer + DCV Controller is that the former increases outdoor air to 100% of the supply air rate in ventilative cooling mode while the latter provides just enough outdoor air to meet the cooling load in economizer mode. The additional outdoor air in ventilative cooling mode provides additional cooling and increases equivalent air exchanges. Because the IAQ-Energy Controller often uses ventilative cooling mode, the economizer mode (Mode 4, less than 100% outdoor air for cooling) is reduced to 1 to 6% of time.

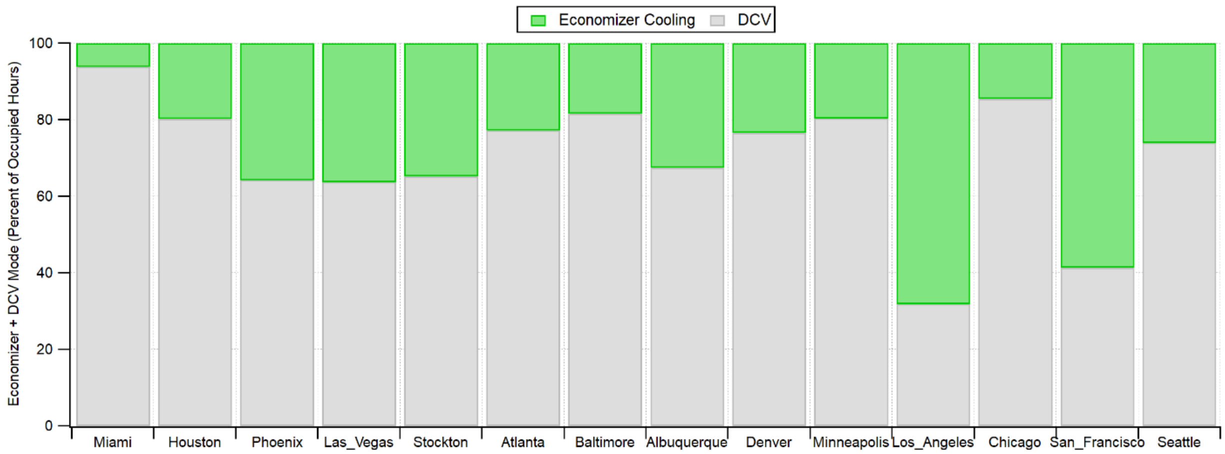

Figure 3-7: Economizer + DCV Controller mode distribution for ventilation system operating hours (2018-2022).

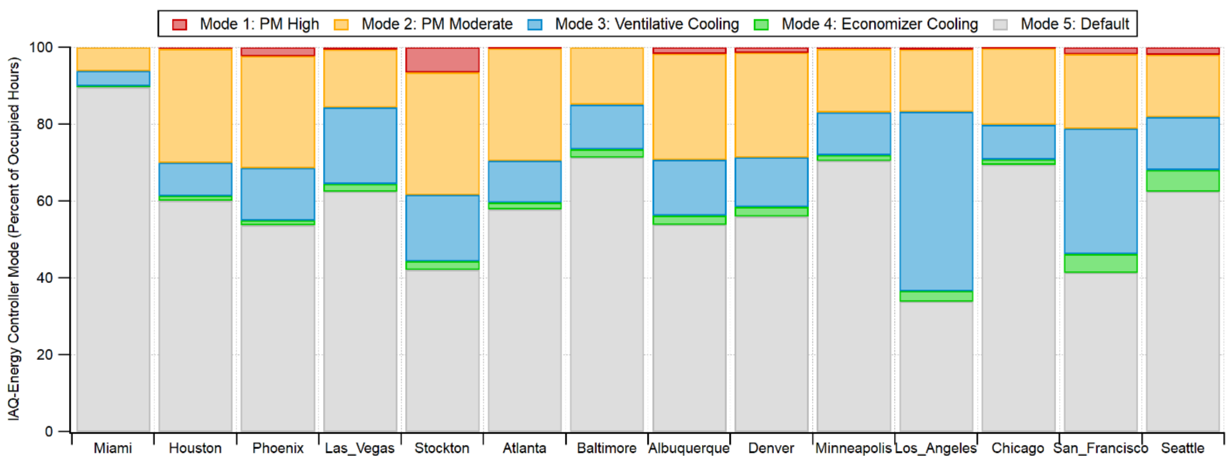

Figure 3-8: IAQ-Energy Controller mode distribution for ventilation system operating hours (2018-2022).

3.3.3 Annual Average Results for all Cities

The simulation output metrics were evaluated on an annual (school year) basis for five years in each city. The results are presented as an average and standard deviation for five years of results (i.e. *n*=5). Annual average outdoor $PM_{2.5}$ concentration is compared to average annual indoor $PM_{2.5}$ concentration (during occupied hours only) for each ventilation system for the five years simulated in Figure 3-9. The same results are presented as average indoor to outdoor $PM_{2.5}$ ratio in Figure 3-10 (note that times when the outdoor $PM_{2.5}$ is zero were excluded from the average ratio calculation). Compared to the fixed rate ventilation system, the Economizer + DCV Controller increased average indoor $PM_{2.5}$ exposure in all cities by 0.1 to 0.9 µg/m^3. For the IAQ-Energy Controller, half the cities had an increase up to 0.4 µg/m^3, while the remainder had no change or a reduction in exposure. In general, cities with PACs had reduced exposure, except for Los Angeles which had the greatest use of the economizer and ventilative cooling.

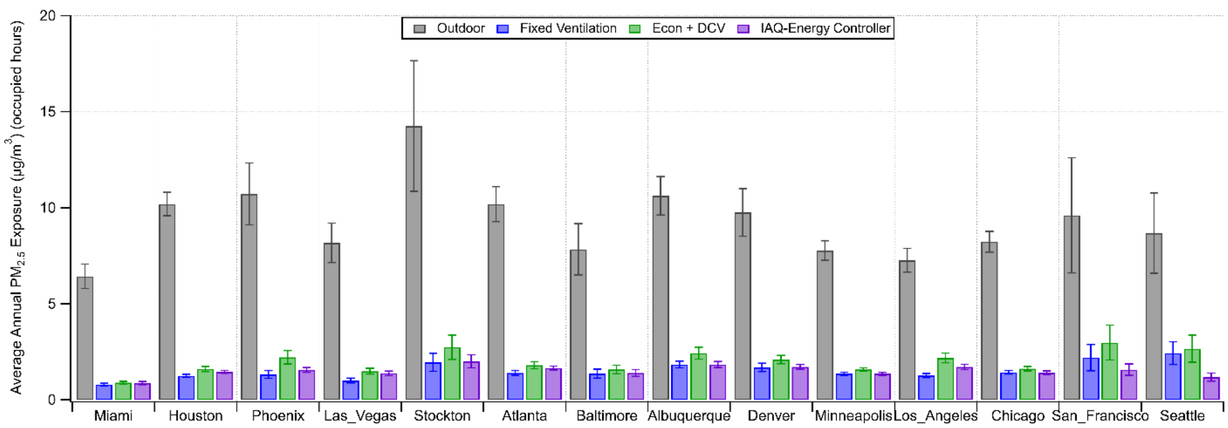

Figure 3-9: Average indoor $PM_{2.5}$ exposure for each city for each ventilation system design. Each bar represents the average annual result for five years of simulation data. Error bars represent the standard deviation for five years of simulation data.

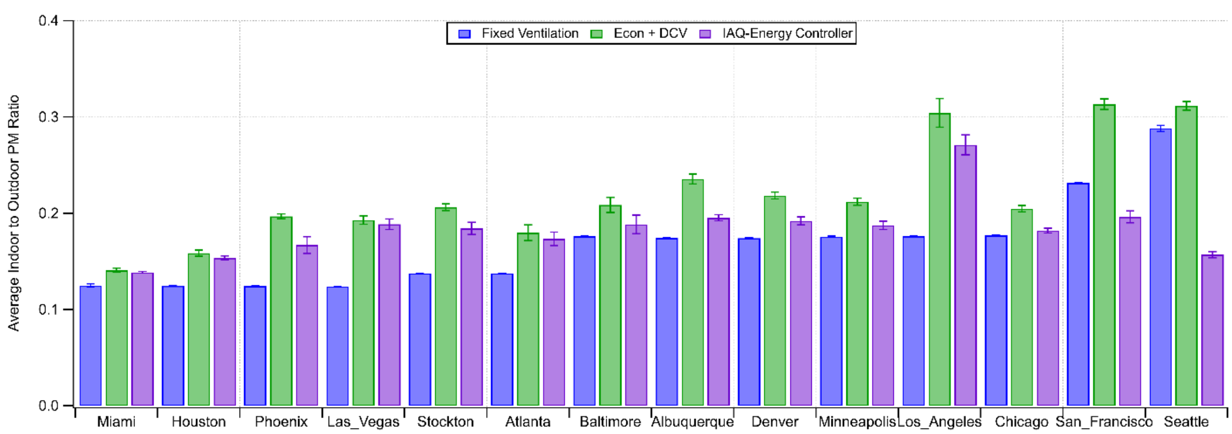

Figure 3-10: Average daily occupied indoor to outdoor $PM_{2.5}$ ratio for each city for each ventilation system design. Each bar represents the average annual result for five years of simulation data. Error bars represent the standard deviation for five years of simulation data.

The reduced $PM_{2.5}$ exposure for the IAQ-Energy Controller compared to the Economizer + DCV Controller is more apparent when considering the maximum average daily exposure for $PM_{2.5}$ (i.e. the average daily exposure on the highest $PM_{2.5}$ day of the year) (Figure 3-11). From 2018 to 2022, Stockton, San Francisco, and Seattle had at least one day with outdoor $PM_{2.5}$ concentration that was in EPA's unhealthy category. Over the five years simulated, the day with the highest outdoor $PM_{2.5}$ concentration during school hours averaged 99, 84, and 94 $\mu g/m^3$ in Stockton, San Francisco, and Seattle respectively. These very high $PM_{2.5}$ days are likely attributed to transient wildfire smoke events. Relative to the fixed ventilation system, the Economizer + DCV Controller increased the highest indoor $PM_{2.5}$ exposure in all cities by 0.4 to 6.4 $\mu g/m^3$. In contrast, the IAQ-Energy Controller decreased the highest indoor $PM_{2.5}$ exposure relative to the fixed ventilation system by 0.3 to 19.9 $\mu g/m^3$. Relative to the Economizer + DCV Controller, the IAQ-Energy Controller reduced average indoor exposure on the worst day of the year in Stockton, San Francisco, and Seattle by 10.8, 19.0, and 24.3 $\mu g/m^3$, respectively. A review by Zhang et al. (2023) summarized acute changes in children's lung function (with asthmatic children more affected) with a 1-day lag to acute exposure to ambient $PM_{2.5}$ increases of 10 $\mu g/m^3$ and greater [79], indicating that the magnitude of reduced indoor $PM_{2.5}$ exposure offered by the IAQ-Energy Controller may protect students from asthma exacerbation. Furthermore, a study by Zhang et al. (2018) demonstrated that the three-day moving average of outdoor $PM_{2.5}$ was associated with increased school absence with an odds ratio of 1.37 (95% CI: 1.07–1.74) per 10 $\mu g/m^3$ in schoolchildren in China [80]. While epidemiology studies generally assess outcomes using outdoor $PM_{2.5}$ as the independent variable, it is reasonable to expect that measures to reduce indoor $PM_{2.5}$ concentration will positively impact students, especially when students are kept indoors during extreme $PM_{2.5}$ events. Anecdotally, facility managers report that they attempt to limit outdoor air intake during wildfire events, but this often involves manual overrides of control systems (which sometimes requires accessing individual systems across rooftops). The systems must then be restored to normal operation when the threat has passed, which may be a low priority. A major benefit of the IAQ-Energy Controller is that the response to poor air quality days is automated and requires no decision making or manual intervention.

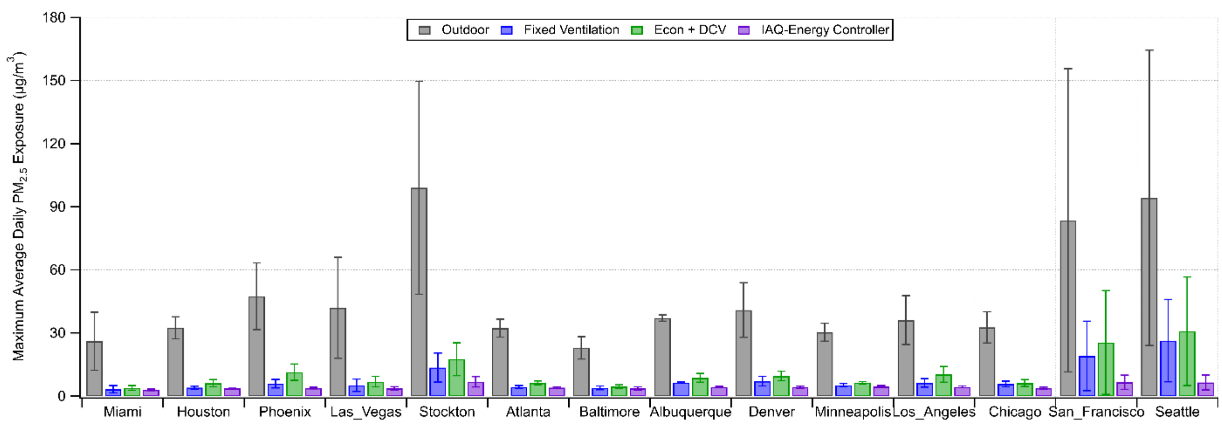

Figure 3-11: Maximum average daily occupied indoor $PM_{2.5}$ exposure for each city for each ventilation system design. Each bar represents the average annual result for five years of simulation data. Error bars represent the standard deviation for five years of simulation data.

The IAQ-Energy Controller also reduced the $PM_{2.5}$ collected on the HVAC system filter over the course of the year (Figure 3-12). Since this metric does not include particles greater than 2.5 µm diameter, and because different MERV 13 filters have different final loading capacities, it is difficult to translate this result to differences in filter lifetime. The Economizer + DCV Controller increased filter loading by more than 15% relative to the fixed ventilation system in five cities: Phoenix (+44%), Las Vegas (+26%), Stockton (+21%), Los Angeles (+61%) and San Francisco (+27%). For comparison, in these cities, the IAQ-Energy Controller generally decreased filter loading relative to the fixed ventilation system, with decreases in Phoenix (-4%), Stockton (-14%), and San Francisco (-8%). In Las Vegas and Los Angeles, the increase was 17% and 27%, respectively, for IAQ-Energy Controller operation, which was an improvement compared to the Economizer + DCV Controller. While the difference in filter accumulation was modest, this difference may yield a meaningful benefit for facility managers that struggle with labor and materials costs to change filters on the scheduled required for best HVAC performance. Note that cities of Baltimore through Seattle on the right side of the chart included a PAC that also requires filter maintenance, although the estimated $PM_{2.5}$ accumulated on the PAC filters was small (≤ 0.5 g) in all cities except San Francisco and Seattle, where it was approximately 1.5 g.

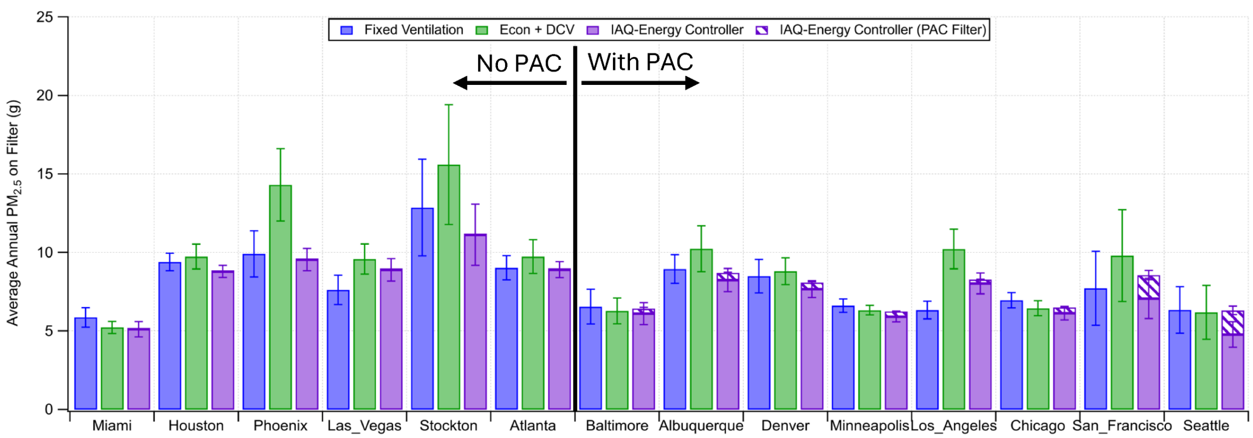

Figure 3-12: Average annual $PM_{2.5}$ collection on filter for each city for each ventilation system design. Each bar represents the average annual result for five years of simulation data. Error bars represent the standard deviation for five years of simulation data.

As expected, the equivalent ACH for classrooms with the fixed ventilation system was dependent on the size of the HVAC system, which impacted recirculation air filtration rates (Figure 3-13). In Figure 3-13, the cities are arranged from largest to smallest HVAC system from left to right. For the Economizer + DCV Controller, cities with the greatest economizer mode frequency (Figure 3-7) had the largest increases in equivalent ACH. By design, the IAQ-Energy Controller had a minimum equivalent ACH of around 6 to comply with ASHRAE Standard 241. This was done by adding PAC capacity to all cities with smaller HVAC systems (supply air rate of 543 L/s or less), which included Baltimore to Seattle on the right side of the plot. For Baltimore through Chicago, the PAC contributed an equivalent ACH of 0.4 to 0.7 1/hr, which was a small fraction of the total. For San Francisco and Seattle, the PAC contributed an equivalent ACH of 2.0 and 2.9 1/hr, which was a larger fraction of the total. Therefore, for cities with the smaller HVAC systems, the improvement in equivalent ACH is mainly attributed to addition of the PAC. The benefit of integration of the PAC with the ventilation control offered by the IAQ-Energy Controller is that it automatically modulates the air cleaner to operate at the lowest speed needed to meet ASHRAE Standard 241 (based on the ventilation system mode). This automated operation minimizes added noise in the classroom, energy use, and filter maintenance. In cities with lager HVAC systems, the equivalent ACH exceeded 6 1/hr for all ventilation system types, and differences among the controllers in each city were 0.1 to 0.4 1/hr. The ACH increase predicted for the ventilation control component of the IAQ-Energy Controller was small due to the high filtration efficiency (77%) modeled for respiratory aerosol removal from recirculated air.

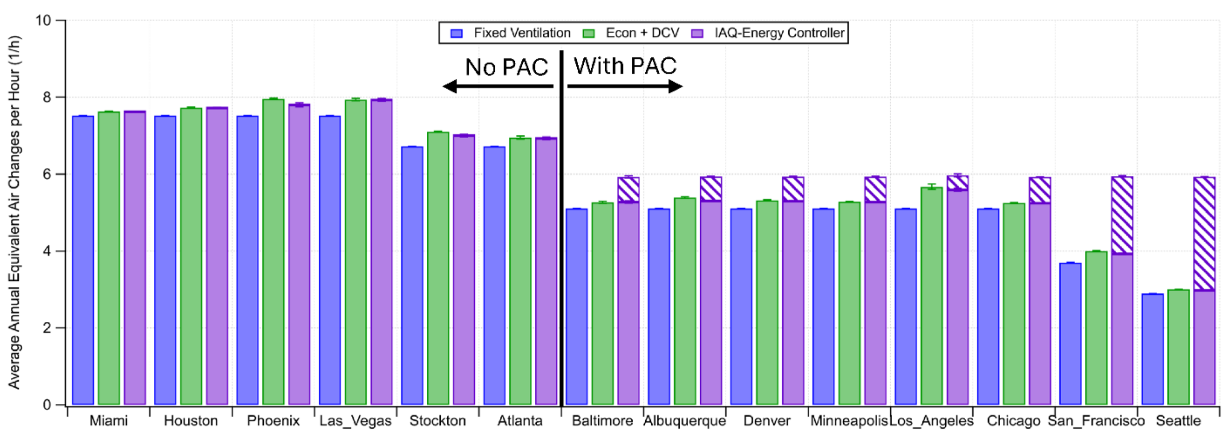

Figure 3-13: Average annual equivalent ACH for each city for each ventilation system design. Each bar represents the average annual result for five years of simulation data. Error bars represent the standard deviation for five years of simulation data.

The Economizer + DCV Controller had the lowest energy use in all cities among the three ventilation system types. Compared to the fixed ventilation system, the Economizer + DCV Controller saved between 235 to 683 kWh per year, with the greatest savings in Minneapolis due to the reduction in heating energy from the DCV control. Excluding San Francisco and Seattle, the IAQ Energy Controller also saved energy relative to the fixed ventilation system. The savings were slightly less than the Economizer + DCV Controller (due to the limitation of not using economizer cooling when outdoor $PM_{2.5}$ was high) and ranged from 154 to 596 kWh per year. This shows the energy tradeoff (~100 kWh) necessary to realize the health benefits from reduced indoor $PM_{2.5}$ exposure offered by the IAQ-Energy Controller. In San Francisco and Seattle, the IAQ-Energy Controller used about 300 kWh more than the Economizer + DCV Controller. This was primarily due to the addition of the PAC needed to achieve ASHRAE 241 compliance. The PAC consumed 204 kWh annually in San Francisco and 298 kWh annually in Seattle.

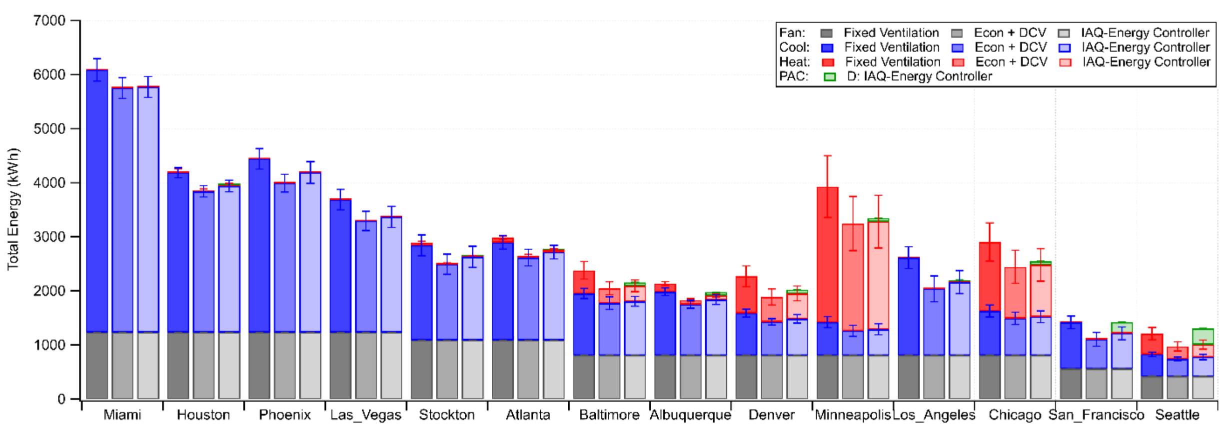

Figure 3-14: Average annual energy use for air handler fan, cooling, heating, and portable air cleaner for each city for each ventilation system design. Each bar represents the average annual result for five years of simulation data. Error bars represent the standard deviation for five years of simulation data.

3.3.4 Impact of Filtration Efficiency on Results

Filters with MERV 13 rating were the modeling focus in this study as they were demonstrated in previous work to be an extremely effective way to reduce both indoor $PM_{2.5}$ and respiratory aerosol exposure with minimal impacts to HVAC energy use [6]. Despite the benefits of MERV 13 filters, MERV 8 filters are still quite common. The simulations were updated to model MERV 8 filters and are briefly discussed to understand how the results change with a reduction in filtration efficiency.

To achieve the average 77% infectious aerosol removal efficiency estimate for MERV 13 filters, we back-calculate that ASHRAE Standard 241 is weighting respiratory aerosols as 77% 1.0 to 3.0 µm diameter particles (85% removal efficiency per Standard 52.2) and 23% 0.3 to 1.0 diameter particles (50% removal efficiency per Standard 52.2) [54, 61]. Applying the same formula to MERV 8 performance yields a respiratory aerosol removal efficiency of 17% (as opposed to the zero credited by Standard 241). Applying the logic in Section 3.2.6 to calculate the $PM_{2.5}$ removal efficiency for MERV 8 filters yields 6%. The final difference between MERV 8 and MERV 13 filters is a reduction in fan power, which was estimated in our previous work as 6% [6]. The methodology was re-run with changes to these variables ($f_{PM25} = 0.17$, $f_{PM25} = 0.06$, and fan power reduced by 6%).

The substantial reduction in central HVAC system filtration efficiency for infectious aerosols increased the PAC sizing required to meet ASHRAE Standard 241 in every city (Table 3-5). Cities that previously had no need for PAC due to larger air handlers (climate zones 1 to 3) would require two consumer grade PAC to meet ASHRAE Standard 241 with the IAQ-Energy Controller.

Table 3-5: HVAC system and PAC sizing with MERV 8 Filters.

IECC Climate Zone	City	Heat Pump Capacity (Cool/Heat) (kW)	Heat Strips (kW)	ECA Target (L/s)	$\dot{V}_{SA}$ (L/s)	Mode 1			Mode 2 and 5			Mode 3 and 4		
						$\dot{V}_{OA,SS}$ (L/s)	ECA_{RA} (L/s)	ECA_{PAC} (L/s)	$\dot{V}_{OA,SS}$ (L/s)	ECA_{RA} (L/s)	ECA_{PAC} (L/s)	$\dot{V}_{OA,SS}$ (L/s)	ECA_{RA} (L/s)	ECA_{PAC} (L/s)
1A	Miami	16.0/15.0	0	540	826	106	122	312	235	100	205	826	0	0
2A	Houston	16.0/15.0	0	540	826	106	122	312	235	100	205	826	0	0
2B	Phoenix	16.0/15.0	0	540	826	106	122	312	235	100	205	826	0	0
3B	Las Vegas	16.0/15.0	0	540	826	106	122	312	235	100	205	826	0	0
3B	Stockton	13.9/12.1	0	540	732	106	106	328	235	84	221	732	0	0
3A	Atlanta	13.9/12.1	0	540	732	106	106	328	235	84	221	732	0	0
4A	Baltimore	10.6/9.3	4	540	543	106	74	360	235	52	253	543	0	0
4B	Albuquerque	10.6/9.3	0	540	543	106	74	360	235	52	253	543	0	0
5B	Denver	10.6/9.3	4	540	543	106	74	360	235	52	253	543	0	0
6A	Minneapolis	10.6/9.3	10	540	543	106	74	360	235	52	253	543	0	0
3B-AC	Los Angeles	10.6/9.4	0	540	543	106	74	360	235	52	253	543	0	0
5A	Chicago	10.6/9.5	8	540	543	106	74	360	235	52	253	543	0	0
3C	San Francisco	6.9/6.6	0	540	378	106	46	388	235	24	281	378	0	162
4C	Seattle	5.1/4.9	4	540	283	106	30	404	235	8	297	283	0	257

With MERV 8 filtration, average indoor $PM_{2.5}$ exposure increased to 4.5 to 10.9 µg/m^3 for fixed rate ventilation and Economizer + DCV systems (Figure 3-15). Average indoor $PM_{2.5}$ exposure was lower for the IAQ-Energy Controller (2.6 to 5.3 µg/m^3) due to the outdoor air controls and PAC use in every city. The impact was also evident in the indoor to outdoor $PM_{2.5}$ ratio results (Figure 3-16).

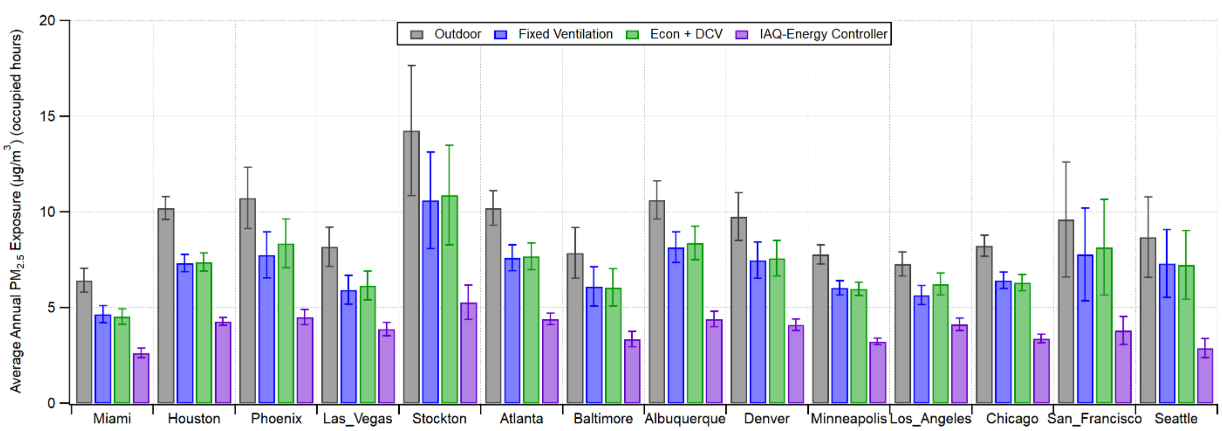

Figure 3-15: Average indoor $PM_{2.5}$ exposure for each city for each ventilation system design with MERV 8 filter.

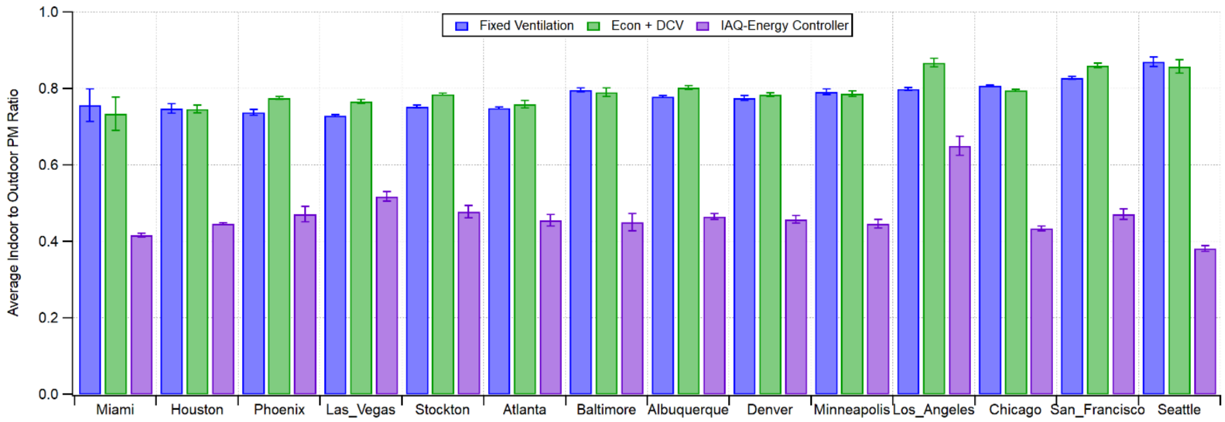

Figure 3-16: Average daily occupied indoor to outdoor $PM_{2.5}$ ratio for each city for each ventilation system design with MERV 8 filter.

With MERV 8 filtration, the maximum average daily indoor $PM_{2.5}$ exposure was very high and exceeded 60 µg/m^3 in Stockton, San Francisco, and Seattle for both fixed ventilation and Economizer + DCV systems (Figure 3-17). In these cities, the IAQ-Energy controller limited the maximum average daily indoor $PM_{2.5}$ exposure to less than 18 µg/m^3. This illustrates that the ventilation rate control and the PAC are more impactful when the central HVAC system has lower filtration efficiency.

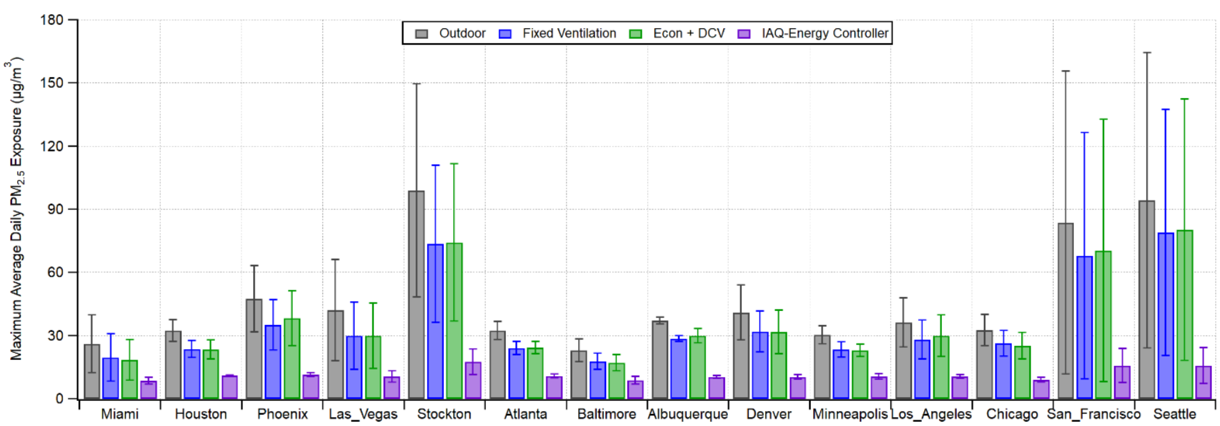

Figure 3-17: Maximum average daily occupied indoor $PM_{2.5}$ exposure for each city for each ventilation system design with MERV 8 filter.

The PAC filters accumulated substantially more $PM_{2.5}$ mass (2.1 to 4.8 g) for the MERV 8 filter simulation because they were the primary sink for outdoor $PM_{2.5}$ (Figure 3-18). Therefore, PACs will require more frequent filter replacements when MERV 8 filters are used.

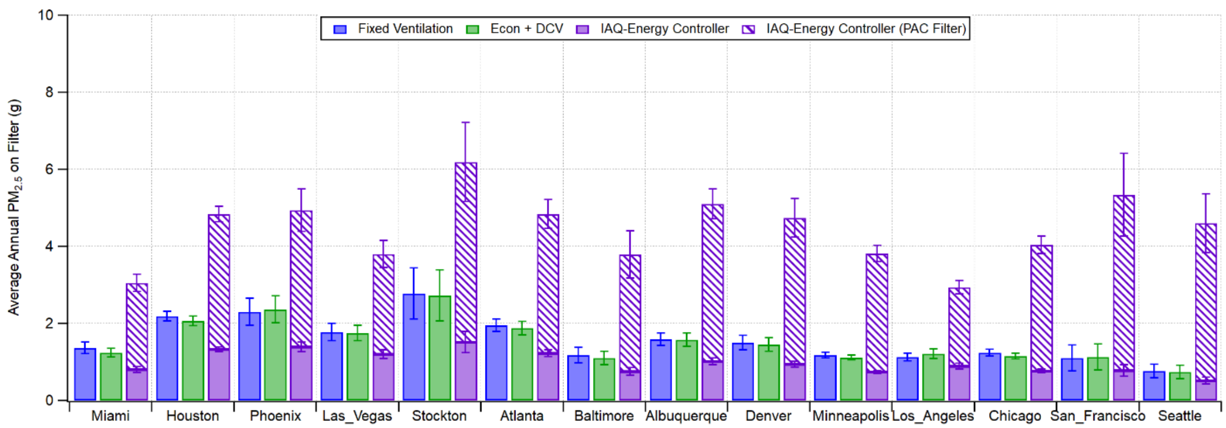

Figure 3-18: Average annual $PM_{2.5}$ collection on filter for each city for each ventilation system design with MERV 8 filter.

The differences in annual average equivalent ACH were larger when MERV 8 filtration was used (Figure 3-19). This is because of the large difference between the 17% infectious aerosol removal efficiency for recirculated air versus 100% for outdoor air. Compared to fixed rate ventilation, the ventilation component of the IAQ-Energy controller increased ACH by 0.4 to 2.0 1/hr, with the largest gains in hot-dry climates. The PAC added an equivalent ACH of 1.3 to 3.2 1/hr so that the target of 6 1/hr was met. In some hot-dry climates with larger air handlers (Phoenix, Las Vegas, and Stockton) the average exceeded 6 1/hr because the ventilative cooling and economizer modes with 100% outside air were frequently used and had an ACH greater than 6 1/hr.

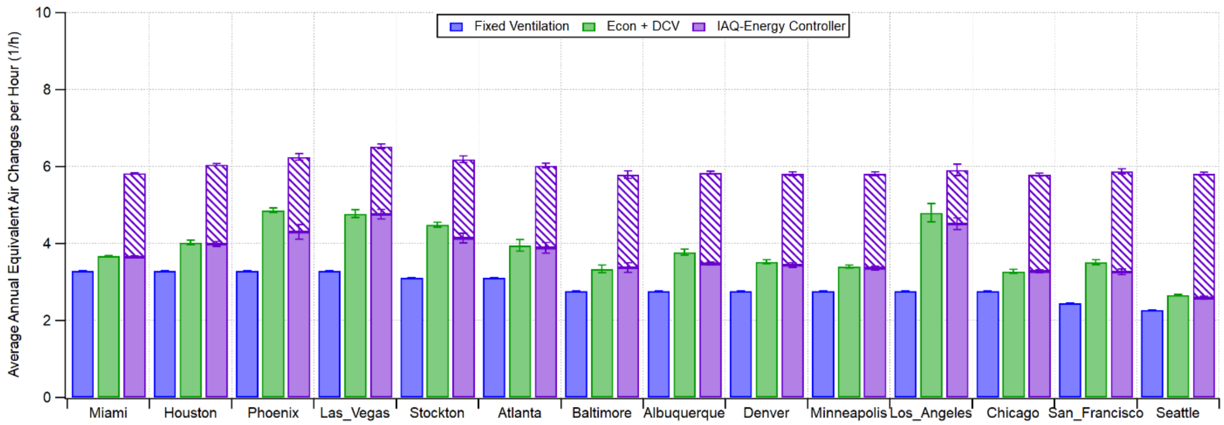

Figure 3-19: Average annual equivalent ACH for each city for each ventilation system design with MERV 8 filter.

Compared to MERV 13 filters, MERV 8 filters reduced HVAC energy use for fixed rate ventilation and the Economizer + DCV system by 1 to 3% (Figure 3-20). For the IAQ-Energy Controller, the HVAC energy use increased by 1 to 7 % for MERV 8 filtration compared to MERV 13. This is because of the increased PAC capacity and use needed to meet ASHRAE Standard 241 requirements. Consistent with our previous study [6], the MERV 13 filter removed infectious aerosols and $PM_{2.5}$ more efficiently than the PAC since the HVAC fan is running continuously during occupied hours and the increased fan power of 6% is small compared to the substantial increase in filtration efficiency.

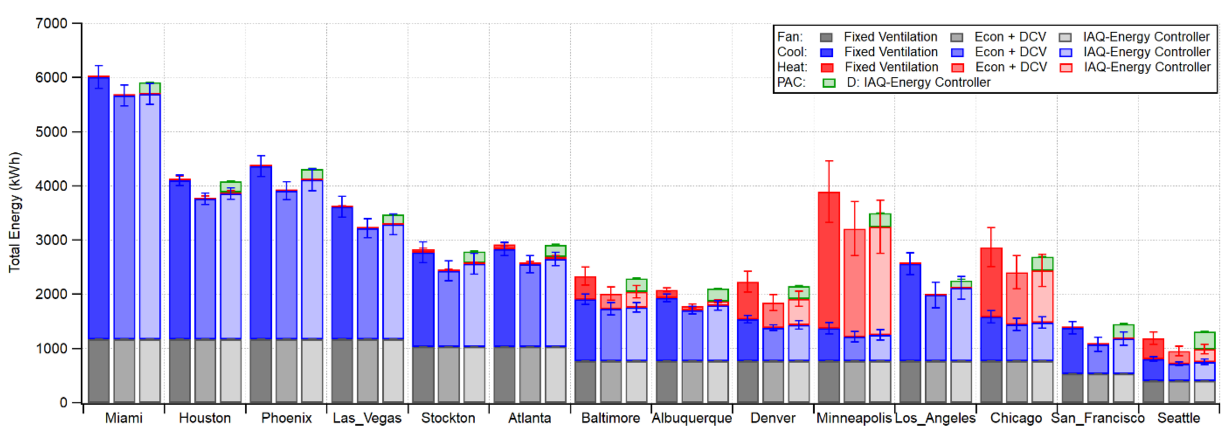

Figure 3-20: Average annual energy use for air handler fan, cooling, heating, and portable air cleaner for each city for each ventilation system design with MERV 8 filter.

3.3.5 Limitations

There are several limitations to this work and a few important ones are discussed here. First, the $PM_{2.5}$ model assumed no generation source inside the building. This is a reasonable simplification for standard classrooms but may be a poor assumption in other building types that have substantial sources of indoor PM2.5 generation (e.g. cooking, smoking, or wood-burning fireplaces). For spaces with no indoor PM2.5 generation, the results from this model are expected to be generalizable to spaces that have a similar occupancy density (e.g. classrooms, conference rooms, or shared office spaces). Because the only source of $PM_{2.5}$ is from outdoors, the controller was designed to use simple open-loop $PM_{2.5}$ sensing to determine the ventilation setting and limit indoor $PM_{2.5}$ exposure. For buildings with substantial indoor $PM_{2.5}$ sources, indoor $PM_{2.5}$ concentration would need to be measured and considered in the controller logic.

Results for the IAQ-Energy Controller were presented only for specific setpoints: $PM_{2.5}$ moderate limit of 12 $\mu g/m^3$, $PM_{2.5}$ high limit of 35 $\mu g/m^3$, and indoor CO_2 setpoints of 1,000 (for Mode 2 and 5) and 1,700 ppm (for Mode 1). These setpoints can be adjusted depending on the desired goals of the implementor. Lowering $PM_{2.5}$ limits will further protect against $PM_{2.5}$ exposure but will increase HVAC energy use and will potentially lower equivalent ACH (in the cases without supplementary PAC). Lowering CO_2 setpoints will increase $PM_{2.5}$ exposure, increase energy use, and increase equivalent ACH. The tradeoff between indoor $PM_{2.5}$ exposure, respiratory aerosols, and energy use is an unavoidable conflict that must be balanced; the limits proposed here are a reasonable solution that offer an improvement over fixed rate ventilation in almost all cases for all assessed metrics.

An important limitation of this work is that the model is not validated by experimental data. The basic components of the simulation (EnergyPlus and mass balance box modeling) have been extensively validated and used in prior work. However, implementation of these tools is prone to user error.

Extensive review and validation of the time series data (as described in Section 3.3.1) was conducted to detect and correct implementation errors in terms of the logic involved. Regardless, laboratory and field testing of the IAQ-Energy Controller are needed to assess the practicality of real-world implementation and to validate the simulation findings. This work is currently underway in two classrooms near Stockton, California and will be discussed in future work.

3.4 Conclusions

Economizers are widely recognized as an important technology that saves cooling energy while maintaining thermal comfort. Building energy efficiency standards often require that HVAC systems be outfitted with economizers. ASHRAE Standard 90.1-2022 [21], which serves as the basis for building energy efficiency standards in many US States, requires economizers in HVAC systems with a cooling capacity of 9.7 kW or greater (except in climate zones 1A, 1B). The lack of consideration for outdoor air quality in current economizer logic is a major shortcoming that is exposing occupants, including schoolchildren, to unnecessarily high levels of $PM_{2.5}$, even when MERV 13 filters are in place. Although the concern is relevant across the United States, this analysis identified cities of Stockton, San Francisco, and Seattle, followed by Los Angeles, Denver, Albuquerque and Phoenix (of the cities simulated) as locations with the highest acute exposure to $PM_{2.5}$ because of outdoor air introduced indoors through ventilations systems (both fixed rate ventilation and economizers). This likely reflects the impact of wildfire smoke on these areas, which can lead to long periods of high concentrations of $PM_{2.5}$, as well as local pollution issues.

Notably, economizers are already equipped with a controllable outdoor air damper and at least a simple controller. Beyond this existing equipment, the IAQ-Energy Controller requires access to outdoor air quality data, an indoor CO_2 sensor that can provide feedback to the DCV algorithm, and control hardware and software that can run the simple rule-based algorithm. Implementation of the IAQ-Energy

Controller is straightforward for HVAC systems with existing economizers already connected to an existing building management system (BMS). The control logic is provided here (Table 3-2) so that it can be easily implemented in any BMS system.

For locations near an existing EPA air quality monitoring station, the hourly outdoor air $PM_{2.5}$ data can be sourced over the internet through EPA's AirNow program, which has an existing easy to use application programming interface (API). Alternatively, a low-cost $PM_{2.5}$ sensor that uses light-scatting technology (e.g. Plantower PMS5003 or Sensirion SPS30) can provide a room, building, or site-level estimate of $PM_{2.5}$ concentration [81]. The benefit of the EPA monitoring station is having validated $PM_{2.5}$ measurements with ongoing service, quality control, and calibration. The benefit of a low-cost sensor located at the building location is that it will represent the air quality at the exact location and report more frequently than once per hour. The decision on what data source to use for $PM_{2.5}$ monitoring will likely come down to how far away the closest EPA station is. Even when a station is nearby, an application could leverage both options by using a low-cost sensor at the building level that is continuously "calibrated" against the EPA reference. It's important to recognize that the rule-based IAQ-Energy controller is built to switch modes when $PM_{2.5}$ concentration reaches specified thresholds (e.g. 12 and 35 $\mu g/m^3$). Therefore, any inaccuracies in the $PM_{2.5}$ measurement will only be relevant when the concentration is near these thresholds. Implementation of a $PM_{2.5}$ sensing strategy, and any calibration adjustments, should aim to increase accuracy near these concentration thresholds.

Chapter 4 Longevity of size-dependent particle removal performance of do-it-yourself box fan air filters

4.1 Introduction

Filtration of indoor air with portable air filters reduces particle concentrations indoors, which is expected to have health benefits for building occupants [10]. Most portable air cleaners that are applied in intervention studies use high efficiency particulate air (HEPA) filters that remove 99.97% of the most penetrating particles from the airstream [11]. Low-cost do-it-yourself portable air cleaners can be built from a box fan and standard filters used in heating, ventilation, and air conditioning (HVAC) systems, which are rated based on their minimum efficiency reporting value (MERV). When MERV-rated filters are arranged in a box configuration, termed a Corsi-Rosenthal box (CR box), the airflow resistance is low, the airflow rates are high, and the particle removal rates exceed most commercially available portable HEPA filters [12]. While the fraction of particles removed on a single-pass through a MERV-rated filter is lower than a HEPA filter, the overall filtration performance can alternatively be compared through a clean air delivery rate (CADR) metric, which is a measure of the volumetric rate of particle-free air delivered by the air cleaner .

Portable filtration has been observed to reduce the concentration of respiratory aerosols and the risk of respiratory infection transmission between occupants in a variety of building types. In a field study in 16 homes with an individual positive for COVID-19, Myers et al. observed a reduction in SARS-CoV-2 RNA positive air samples in the room most often occupied by the infected individual when a portable HEPA filter was operated [82]. In a field study of a hospital patient room and adjacent corridor and nurses' station, Buising et al. demonstrated that a surrogate for respiratory aerosol rapidly travelled from the patient room to adjacent spaces and that portable HEPA filters increased aerosol removal rates and decreased spread outside the patient room [83]. In a field study in a secondary school with 90 students, Banholzer et al. found that air samples positive for SARS-CoV-2 were reduced from 8% to 5% when a portable HEPA filter was operated in classrooms [84]. Additionally, average viral concentrations of positive air samples were substantially reduced by operation of the HEPA filter. Although the infection transmission risk odds ratio for SARS-CoV-2 was calculated to be comparable for the periods with and without portable air filters, the short two-week intervention and low number of infections resulted in high uncertainty in this conclusion. In a six-month study comparing two daycare centers with a portable HEPA filter intervention to a large reference population, Vartiainen et al. demonstrated that absenteeism due to child illness was reduced by 32% in the daycare centers with HEPA filters [85]. These field results are consistent with infection transmission risk modelling that predicts a reduced number of infections when using air filters that remove respiratory aerosols from the indoor air [6].

Filtration has additional health benefits in reducing occupant exposure to particles including pollen, pet dander, indoor cooking generated particle pollution, and outdoor-source particle pollution (e.g. vehicle exhaust, forest fire and residential wood smoke). A general review of the health benefits of particle filtration by Fisk in 2013 concluded that the majority of well-designed intervention studies employing particle filtration report modest statistically significant improvements in health, particularly for people with allergies or asthma [86]. Notably, two of the studies reviewed demonstrated portable HEPA filtration used in homes reduced both particulate matter exposure and health markers (vascular and endothelial function) that are predictors of future coronary events [87],[88]. A 2021 review of 21 papers related to portable air cleaners and published between 2005 and 2020 by Cheek et al. showed substantial reductions (22 to 90%) of indoor particulate matter less than 2.5 microns ($PM_{2.5}$) when portable air filters were in use [10]. Health benefits of reduced particulate matter exposure assessed by these studies were also summarized, but evidence of benefits was limited and inconsistent. However, the authors note that the cumulative body of scientific evidence supports that there are positive health benefits associated with reduced $PM_{2.5}$ exposure.

A limitation of the widespread deployment of portable HEPA filters is cost. In a cost-benefit analysis of HEPA filtration in 2017, Fisk and Chan estimated the cost of procuring HEPA filtration for a home at \$0.55 to \$1.40 per m^3/h of clean air delivered (CADR) and determined that the mortality-related economic benefits exceed the cost of purchasing and operating air cleaners when used over their multi-year life [89]. In 2022, Dal Porto et al. estimated the cost of HEPA filtration at \$0.44 to \$0.51 per m^3/h of CADR. The American Home Appliance Manufacturers (AHAM) recommend a CADR target of 12 m^3/h per m^2 of floor area, which equates to \$5.39 to \$6.25 per m^2 of floor area when applying costs from Dal Porto et al. [90] Therefore, HEPA filtration may not be a priority or may be too costly for some residents and operators of commercial buildings (e.g. schools, daycares, offices). The CR box offers a first-cost that is an order of magnitude below HEPA at \$0.05 to \$0.07 per m^3/h of CADR [12]. While multiple papers have been published documenting the filtration performance of new CR boxes [12-17], there is no published data on the longevity of the devices and their long-term performance. The purpose of this research was to assess the filtration performance of CR boxes operated daily over a 9-month academic year to determine how well these low-cost do-it-yourself filters perform over time.

4.2 Experimental

Four CR boxes were constructed, tested in new condition, and deployed across the UC Davis campus where their use was continuously monitored via power measurement. The CR boxes were collected every 10 weeks, retested, and redeployed for a total of 40 weeks of operation and five performance measurements. Each round of testing included measurement of the particle-size dependent CADR and single pass filtration efficiency (SPFE).

4.2.1 Construction

Four CR boxes were constructed with the following materials each: Three-speed box fan (Lasko model 3129342), 5 cm deep MERV 13 filters (two 50 x 50 cm and two 40 x 50 cm), cardboard shroud with opening of diameter 42 cm to reduce backflow through the corners of the fan, cardboard base, and duct tape. Filters for Box 1 were from Air Handler (AH) and filters for Boxes 2-4 were from Tex-Air (TA). Although both brands of filters had the same MERV 13 filtration efficiency rating, the filters looked visibly different, with the AH filters having a fuzzier appearance. The cost of each CR box was approximately $70 ($24 fan, $11 x 4 filters, $2 duct tape), consistent with the cost reported by Dal Porto et al.

4.2.2 Deployment and Long-Term Monitoring

The CR boxes were deployed in four locations across the UC Davis campus, two lab environments and two office spaces (Table 4-1). Ventilation with 100% outdoor air (OA) and activities occurring in the selected labs were expected to be large sources of particles to load the CR boxes. The Bainer laboratory is used primarily as a teaching laboratory for several undergraduate civil and environmental engineering courses and also as a general workshop space with a variety of sporadic activities (cutting, drilling, hand tools) that may generate particles. Within the Western Cooling Efficiency Center (WCEC) research laboratory particles were periodically generated from typical shop activities (cutting and drilling wood and metal).

Table 4-1: Deployment locations for four CR boxes on the UC Davis Campus

CR box	Space	Building Ventilation Type	Ventilation Schedule
1	Bainer - Lab	100% OA	All hours
2	WCEC - Lab	Local Exhaust	Varies (manual)
3	Kemper - Office	100% OA	All hours
4	Ghausi - Office	Recirculated	M-F 6:00 – 18:00

4.2.3 Power

Power draw of each CR box was continuously measured and logged every 5 minutes by an Onset HOBO Plug Load Data Logger (UX120-018). Power data was used to determine run time at each fan speed and assess changes in the power draw for a particular speed over time. A digital programmable timer turned on the fan daily at 8:00 and off at 17:00. The users could change the fan speed (low, medium, high) to suit their preference but were asked to leave the fan turned on (so that the on-off status would be controlled by the timer). The power used by the timer (about 1 W) was included in the power measurements. The change in power over time was assessed with a linear fit of the power data when the fan was running.

4.2.4 Clean Air Delivery Rate (CADR)

The CADR was calculated from the measured decay of salt particles in a room with and without the CR box operating. The methods generally followed Dal Porto et al. [12] The salt particles were generated using a portable mesh nebulizer (Wellue or equivalent) using an aqueous table salt solution (50 g/L).

Measurements were conducted in a conference room at WCEC with measured volume of 120 m^3. The mechanical heating, cooling, ventilation and filtration system for the conference room was shut off so that the only particle loss mechanisms in the room were deposition, air exchange through infiltration, and removal by the CR box. The total particle loss rate for combined deposition and infiltration was measured without the CR box operating. This loss rate was subtracted from the particle loss rate calculated with the CR box operating to obtain the particle loss rate attributable to the CR box.

Figure 4-1: CR box experimental test setup in a conference room.

The following procedure was used to collect the data required to calculate the CADR:

1. Salt particles were generated for 10 minutes while the CR box was off. Two fans placed on the table mixed the room air at low speed during this period.

2. The mixing fans were turned off. The room was left undisturbed for 10 minutes.

3. The CR box was turned on for 30 minutes to measure the exponential decay of the particles.

In the first round of testing, particle concentrations by size bin were measured every 5 seconds with two types of instruments, a laboratory-grade aerodynamic particle sizer (APS; TSI model 3321) and two low-cost optical particle counters (OPC; Alphasense OPC-N3 packaged into QuantAQ-MODULAIR-PM). This was done to correlate the particle concentration measurements for the lower-accuracy OPCs, which were available for the duration of the yearlong study, with the higher accuracy APS, which was only available intermittently. Kaur and Kelly evaluated nine Alphasense OPC-N3 sensors and reported a negative bias for particle concentration relative to the APS, as well as substantial inter-sensor variability [91]. Since CADR is calculated based on the change in particle concentration over time, an error in absolute sensor accuracy (i.e. gain) does not impact the results. However, sensor non-linearity does impact the results and is important to correct for.

As described in the Supplementary Information, the particle aerodynamic diameters defining each APS bin were converted to physical diameter (assuming spherical particles) to account for particle density and aligned with the optical diameter bins for the OPC. A set of empirical correlations were then developed to convert OPC particle concentrations to APS-equivalent particle concentrations. The APS-equivalent values were then used to calculate the air changes per hour (ACH) for particle removal (Bins 0-6) as described by Dal Porto et al. for the CR box including filtration and air movement (f), deposition (d), and infiltration (i), termed ACH_{f+d+i} [12]. Particle removal by deposition may be enhanced by the increased turbulence engendered by the fan on the CR box, enhancing the apparent losses due to filtration alone. We distinguish below between depositional losses with (*d+fan*) and without (*d*) the CR box fan.

Curve fits were calculated with Igor Pro v9.02 using the Levenberg-Marquardt least-squares method. The 95% confidence interval for each fit coefficient for ACH_{f+d+i} is also reported.

The ACH for deposition (d) and infiltration (i), termed ACH_{d+i}, was measured in an experiment in the conference room where:

1. Salt particles were generated for 10 minutes. Two fans placed on the table mixed the room air at low speed during this period.

2. The mixing fans were turned off. The room was left undisturbed for 24 hours.

The APS-equivalent values were then used to calculate ACH_{d+i} for particle removal as described by Dal Porto et al. Particle concentrations for larger particle diameters dropped below the detection limit of the OPC before the end of the 24-hour settling period. The particle loss rate analysis was limited to the period where the particle concentration was above 0. The particle loss rate for deposition and infiltration and analysis period for each bin are shown in Table 4-2. As generally expected, ACH_{d+i} increased with particle size.

Table 4-2: Particle loss rates, deposition and infiltration

Bin (j)	APS Physical Diameter (µm)	OPC Optical Diameter (µm)	ACH_{i+d} (1/hr)	Analysis Period (hr)
0	≤ 0.46	0.35 – 0.46	0.141	24.0
1	0.46 – 0.66	0.46 – 0.66	0.166	24.0
2	0.66 – 1.03	0.66 – 1.0	0.202	21.7
3	1.03 – 1.28	1.0 – 1.3	0.245	14.7
4	1.28 – 1.72	1.3 – 1.7	0.284	12.0
5	1.72 – 2.30	1.7 – 2.3	0.378	6.5
6	2.30 – 3.07	2.3 – 3.0	0.523	1.9

The CADR for the air cleaner for each particle size bin “j” was then calculated from Equation 4-1:

$$CADR_{(j)} = (ACH_{f+d+i(j)} - ACH_{d+i(j)})\,V \qquad \text{Equation 4-1}$$

where V is the volume of the conference room (120 m^3). The 95% confidence interval for each $ACH_{f+d+i(j)}$ was used to estimate the confidence interval for $CADR_{(j)}$. Although there are also uncertainties in calculation of $ACH_{d+i(j)}$ and V, these values were only measured once and were held constant in the long-term performance analysis. Therefore, uncertainties in these values do not impact the analysis of the change in performance of the CADR boxes over time. Note that the CADR obtained from Equation 4-1 includes the combined effects of removal by the filter and enhanced depositional losses.

To simplify the presentation of the data, the CADR results from bins 0 to 6 were averaged into two groups: particles with optical diameter less than 1 µm (more representative of particle diameters observed in wildfire smoke) and particles with optical diameters between 1 to 3 µm (more representative of particle diameters observed in infectious respiratory aerosols) [92, 93]. The average CADR for all bins was also calculated. All averaging calculations weighted the CADR measurement for each bin equally. To estimate the uncertainty of the CADR measurement method, at the end of the experiment the CADR of Box 3 on speed high was measured 10 times. The repeat measurement included setup and takedown of the CR Box and the instrumentation to account for minor differences in setup. The uncertainty (two standard deviations) was 6% of the average measurement for 0.35 to 1 µm optical diameter particles and 5% for 1 to 3 optical diameter particles. This uncertainty (as a percentage) was applied to all CADR measurements.

4.2.5 Single Pass Filtration Efficiency and Pressure Drop

The single pass filtration efficiency of the air filters for each particle size bin "j" was calculated with Equation 4-2:

$$SPFE_{(j)} = \left(\frac{C_{filter\ inlet(j)} - C_{filter\ outlet(j)}}{C_{filter\ \ inlet(j)}} \right) \qquad \text{Equation 4-2}$$

where $C_{filter\ inlet}$ is the particle concentration in the room as measured by OPC-1 and $C_{filter\ outlet}$ is the particle concentration inside the CR box as measured simultaneously by OPC-2. Sensor OPC-2 was placed inside the filter box by cutting an access door in the cardboard bottom and taping the door shut during testing. Both OPC-1 and OPC-2 were sampled every 5 s for 2 min and the average result was calculated. The average OPC measurements were converted to equivalent APS values prior to calculation of the SPFE with Equation 2. Static pressure drop across the filters was measured using plastic tubing and a differential pressure sensor (The Energy Conservatory DG-500).

While the SPFE and pressure drop data were collected every 10 weeks, the door was unintentionally not taped during SPFE testing that occurred on weeks 10 and 20. Leaks in the bottom of the box made the results unreliable and therefore only SPFE results from 0, 30, and 40 weeks are presented. The access door was securely taped for the CADR testing and those results were unaffected.

4.2.6 Enhanced Particle Deposition

As noted above, the air movement from the fan increases particle deposition by increasing the turbulent kinetic energy in the room. While such enhanced loss is attributable to the CR box it is not attributable to removal by the filters. To separate particle removal by the filter from enhanced deposition we followed the same procedure as used to measure the ACH_{d+i} but with a "mock" CR box that had the fan in the same orientation as a standard CR box but with the filters removed. The resulting loss rate, $ACH_{d+i,fan(j)}$, includes the enhanced particle deposition of the CR box fan (Table 4-3). As expected, the $ACH_{d+i+fan(j)}$ values at all sizes exceeded the ACH_{d+i} values.

Table 4-3: Particle loss rates, deposition and infiltration with box fan on (no filter)

Bin (j)	OPC Optical Diameter (µm)	Low Speed (1/hr)	Medium Speed (1/hr)	High Speed (1/hr)	Analysis Period (hr)
0	0.35 – 0.46	0.44	0.37	0.55	2.0
1	0.46 – 0.66	0.68	0.60	0.76	2.0
2	0.66 – 1.0	0.79	0.72	0.89	2.0
3	1.0 – 1.3	0.91	0.86	1.06	2.0
4	1.3 – 1.7	1.02	0.97	1.17	2.0
5	1.7 – 2.3	1.17	1.17	1.35	2.0
6	2.3 – 3.0	1.38	1.58	1.69	0.6-0.9

A modified $CADR_{filter_{(j)}}$, meaning the CADR attributed to the filters only, was calculated from Equation 4-3:

$$CADR_{filter_{(j)}} = (ACH_{f+d+i(j)} - ACH_{d+i,fan(j)})\,V \qquad \text{Equation 4-3}$$

4.2.7 Total Airflow Rate

Airflow rate of the fan was analyzed over the 40 weeks of testing to determine if performance losses were attributed to a reduction in filtration efficiency and/or a reduction in total fan flow rate (due to increased resistance to flow as filters accumulated particulate matter). The total airflow rate of the fan, Q, was estimated from $CADR_{filter}$ divided by the SPFE for each bin "j".

However, because the air movement from the fan increases particle deposition (which is not attributable to removal by the filters), the ACH_{d+i} measurement was repeated with the fan on and filters removed to obtain a loss rate $ACH_{d+i,fan(j)}$ that includes the effect of the fan operating without the filters (Table 4-3).

$$Q_{(j)} = (CADR_{filter_{(j)}}/SPFE_{(j)}) \qquad \text{Equation 4-4}$$

The $CADR_{filter_{(j)}}$ values were used here instead of the CADR values so as to focus on just the airflow through the filters. The calculated flow rate for a CR box should be the same across all particle size bins. Any size-dependent differences in the flow result are attributed to the uncertainty in the measurements of CADR and SPFE. The average flow rate ($\bar{Q}$) was calculated as the average across all seven size bins. The 95% confidence interval was calculated as two standard deviations across the seven measurements.

4.2.8 Estimate of Mass Collected on Filters

Indoor air particle concentrations in each space with a CR box deployed were monitored with a low-cost Purple Air sensor (PA-II-SD) that reported an average result from two Plantower PMS5003 nephelometers. Nephelometers measure total light scattered by an air sample and estimate the total particle mass concentration [94]. Since the CR box will collect particles of all sizes, the Purple Air signal for particulate matter less than 10 µm (PM_{10}) was used, which is the best measurement available from these low-cost sensors to represent the total particle mass concentration of the air being filtered. While a field evaluation by the South Coast Air Quality Management District determined outdoor PM_{10} measured by Purple Sensors was only moderately correlated (R^2<0.41) with PM_{10} measured by federal equivalent reference methods, the study of six sensors showed good agreement between devices [95]. It has also been demonstrated that Purple Air PM10 measurement accuracy varies substantially based on indoor particle source and that accuracy generally decreases as particle size and concentration increase [96, 97]. While the spaces monitored had similar sources of outdoor particles due to their proximity on the same campus, the two laboratories had different sources of indoor particles. Low accuracy of the nephelometer-based PM_{10} measurements, and lack of a true mass-based PM_{10} reference measurement, is a limitation of this study and thus the cumulative mass is labelled as “estimated” to reinforce the accuracy limitation of the sensors used.

The mass deposited on the filters over each deployment period was estimated per Equation 4-4. For each fan speed i, the cumulative mass deposited was estimated by multiplying the number of hours (t) of operation (as measured by the power meter), the average particle mass concentration as measured by Purple Air ($\overline{PM10}$)), and the average CADR for all particle bins ($\overline{CADR}$). The total estimated mass was calculated as the sum of the mass collected at each fan speed (low, medium, high). These data were used to estimate the cumulative mass deposited on the box at the time each set of CADR and SPFE measurements were taken.

$$m_{total} = \sum_{i=low}^{high} \overline{CADR}_i \times \overline{PM10}_i \times t_i \qquad \text{Equation 4-5}$$

4.3 Results & Discussion

4.3.1 Power

The complete power data collected for each box fan are included in the Supplementary Information in Figure S3. The initial power and final power for each box fan were estimated using a linear fit of the power data collected at the speed used most frequently (Table 4-4). For Box 2, power data did not log during the final deployment period, so the final power is predicted based extrapolation of the measurements from the first three deployment periods and an additional day of power measurements collected at the end of the experiments. Overall, changes in power were small and, for Boxes 1, 3, and 4, were within the accuracy specification of the power meter. Box 2 measurements showed a power decrease of about 3 W, potentially indicating that the airflow through the fan was slightly reduced.

Table 4-4: Initial power and final power for each box fan estimated using a linear fit of the power data collected at the most used speed.

Box	Main Speed	Initial Power (W)	Final Power (W)	% Change
1	Medium	72.6	73.3	1.0%
2	Low	63.2	60.3	-4.5%
3	High	86.5	87.1	0.7%
4	Low	60.1	60.3	0.4%

4.3.2 Clean Air Delivery Rate

The average CADR for the size bin as a function of the estimated cumulative mass deposited on the filter is plotted in Figure 4-2 for high, medium, and low fan speeds. As a reminder, the CADR values include the combined effects of removal by the filters and enhanced depositional losses. Complete CADR results for each particle diameter bin are available in the supplementary information (Table S4 to S6). Further details about the cumulative mass results displayed on the x-axis are provided in the next section. Note that particle accumulation combines the effects of operating time with the average particle concentration; here, an increase in particle accumulation for a given box corresponds to an increasing overall deployment time.

Overall the CADR measurements (and associated cost-effectiveness) for new CR boxes (514 to 1387 m^3/hr, depending on Box, fan speed, and particle size) were within range of others reported in the literature (Figure 4-2) [17]. Box 1 (AH filters) outperformed the other CR boxes, both when new and throughout the study. This illustrates that filter selection, even among those rated MERV 13, may impact performance. In addition to differences in box fans, filter selection likely contributes to the wide range of CADR results reported in the literature [17]**.** In addition to actual differences in CR box performance due to material selection, measurement methods will influence results because of CADR dependence on particle size. For example, use of sensors and methods that calculate CADR based on particle mass removal rates (as opposed to particle count removal rates) are likely to yield higher CADR results because MERV 13 filters have higher removal rates of larger particles that dominate mass-based measurements.

This study was designed to assess the long-term performance of CR Boxes and was not designed to assess differences between MERV 13 filter brands, and we did not expect the results to be different for the box built with a different brand of filter. The minimum 0.3 to 1.0 μm diameter particle removal efficiency must be at least 50% for MERV 13 filters and 75% for MERV 14 filters. The large jump in filtration efficiency between MERV 13 and MERV 14 shows that there could be variation among MERV 13 filters brands that meet or exceed the MERV 13 standard but do not meet MERV 14 standards [53]. Both types of filters used in this study met requirements of MERV 13 filters, with a small difference between the filters' initial filtration efficiency (e.g. AH 61% and TA 55% for 0.3 to 1.0 μm particles) per the ASHRAE 52.2-2017 test reports, which were obtained from the manufacturers [98, 99]. Although initial filtration efficiency differences were small and long-term filtration efficiency is generally not available, CR Box builders may benefit from reviewing manufacturer provided filtration performance data when making filter selection instead of only considering MERV rating (in addition to consideration of filter cost).

As expected for MERV 13 filters, the CADR for 1.0-3.0 µm optical diameter particles was consistently higher than the CADR for 0.35-1.0 µm optical diameter particles because they are more easily removed by impaction with filter fibers [100]. Across four CR boxes tested at three speeds at five times during the 40-week deployment (n=60), the CADR for 1.0-3.0 µm optical diameter particles was, on average, 34% higher than the CADR for 0.35-1.0 µm optical diameter particles.

The CADR for CR boxes 2, 3, and 4 (TA filters) declined approximately linearly with particle accumulation on the filters (Figure 4-2). Considering these three CR boxes as one dataset, a linear least-squares regression estimated that, after 4.8 g of particles was deposited, the CADR was 62-63% of the new CR box performance for particles 0.35 to 1.0 µm optical diameter and 69-70% of the new CR box performance for particles 1.0 to 3.0 µm optical diameter.

The CADR for CR box 1 was higher than CR boxes 2, 3, and 4. A two-sample t-test comparing all CADR measurements for Box 1 to all CADR measurements for Box 2, 3, and 4 (at the same speed) determined that the higher value of CADR for Box 1 was statistically significant at high speed ($p = 6.6 \times 10^{-7}$) and medium speed ($p = 1.5 \times 10^{-3}$) but not at low speed ($p = 0.20$). Coincidentally, Box 1 was deployed in the dustiest environment and accumulated an estimated 9.6 g of particles on the filters over the course of the deployment. Box 1 appeared to have an increase in CADR in almost all cases between the first and second measurements (except high speed, 0.35 to 1.0 µm optical diameter particles). Clean air delivery rate generally decreased in subsequent measurements. A quadratic least-squares regression estimated that, after 9.6 g of particles was deposited, the CADR was 63-75% of the new CR box performance for particles 0.35 to 1.0 µm optical diameter and 70-84% of the new CR box performance for particles 1.0 to 3.0 µm optical diameter. Clean air delivery rate was better maintained at high and medium speed than low speed. The sample size of one box with AH filters is too limited to draw general conclusions; it is unknown if a larger sample size would exhibit similar behavior.

Analysis of the CADR results alone cannot determine if the CADR is decreasing due to a loss of filtration efficiency or due to a reduction in flow rate due to increased resistance of the filters. The SPFE measurements, flow rate calculations, and power measurements provide insight to the reasons for the performance decrease.

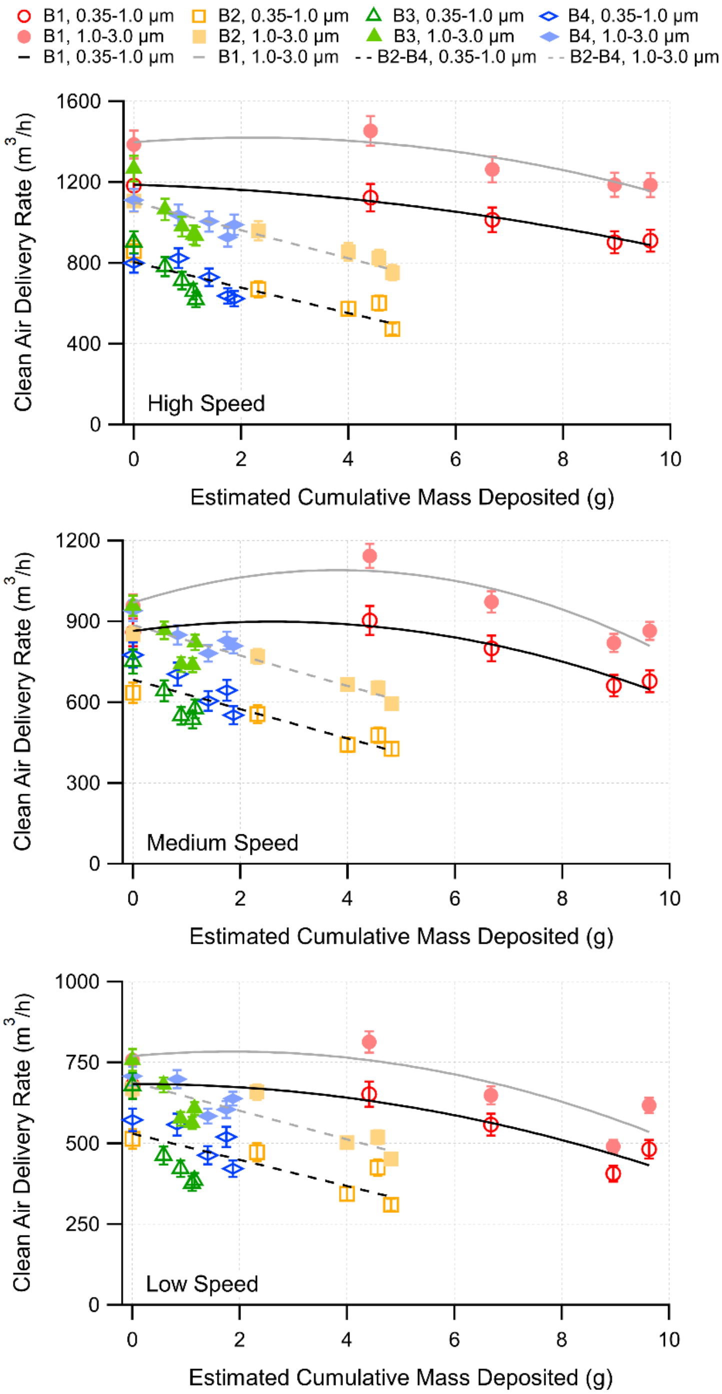

Figure 4-2: CADR results for CR boxes as a function of cumulative mass deposited over the 40-week field trial. Coefficients for the linear and quadratic fits are provided in Table S2 and Table S3. Error bars represent an estimated uncertainty of 6% for 0.35 to 1 μm optical diameter particles and 5% for 1 to 3 optical diameter particles.

4.3.3 Cumulative Mass Deposited

For each CR box and deployment period, the hours of operation at each speed, the average CADR calculated for that speed (from Figure 4-2), the average PM_{10} measurement during that period and speed, and the PM_{10} deposited are detailed in Table 4-5. The average PM_{10} measurement was calculated from the available data and was used as the average for the deployment period. Box 1, which had a higher CADR than the other boxes and was placed in a lab environment with high particle concentration, accumulated the highest amount of estimated particle mass of 9.6 g over the 40 weeks of measurement. Box 2, which was also placed in a lab environment with high particle concentration, accumulated an estimated particle mass of 4.8 g. Boxes 3 and 4, which operated in cleaner office environments, accumulated an estimated particle mass of 1 and 2 g respectively. Photographs of the filters at the end of the study are shown in Figure 4-3.

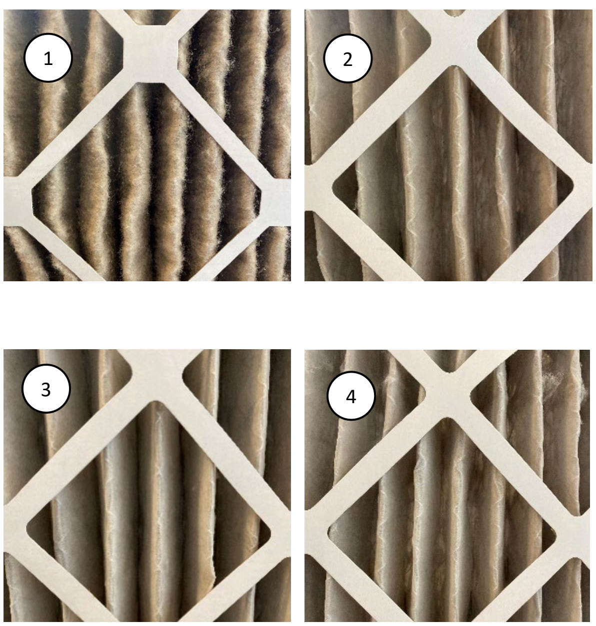

Figure 4-3: Photographs of filters for each CR box at the end of the last deployment period.

Table 4-5: Hours of operation at each speed for each deployment period for each CR box. The average CADR was calculated as the average of the measurements taken before and after the deployment period. The average PM_{10} measurement during each period is reported as well as the estimated amount of particle mass deposited. *Power measurements did not log for Box 2, deployment period 4. Hours of operation were calculated from the programmable timer schedule and observations that the CR box as working as expected.

CR Box	Period	Hours of Operation	Speed	$\overline{CADR}$ (m^3/h)	Average PM_{10} (μg/m^3)	PM_{10} 10th Percentile (μg/m^3)	PM_{10} 90th Percentile (μg/m^3)	% PM_{10} Data Available	Estimated PM_{10} Deposited (g)	Estimated Cumulative PM_{10} Deposited (g)
1	1	639	Med	978	7.05	2.21	13.24	45%	4.41	4.41
	2	63	Med	969	2.15	0.06	2.55	100%	0.13	4.54
		585	Low	677	5.41	0.47	11.48	73%	2.14	6.68
	3	369	Med	825	5.14	0.06	13.81	100%	1.57	8.25
		261	Low	555	4.94	0.20	11.55	100%	0.72	8.96
	4	432	Med	768	2.00	0.05	7.26	25%	0.66	9.63
Total Box 1		2349								9.6
2	1	639	Low	591	6.14	1.08	12.13	100%	2.43	2.32
	2	648	Low	507	5.14	0.31	10.56	100%	1.69	4.00
	3	630	Low	456	1.98	0.04	5.66	100%	0.57	4.57
	4	693	Low*	435	0.83	0.03	1.80	100%	0.25	4.82
Total Box 2		2610								4.8
3	1	297	Med	820	0.92	0.05	2.19	100%	0.22	0.22
	1	342	High	1027	1.02	0.03	1.96	92%	0.45	0.58
	2	648	High	904	0.54	0.00	1.48	100%	0.32	0.90
	3	459	High	842	0.45	0.00	1.24	100%	0.17	1.07
		171	Med	654	0.35	0.00	1.14	100%	0.04	1.11
	4	135	Med	683	0.18	0.00	0.44	100%	0.02	1.13
		558	High	808	0.07	0.00	0.19	100%	0.03	1.16
Total Box 3		2610								1.2
4	1	639	Low	644	2.01	0.11	4.54	100%	0.94	0.83
	2	648	Low	585	1.52	0.05	3.66	100%	0.57	1.40
	3	576	Low	550	1.09	0.01	3.28	100%	0.34	1.75
	4	693	Low	557	0.30	0.01	0.91	100%	0.12	1.87
Total Box 4		2556								1.9

4.3.4 Single Pass Filtration Efficiency

The average SPFE as a function of the estimated cumulative mass deposited on the filter is plotted in Figure 4-4 for high, medium, and low fan speeds. Complete SPFE results for each particle diameter bin are available in the supplementary information (Table S7 to S9). In agreement with the CADR measurements, the SPFE for the 1.0-3.0 µm optical diameter particles was consistently higher than for 0.35-1.0 µm optical diameter particles because larger particles are more easily removed by impaction with filter fibers. Across four CR boxes tested at three speeds at five times during the 40-week deployment (n=60), the SPFE for 1.0-3.0 µm optical diameter particles was, on average, 23% higher than the SPFE for 0.35-1.0 µm optical diameter particles. It is difficult to estimate the uncertainty of the SPFE measurements (which are more sensitive to accurate measurement of absolute particle concentration than the CADR measurements). Assuming a best-case scenario where the measured particle concentrations have an accuracy of ±10% of reading (which is the reported accuracy of the APS), uncertainty propagation of the SPFE formula is a 20% relative uncertainty. While there is substantial uncertainty in these measurements, the results are still helpful to understand the change in CR box performance over time.

The SPFE for CR box 1 was consistently higher than CR boxes 2, 3, and 4. The SPFE declined over time for all boxes. Collectively for CR boxes 2, 3, and 4, the decline in SPFE was correlated with the cumulative mass deposited. This likely results from the filters having an initial electrostatic effect that is reduced as the filter accumulates particles [101]. Both manufacturers confirmed that the filters use both charged fibers and mechanical principles to remove particles. Testing with ASHRAE Standard 52.2 to determine MERV rating does not take into account electrostatic discharge. The difference in the SPFE between the CR boxes indicates that Box 1 filters rely less on initial electrostatic forces to meet their stated initial MERV performance (since the Box 1 removal efficiency better persists with particle accumulation).

Unfortunately, performance data after electrostatic discharge are not generally available to the consumer in ASHRAE 52.2 test reports (unless optional Appendix J is used).

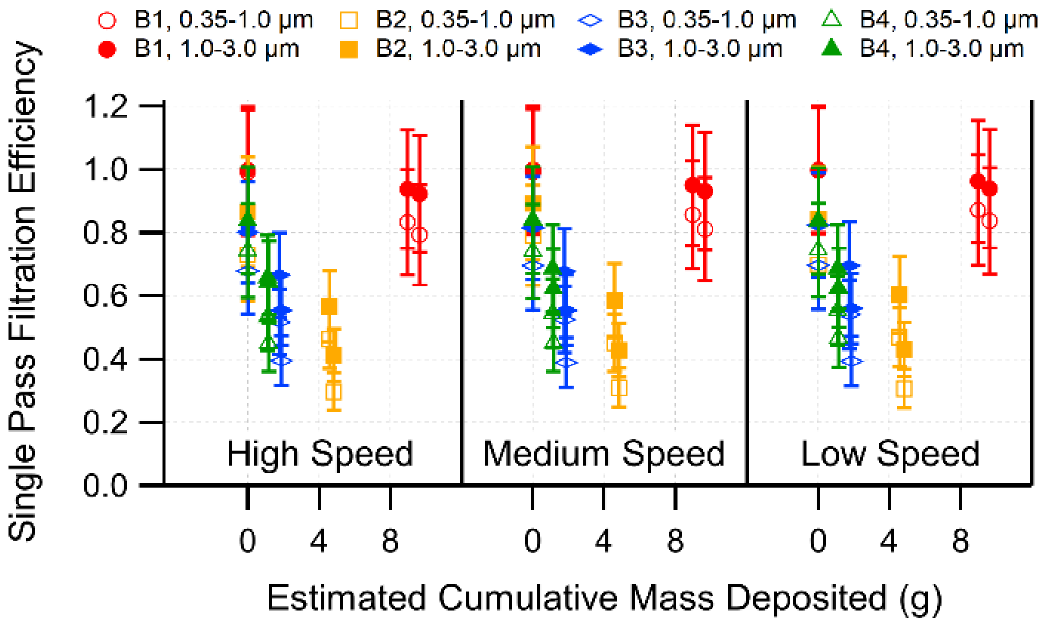

Figure 4-4: SPFE results for CR boxes as a function of cumulative mass deposited at 0, 30, and 40 weeks. Error bars represent an estimate 20% relative error on the SPFE measurement.

4.3.5 Total Airflow Rate and Pressure Drop

For each test, there was substantial variation in the derived flow rates between the 7 particle size bins owing to the variability and uncertainty in the SPFE measurement (supplementary information Table S10 to S12). This leads to relatively large standard deviations for each average flow rate determination (Figure 4-5). Nonetheless, there is no strong indication that the flow rates decreased appreciably over time for any of the fans. In comparison, there were clearer trends in loss of SPFE with particle accumulation, particularly for boxes 2 to 4. This suggests that the declines in CADR over time are likely not due to a change in airflow, but rather due to a loss of filtration efficiency. This is counterintuitive to the expectation that the accumulation of particles will increase resistance on the filters and reduce airflow. MERV filters for HVAC applications are generally designed for an air velocity of 2.5 m/s, whereas the air velocity of the CR box (with approximately 1 m^2 of surface area) is 0.1 to 0.4 m/s for airflow rates of 500 to 1500 m^3/h.

Complete pressure drop measurements are available in the Supplementary Information, Table S13. At high speed, the static pressure drop across new boxes was 7.1 to 7.2 Pa and the final pressure drop was 8.2 to 10.9 Pa, where the highest final pressure drop was observed for Box 1. This increase in pressure is small relative to the total external static pressure across the fan. For example, an increase of static pressure of 3 Pa at a flow rate of 1500 m^3/h is equal to a fluid power loss of only 1.3 W. Although the efficiency of the fan and motor assembly is not known (so conversion to electrical power cannot be estimated), 1.3 W is small compared to the electrical input of the box fan at high speed (86 W). Therefore, while particle accumulation on the filters will increase resistance, the change is small relative to the external static pressure across the fan system and thus is expected to have minimal impact on total flow rate.

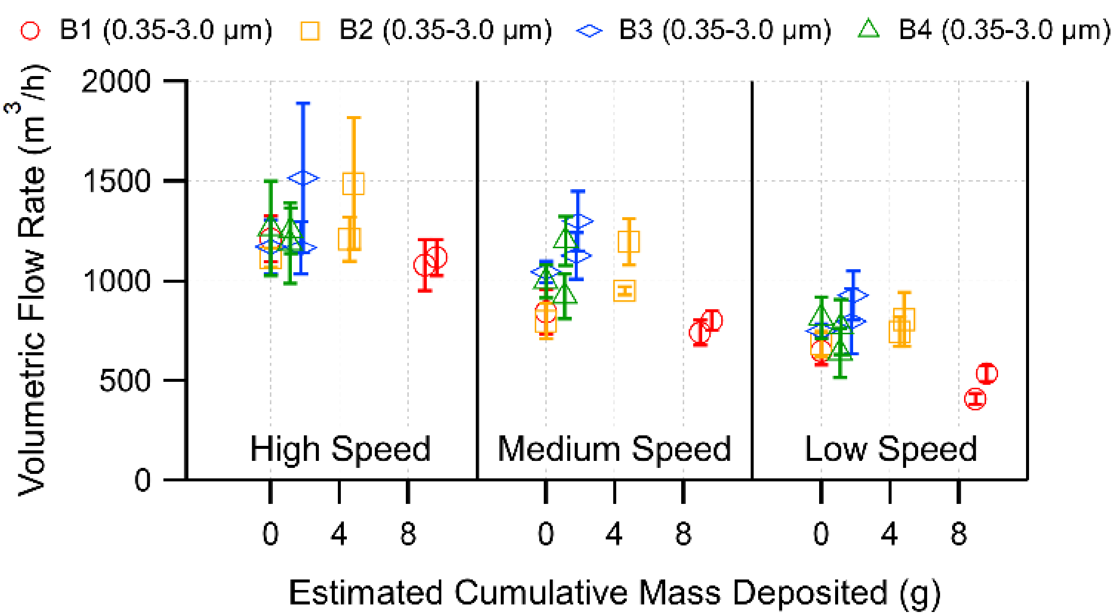

Figure 4-5: Calculated flow results for CR boxes as a function of cumulative mass deposited at 0, 30, and 40 weeks. Error bars represent the 95% confidence interval for the average result calculated from 7 particle size

bins for each test.

4.4 Limitations

This study had several limitations that should be considered in interpretation of the results and conclusions. It was designed to assess the long-term performance of CR boxes and was not designed to assess differences between MERV 13 filter brands. We did not expect the results to be different for the box built with a different brand of filters. While a clear difference was observed, the sample size of one box with AH filters is too limited to draw general conclusions; it is unknown if a larger sample size would exhibit similar behavior. A study with larger sample sizes of CR boxes built with different filter brands could explore this further.

A second limitation was the estimate of PM_{10} cumulative mass. This metric was used to provide more information than the cumulative runtime because particle concentrations in the indoor environment vary widely. As discussed in the methodology, low-cost Purple Air sensors have only moderate correlation with PM_{10} reference measurements. An improvement to this study methodology would be to deploy periodic PM_{10} reference instruments (e.g. 1 week per deployment period) to calibrate the Purple Air sensors for the specific environments in which they are deployed.

Finally, in this study we did not directly measure airflow through the CR box. Methods that measure air velocity are challenging because they require many individual measurements and assumptions on the applicable area for the measured velocity to calculate flow[12]. As such, we estimated airflow as the ratio of measured CADR and SPFE. A limitation of this approach is a high uncertainty of the SPFE measurement, which impacts uncertainty of the total flow calculation.

4.5 Conclusions

Four CR boxes deployed across a university campus in labs and offices demonstrated robust performance over 40 weeks of operation. Across four CR boxes tested at three speeds at five times during the deployment (n=60), the CADR for 1.0-3.0 µm optical diameter particles was, on average, 34% higher than the CADR for 0.35-1.0 µm optical diameter particles. This result is consistent with rating requirements for MERV 13 filters. While CR boxes are effective at filtering all particle sizes, the results show they are particularly well suited for filtering most of the volume of respiratory aerosol particles. Programmable timers are a useful tool to efficiently operate the CR boxes automatically when people are expected to be present.

Considering all three boxes with the same filter brand (TA) as one dataset, a linear least-squares regression estimated that, after 4.8 g of particles were deposited, the CADR was 62-63% of its initial value for particles 0.35 to 1.0 µm optical diameter and 69-70% of its initial value for particles 1.0 to 3.0 µm optical diameter. For the CR box with a different filter brand (AH), a quadratic least squares regression estimated that, after 9.6 g of particles deposited, the CADR was 63-75% of its initial value for particles of 0.35 to 1.0 µm optical diameter and 70-84% of its initial value for particles 1.0 to 3.0 µm optical diameter. Since CR boxes are an order of magnitude less in cost than HEPA filters and they maintain at least 60% of their initial CADR (even after 40-weeks of daily operation in dirty lab environments), they are a cost-effective long-term tool to manage air quality. The results indicate that annual filter replacements are sufficient in dirty environments and that filters may last 2-3 years in clean office environments. No substantial wildfire smoke was observed during the study period. A study by Liang et al. quantified that indoor air $PM_{2.5}$ was approximately 2.7 times higher on “fire days” versus “non-fire days” [102]. Thus, the occasional and short-term presence of wildfire smoke is not expected to appreciably affect the 1-3 year lifetime of the CR Box.

Performance losses as particles accumulated were attributed to loss of single pass filtration efficiency (likely due to loss of initial electrostatic charge on the filters). Although total airflow rate measurements had high uncertainty, there were no indications that minimally increased filtration resistance significantly affected airflow, even for CR boxes operating in laboratory environments with high average particle concentrations.

4.6 Supplementary Information

4.6.1 Conversion of OPC Measurement to APS-Equivalent Values

The APS measures particle concentrations in 52 bins for particle aerodynamic diameters of ~0.5 to 20 µm, and the OPC measures particle concentrations in 24 bins for particle optical diameters of 0.35 to 40 µm. Salt particle concentrations generated by the nebulizer were negligible above 3 µm optical diameter. Therefore, evaluation of the CR box performance was limited to particles with optical diameters of 0.35 to 3 µm, which covers the primary range of interest for air cleaners due to the known health impacts of particles in this size range.

The APS particle size bins were converted from aerodynamic diameter to mobility diameter using Equation S 4-1:

$$D_m = \left(\frac{\rho_o}{\rho_p}\right)^{0.5} D_a \qquad \text{Equation S 4-1}$$

Where D_m is the mobility diameter for a theoretical spherical particle, ρ_o is the density of water (1 g/cm^3), ρ_p is the density of the particle (2 g/cm^3 for NaCl), and D_a is the aerodynamic diameter as measured by the APS. After the APS particle diameter bins were converted to mobility diameter using Equation 1, they were aligned with the corresponding OPC optical diameter bins (which assumes that the particles are spherical). The particle concentrations for the matched bins were then correlated using the available data from the first round of testing with both instruments. A cubic equation was fit to correlate each OPC to the APS data for each particle size bin "j", with the following empirical form:

$$APS_{(j)} = a1_{(j)} OPC_{(j)} + a2_{(j)} OPC_{(j)}{}^{2} + a3_{(j)} OPC_{(j)}{}^{3} \qquad \text{Equation S 4-2}$$

Where OPC and APS are the respective measured particle concentrations in particles per cubic centimeter. The coefficients for Equation S 4-2 for each bin are listed in Table S4-1. The data used to determine each correlation for Table S4-1 is shown in Figure S4-1 and Figure S4-2.

Table S4-1: APS and OPC particle diameter bins and coefficients for cubic OPC and APS correlation

Bin (j)	APS Mobility Diameter (µm)	OPC Optical Diameter (µm)	Coefficients for OPC-1, Eq 2			Coefficients for OPC-2, Eq 2		
			a1 (-)	a2 (cm^3/p)	a2 (cm^6/p^3)	a1 (-)	a2 (cm^3/p)	a2 (cm^6/p^3)
0	≤ 0.46	0.35 – 0.46	2.97E+00	-1.08E-01	4.33E-03	2.76E+00	-8.77E-02	3.79E-03
1	0.46 – 0.66	0.46 – 0.66	2.23E+00	1.72E-03	4.10E-04	2.27E+00	3.74E-03	4.14E-04
2	0.66 – 1.03	0.66 – 1.0	3.31E+00	5.74E-03	3.55E-04	3.22E+00	1.49E-02	1.98E-04
3	1.03 – 1.28	1.0 –1.3	2.52E+00	3.49E-02	-9.06E-04	2.61E+00	2.86E-02	-8.04E-04
4	1.28 – 1.72	1.3 – 1.7	1.49E+00	-1.24E-03	-1.50E-04	1.50E+00	-1.99E-03	-1.19E-04
5	1.72 – 2.30	1.7 – 2.3	1.64E+00	-5.08E-03	-1.84E-03	1.60E+00	-1.18E-02	-1.13E-03
6	2.30 – 3.07	2.3 – 3.0	1.46E+00	3.19E-02	-3.73E-02	1.43E+00	2.96E-02	-3.46E-02

For each CR Box test, the particle loss rate was measured with OPC-1. For consistency, the test data were analyzed starting at the time the particle concentration for bin 0 dropped below 26 p/cm^3 (per the OPC-1 measurement) for a period of 20 minutes. In 6 of 60 tests, there was not 20 minutes of data available after the concentration dropped below 26 p/cm^3, and the available data (14-19 minutes) was used in these cases. The OPC-1 values were converted to corresponding APS values with Equation S 4-2.

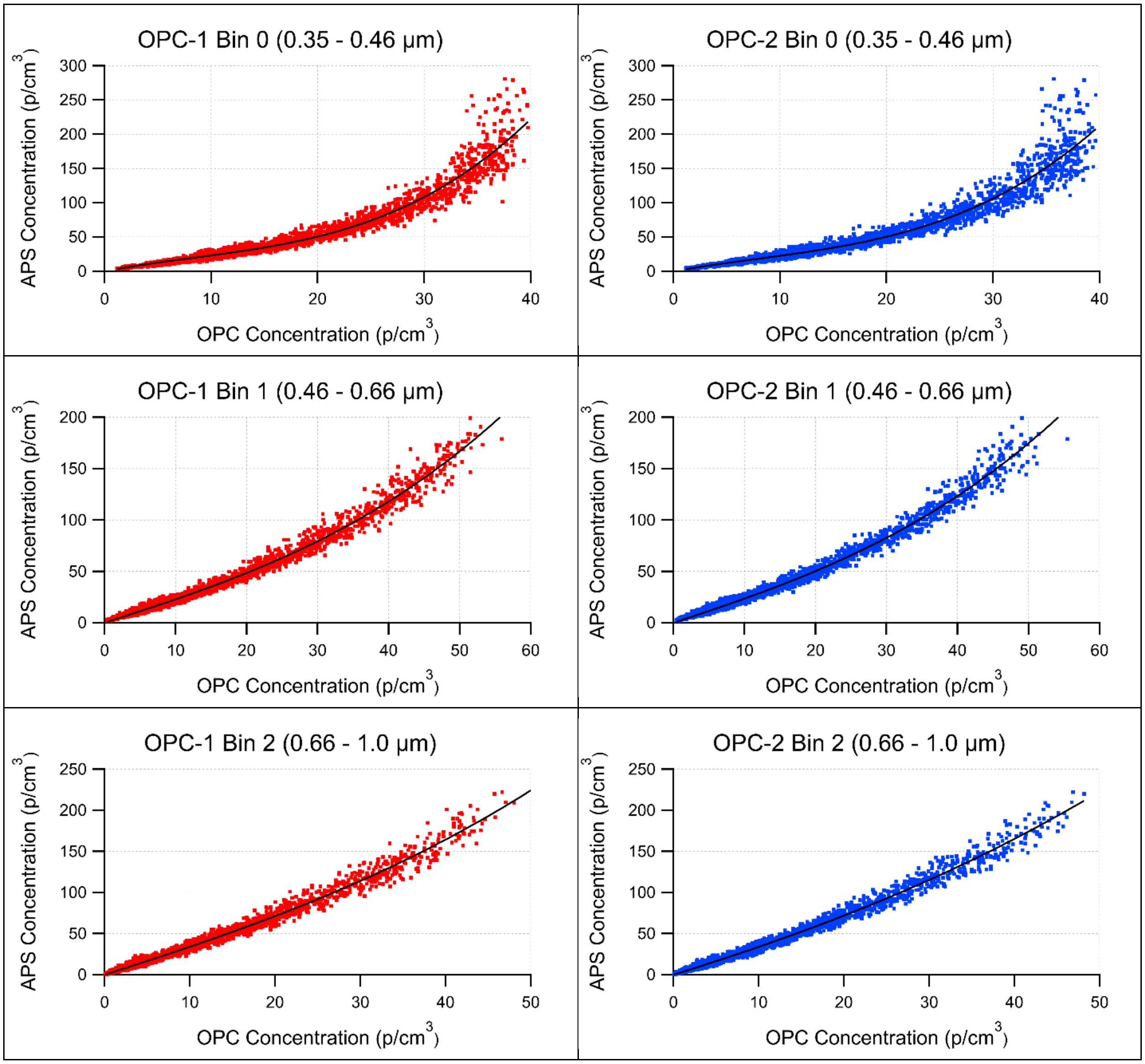

Figure S4-1: Empirical cubic correlations between low-cost OPC and laboratory grade APS data for bins 0 to 2 of the OPC. Coefficients for least-squares regression are contained in Table 2.

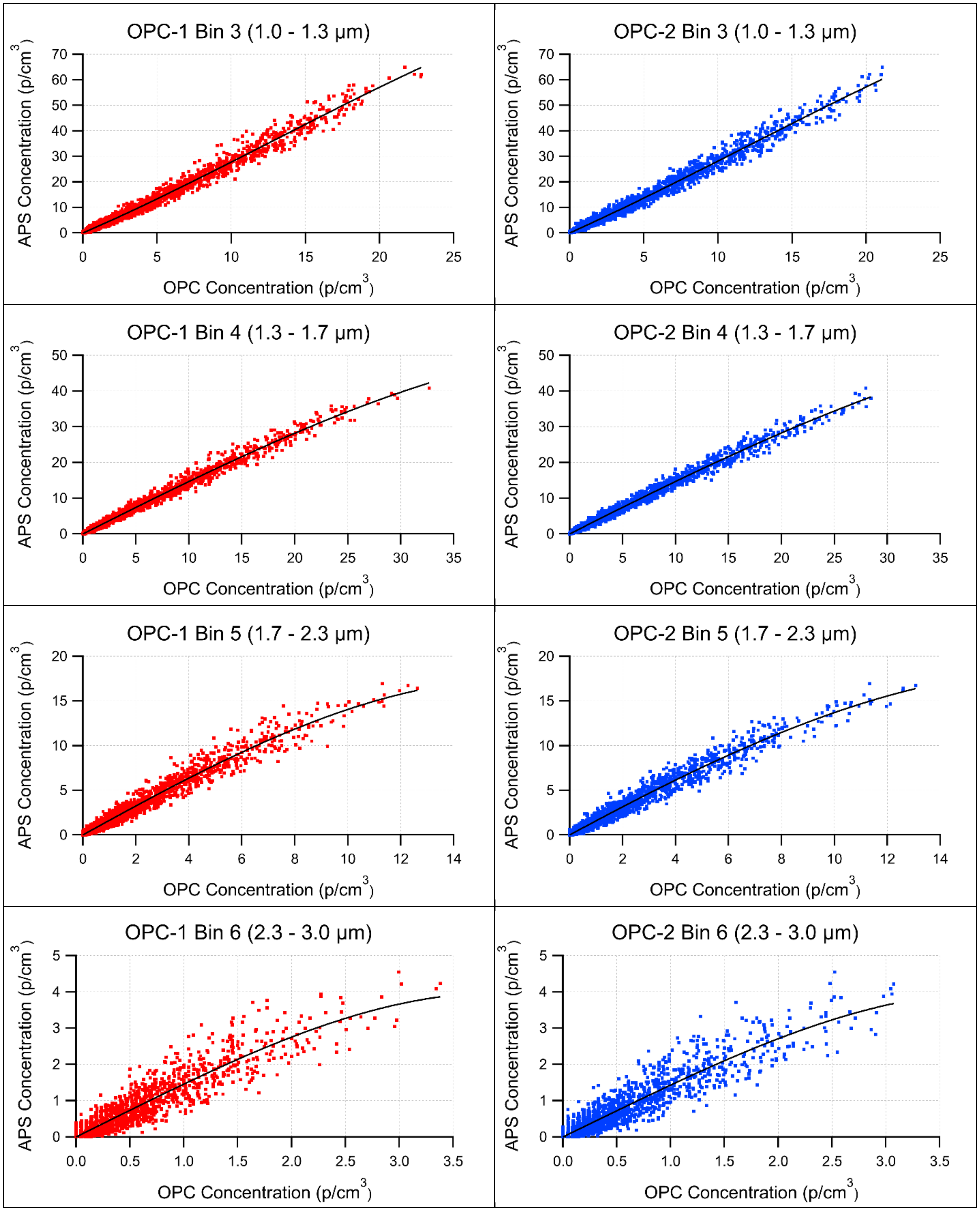

Figure S4-2: Empirical cubic correlations between low-cost OPC and laboratory grade APS data for bins 3 to 6 of the OPC. Coefficients for least-squares regression are contained in Table 2.

4.6.2 CADR Versus Cumulative Mass correlations

The fit coefficients for each box for CADR versus cumulative mass are shown in Table S4-2 and Table S4-3.

Table S4-2: Linear fit coefficients for Box 2, 3, and 4 from Figure 2 (y=K0+K1x)

	High Speed		Medium Speed		Low Speed	
Size Range (um)	**K0**	**K1**	**K0**	**K1**	**K0**	**K1**
0.35-1.0	8.034E+02	-6.291E+01	6.834E+02	-5.458E+01	5.301E+02	-4.061E+01
1.0-3.0	1.101E+03	-6.949E+01	8.865E+02	-5.658E+01	6.891E+02	-4.422E+01

Table S4-3: Quadratic fit coefficients for Box 1 from Figure 2 ($y=K0+K1x+K2x^2$)

	High Speed			Medium Speed			Low Speed		
Size Range (um)	**K0**	**K1**	**K2**	**K0**	**K1**	**K2**	**K0**	**K1**	**K2**
0.35-1.0	1.187E+03	-7.794E+00	-2.411E+00	8.643E+02	2.658E+01	-5.100E+00	6.834E+02	5.407E-01	-2.767E+00
1.0-3.0	1.397E+03	2.102E+01	-4.787E+00	9.694E+02	6.339E+01	-8.314E+00	7.700E+02	1.521E+01	-4.110E+00

4.6.3 CADR Results Tables

CADR values for each bin with specified particle optical diameter range, as well as average CADR values presented in Figure 4-2, are shown for high speed (Table S4-4), medium speed (Table S4-5), and low speed (Table S4-6).

Table S4-4: CADR results for all CR boxes for high speed. CADR units are m^3/hr.

CR Box	Days Elapsed	0.35 – 0.46 µm	0.46 – 0.66 µm	0.66 – 1.0 µm	1.0 – 1.3 µm	1.3 – 1.7 µm	1.7 – 2.3 µm	2.3 – 3.0 µm	Avg 0.35 – 1.0 µm	Avg 1.0 – 3.0 µm	Avg 0.35 – 3.0 µm
1	0	1109	1196	1244	1371	1366	1393	1415	1183	1386	1299
1	70	933	1152	1284	1414	1381	1454	1563	1123	1453	1312
1	140	858	1062	1120	1198	1259	1303	1293	1013	1263	1156
1	210	710	968	1028	1099	1155	1174	1318	902	1187	1065
1	280	753	943	1033	1103	1196	1199	1245	910	1186	1067
2	0	734	870	970	1057	1096	1115	1159	858	1106	1000
2	70	528	695	783	890	921	1002	1026	669	960	835
2	140	472	574	673	742	816	858	1004	573	855	734
2	210	516	612	678	761	785	851	902	602	825	729
2	280	377	484	557	651	702	776	882	473	753	633
3	0	785	917	1002	1118	1177	1361	1412	902	1267	1110
3	70	617	836	892	989	1057	1058	1154	782	1064	943
3	140	605	731	802	899	943	999	1077	712	979	865
3	210	574	664	737	819	889	979	1067	659	938	818
3	280	506	625	720	817	883	970	1060	617	933	798
4	0	668	809	923	1011	1028	1150	1257	800	1112	978
4	70	697	844	929	1008	1026	1047	1067	823	1037	945
4	140	627	736	822	912	965	1013	1133	728	1006	887
4	210	471	669	771	853	900	975	979	637	927	803
4	280	513	634	722	841	890	1006	1220	623	989	832

Table S4-5: CADR results for all CR boxes for medium speed. CADR units are m^3/hr.

CR Box	Days Elapsed	0.35 – 0.46 µm	0.46 – 0.66 µm	0.66 – 1.0 µm	1.0 – 1.3 µm	1.3 – 1.7 µm	1.7 – 2.3 µm	2.3 – 3.0 µm	Avg 0.35 – 1.0 µm	Avg 1.0 – 3.0 µm	Avg 0.35 – 3.0 µm
1	0	807	859	913	958	1002	1002	869	860	958	916
1	70	788	925	996	1094	1128	1133	1216	903	1143	1040
1	140	661	825	913	943	983	960	1003	800	972	898
1	210	530	696	758	803	812	854	810	661	820	752
1	280	577	703	753	818	861	845	934	678	865	784
2	0	563	632	709	816	823	867	898	635	851	758
2	70	469	561	637	703	736	804	836	555	770	678
2	140	377	440	510	574	624	693	770	442	665	570
2	210	398	486	549	601	620	686	705	478	653	578
2	280	367	421	491	560	590	611	618	426	595	523
3	0	649	786	818	919	948	992	973	751	958	869
3	70	522	663	741	831	841	913	883	642	867	771
3	140	457	560	633	692	727	787	751	550	739	658
3	210	488	526	591	658	689	765	837	535	737	651
3	280	502	570	654	743	783	895	867	575	822	716
4	0	727	777	821	885	940	964	970	775	940	869
4	70	649	705	758	828	858	873	837	704	849	787
4	140	522	637	654	745	759	794	826	604	781	705
4	210	567	656	710	765	804	837	912	644	830	750
4	280	474	560	623	733	769	875	858	552	808	699

Table S4-6: CADR results for all CR boxes for low speed. CADR units are m^3/hr.

CR Box	Days Elapsed	0.35 – 0.46 µm	0.46 – 0.66 µm	0.66 – 1.0 µm	1.0 – 1.3 µm	1.3 – 1.7 µm	1.7 – 2.3 µm	2.3 – 3.0 µm	Avg 0.35 – 1.0 µm	Avg 1.0 – 3.0 µm	Avg 0.35 – 3.0 µm
1	0	632	683	719	768	797	761	704	678	758	724
1	70	606	654	697	779	792	832	851	652	814	744
1	140	453	575	646	684	686	603	621	558	649	610
1	210	335	421	462	481	496	511	472	406	490	454
1	280	494	497	534	566	581	613	601	508	590	555
2	0	484	507	550	655	659	703	660	514	669	603
2	70	426	477	514	601	616	639	779	472	659	579
2	140	308	339	385	444	479	510	575	344	502	434
2	210	401	416	459	500	523	522	530	425	519	479
2	280	253	320	358	407	442	472	484	310	451	391
3	0	632	683	719	768	797	761	704	678	758	724
3	70	284	507	595	687	708	672	654	462	680	587
3	140	374	420	471	522	554	620	605	421	575	509
3	210	274	398	455	514	568	625	547	376	563	483
3	280	277	399	480	517	573	674	667	385	608	512
4	0	533	566	619	674	690	714	753	573	708	650
4	70	502	566	606	678	681	726	709	558	698	638
4	140	430	462	499	540	572	615	612	463	584	533
4	210	487	514	560	615	612	628	564	520	605	568
4	280	340	434	490	569	599	679	707	422	639	546

4.6.4 SPFE Results Tables

SPFE values for each bin with specified particle optical diameter range, as well as average SPFE values presented in Figure 4, are shown for high speed (Table S4-7), medium speed (Table S4-8), and low speed (Table S4-9).

Table S4-7: SPFE results for all CR boxes for high speed. SPFE is a unitless ratio.

CR Box	Days Elapsed	0.35 – 0.46 µm	0.46 – 0.66 µm	0.66 – 1.0 µm	1.0 – 1.3 µm	1.3 – 1.7 µm	1.7 – 2.3 µm	2.3 – 3.0 µm	Avg 0.35 – 1.0 µm	Avg 1.0 – 3.0 µm	Avg 0.35 – 3.0 µm
1	0	0.98	0.99	1.00	1.00	1.00	1.00	1.00	0.99	1.00	0.99
1	210	0.72	0.87	0.91	0.92	0.93	0.94	0.96	0.83	0.94	0.89
1	280	0.67	0.83	0.88	0.89	0.91	0.94	0.95	0.79	0.92	0.87
2	0	0.69	0.72	0.78	0.84	0.86	0.86	0.90	0.73	0.87	0.81
2	210	0.41	0.47	0.50	0.52	0.58	0.57	0.59	0.46	0.57	0.52
2	280	0.20	0.29	0.40	0.39	0.40	0.45	0.41	0.30	0.41	0.36
3	0	0.72	0.73	0.78	0.82	0.82	0.83	0.88	0.74	0.84	0.80
3	210	0.44	0.56	0.61	0.64	0.65	0.64	0.70	0.53	0.66	0.61
3	280	0.36	0.45	0.55	0.60	0.60	0.70	0.68	0.45	0.65	0.56
4	0	0.64	0.67	0.72	0.75	0.78	0.80	0.87	0.68	0.80	0.75
4	210	0.39	0.56	0.61	0.61	0.68	0.66	0.72	0.52	0.67	0.60
4	280	0.29	0.41	0.49	0.49	0.52	0.65	0.56	0.40	0.56	0.49

Table S4-8: SPFE results for all CR boxes for medium speed. SPFE is a unitless ratio.

CR Box	Days Elapsed	0.35 – 0.46 µm	0.46 – 0.66 µm	0.66 – 1.0 µm	1.0 – 1.3 µm	1.3 – 1.7 µm	1.7 – 2.3 µm	2.3 – 3.0 µm	Avg 0.35 – 1.0 µm	Avg 1.0 – 3.0 µm	Avg 0.35 – 3.0 µm
1	0	0.98	0.99	1.00	1.00	1.00	1.00	1.00	0.99	1.00	0.99
1	210	0.72	0.87	0.91	0.92	0.93	0.94	0.96	0.83	0.94	0.89
1	280	0.67	0.83	0.88	0.89	0.91	0.94	0.95	0.79	0.92	0.87
2	0	0.69	0.72	0.78	0.84	0.86	0.86	0.90	0.73	0.87	0.81
2	210	0.41	0.47	0.50	0.52	0.58	0.57	0.59	0.46	0.57	0.52
2	280	0.20	0.29	0.40	0.39	0.40	0.45	0.41	0.30	0.41	0.36
3	0	0.72	0.73	0.78	0.82	0.82	0.83	0.88	0.74	0.84	0.80
3	210	0.44	0.56	0.61	0.64	0.65	0.64	0.70	0.53	0.66	0.61
3	280	0.36	0.45	0.55	0.60	0.60	0.70	0.68	0.45	0.65	0.56
4	0	0.64	0.67	0.72	0.75	0.78	0.80	0.87	0.68	0.80	0.75
4	210	0.39	0.56	0.61	0.61	0.68	0.66	0.72	0.52	0.67	0.60
4	280	0.29	0.41	0.49	0.49	0.52	0.65	0.56	0.40	0.56	0.49

Table S4-9: SPFE results for all CR boxes for low speed. SPFE is a unitless ratio.

CR Box	Days Elapsed	0.35 – 0.46 µm	0.46 – 0.66 µm	0.66 – 1.0 µm	1.0 – 1.3 µm	1.3 – 1.7 µm	1.7 – 2.3 µm	2.3 – 3.0 µm	Avg 0.35 – 1.0 µm	Avg 1.0 – 3.0 µm	Avg 0.35 – 3.0 µm
1	0	0.99	1.00	1.00	1.00	1.00	1.00	1.00	0.99	1.00	1.00
1	210	0.77	0.91	0.94	0.95	0.96	0.98	0.95	0.87	0.96	0.92
1	280	0.73	0.87	0.91	0.93	0.94	0.94	0.95	0.84	0.94	0.90
2	0	0.64	0.70	0.75	0.82	0.81	0.83	0.82	0.70	0.82	0.77
2	210	0.39	0.49	0.52	0.56	0.62	0.63	0.61	0.47	0.61	0.55
2	280	0.24	0.30	0.38	0.43	0.39	0.50	0.55	0.31	0.46	0.40
3	0	0.69	0.75	0.79	0.81	0.82	0.84	0.87	0.75	0.83	0.80
3	210	0.42	0.59	0.65	0.68	0.67	0.69	0.70	0.55	0.69	0.63
3	280	0.36	0.49	0.55	0.57	0.63	0.63	0.69	0.47	0.63	0.56
4	0	0.62	0.71	0.76	0.80	0.80	0.82	0.85	0.70	0.82	0.77
4	210	0.39	0.59	0.64	0.66	0.68	0.73	0.77	0.54	0.71	0.64
4	280	0.28	0.42	0.48	0.57	0.52	0.59	0.73	0.39	0.60	0.51

4.6.5 Total Flow Rate Results Tables

Total flow rate for each bin with specified particle optical diameter range, as well as average flow rate and standard deviation values presented in Figure 5, are shown for high speed (Table S4-10), medium speed (Table S4-11), and low speed (Table S4-12).

Table S4-10: Total flow rate results for all CR boxes for high speed. Flow rate units are m^3/hr.

CR Box	Days Elapsed	0.35 – 0.46 µm	0.46 – 0.66 µm	0.66 – 1.0 µm	1.0 – 1.3 µm	1.3 – 1.7 µm	1.7 – 2.3 µm	2.3 – 3.0 µm	Avg 0.35 – 3.0 µm	Standard Deviation 0.35– 3.0 µm
1	0	1083	1132	1165	1278	1261	1276	1275	1210	58
1	210	917	1027	1044	1088	1123	1128	1228	1079	66
1	280	1049	1057	1079	1129	1200	1147	1166	1118	47
2	0	999	1109	1132	1141	1153	1154	1125	1116	23
2	210	1132	1142	1187	1276	1163	1279	1283	1209	56
2	280	1628	1438	1178	1429	1491	1452	1795	1487	168
3	0	1021	1165	1174	1248	1307	1489	1442	1264	121
3	210	1206	1063	1074	1123	1199	1338	1325	1190	103
3	280	1276	1242	1168	1199	1287	1217	1361	1250	59
4	0	966	1100	1158	1218	1176	1282	1286	1169	69
4	210	1093	1066	1135	1234	1175	1293	1170	1167	67
4	280	1602	1378	1310	1510	1503	1370	1930	1515	191

Table S4-11: Total flow rate results for all CR boxes for medium speed. Flow rate units are m^3/hr.

CR Box	Days Elapsed	0.35 – 0.46 µm	0.46 – 0.66 µm	0.66 – 1.0 µm	1.0 – 1.3 µm	1.3 – 1.7 µm	1.7 – 2.3 µm	2.3 – 3.0 µm	Avg 0.35 – 3.0 µm	Standard Deviation 0.35– 3.0 µm
1	0	791	812	853	886	920	908	742	845	58
1	210	673	723	744	770	767	805	704	741	32
1	280	783	768	778	830	835	794	827	802	24
2	0	728	732	762	853	826	860	831	799	45
2	210	999	929	939	949	942	952	934	949	11
2	280	1481	1206	1083	1177	1185	1125	1117	1196	59
3	0	883	998	962	1035	1048	1076	972	996	42
3	210	1024	837	852	896	887	943	1015	922	58
3	280	1415	1112	1069	1154	1206	1220	1218	1199	63
4	0	1083	1045	1012	1032	1086	1060	1002	1046	27
4	210	1458	1066	1009	1095	1097	1056	1104	1126	59
4	280	1676	1229	1141	1248	1307	1288	1209	1300	77

Table S4-12: Total flow rate results for all CR boxes for low speed. Flow rate units are m^3/hr.

CR Box	Days Elapsed	0.35 – 0.46 µm	0.46 – 0.66 µm	0.66 – 1.0 µm	1.0 – 1.3 µm	1.3 – 1.7 µm	1.7 – 2.3 µm	2.3 – 3.0 µm	Avg 0.35 – 3.0 µm	Standard Deviation 0.35– 3.0 µm
1	0	601	624	650	689	709	666	600	649	35
1	210	391	395	417	421	424	426	386	408	14
1	280	628	497	511	522	525	549	523	536	20
2	0	701	632	640	700	705	734	674	684	34
2	210	939	718	740	747	696	676	703	745	38
2	280	901	864	751	766	912	756	695	806	70
3	0	684	34	861	826	820	846	865	815	53
3	210	745	38	568	567	594	635	714	640	64
3	280	806	70	677	686	740	768	770	769	70
4	0	796	711	724	743	752	750	763	749	18
4	210	1150	770	759	813	768	732	598	799	83
4	280	1082	890	870	858	983	986	822	927	62

4.6.6 Raw Power Data

The complete set of power monitoring data is shown in Figure S4-3. As explained in the main text, the power meter for Box 2 did not log data for the last deployment period. Periodic observations of the box recorded that it was running at low speed as expected during this period.

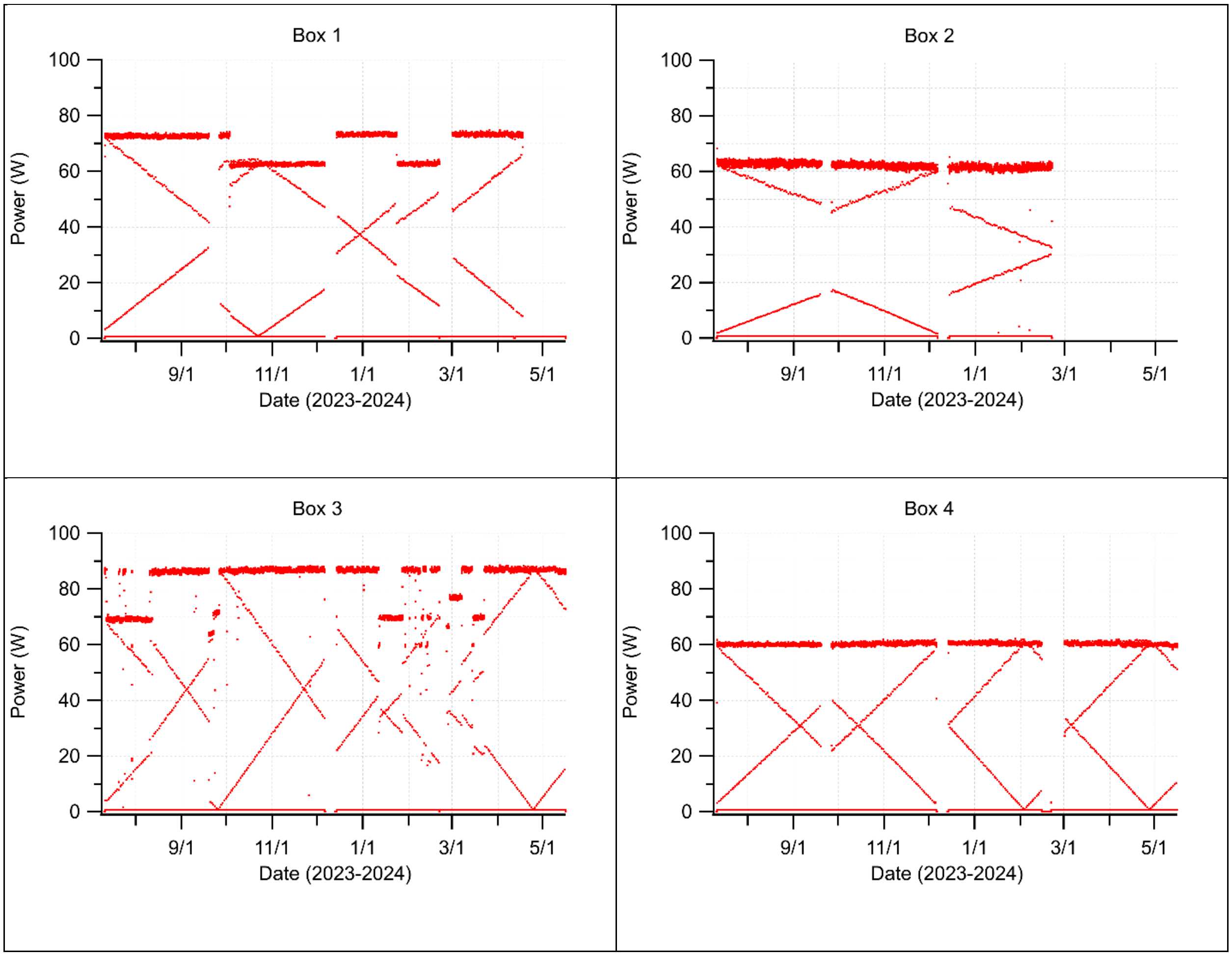

Figure S4-3: All power motoring data for CR Boxes 1 to 4. Each steady state power level indicates distinct fan speed (only Box 1 and Box 3 were used at multiple speeds by the occupants).

4.6.7 Pressure Drop Data

The differential pressure measurements for each CR box at each speed are shown in Table S4-13.

Table S4-13: Pressure differential across CR Box filters by box, speed, and days elapsed.

	High Speed				Medium Speed				Low Speed			
Days Elapsed	Box 1 (Pa)	Box 2 (Pa)	Box 3 (Pa)	Box 4 (Pa)	Box 1 (Pa)	Box 2 (Pa)	Box 3 (Pa)	Box 4 (Pa)	Box 1 (Pa)	Box 2 (Pa)	Box 3 (Pa)	Box 4 (Pa)
0	7.2	7.2	7.1	7.2	5.4	5.6	5.7	5.7	4.0	4.1	4.2	4.2
210	10.3	8.2	8.6	8.7	6.7	5.5	6.2	6.0	5.7	4.4	4.9	4.8
280	10.9	8.2	8.9	9	8.1	6.2	7	7.2	5.7	4.6	5.1	5.2

4.6.8 CADR Measurement Uncertainty

To estimate the uncertainty of the CADR measurement method, at the end of the experiment the CADR of Box 3 on speed high was measured 10 times (Table S4-14). Box 3 had been used intermittently over two months since testing concluded, so the results are slightly lower than the 40-week measurement. The uncertainty (two standard deviations) was 6% of the average measurement for 0.35 to 1 µm optical diameter particles and 5% for 1 to 3 optical diameter particles.

Table S4-14: Repeat CADR measurement for Box 3 for medium speed. CADR units are m^3/hr.

Test	0.35 – 0.46 µm	0.46 – 0.66 µm	0.66 – 1.0 µm	1.0 – 1.3 µm	1.3 – 1.7 µm	1.7 – 2.3 µm	2.3 – 3.0 µm	Average 0.35 – 1.0 µm	Average 1.0 – 3.0 µm
1	389	613	707	807	874	926	1014	570	905
2	459	604	674	770	791	883	940	579	846
3	464	604	686	767	815	880	1022	585	871
4	449	612	694	767	834	902	1028	585	883
5	477	614	690	780	824	931	937	594	868
6	393	582	661	736	814	917	948	545	854
7	447	585	668	746	818	903	1008	567	869
8	458	596	678	769	797	923	976	577	866
9	394	607	683	775	818	842	898	562	833
10	489	626	697	821	845	879	971	604	879
							Average	577	867
							2*STD	34	40
							Percent	6%	5%

Chapter 5 References

1. United States Environmental Protection Agency, *Child-Specific Exposure Factors Handbook, Final Report*. 2008: Washington, DC.
2. Sadrizadeh, S., et al., *Indoor air quality and health in schools: A critical review for developing the roadmap for the future school environment.* Journal of Building Engineering, 2022. **57**.
3. Fisk, W.J., *The ventilation problem in schools: literature review.* Indoor Air, 2017. **27**(6): p. 1039-1051.
4. Chan, R., et al., *Ventilation rates in California classrooms: Why many recent HVAC retrofits are not delivering sufficient ventilation.* Building and Environment, 2020. **167**.
5. United States Energy Information Administration. *Commercial Buildings Energy Consumption Survey (CBECS)*. 2018 CBECS Survey Data 2018 [cited 2023 February 15]; Available from: https://www.eia.gov/consumption/commercial/data/2018/index.php?view=consumption.
6. Pistochini, T., C. Mande, and S. Chakraborty, *Modeling impacts of ventilation and filtration methods on energy use and airborne disease transmission in classrooms.* Journal of Building Engineering, 2022. **57**.
7. Morawska and J. Cao, *Airborne transmission of SARS-CoV-2: The world should face the reality* Environment International, 2020. **139**.
8. Centers for Disease Control and Prevention. *COVID-19: How to Protect Yourself and Others*. Improving Ventilation and Spending Time Outdoors 2023 [cited 2023 February 15]; Available from: https://www.cdc.gov/coronavirus/2019-ncov/prevent-getting-sick/prevention.html#ventilation.
9. National Interagency Fire Center. *Total Wildland Fires and Acres (1983-2022)*. 2022 [cited 2023 February 15]; Available from: https://www.nifc.gov/fire-information/statistics/wildfires.
10. Cheek, E., et al., *Portable air purification: Review of impacts on indoor air quality and health.* Science of the Total Environment, 2021. **766**.
11. International Standards Organization, *ISO 29463-5:2022 High-efficiency filters and filter media for removing particles in air*. 2022. p. 28.
12. Dal Porto, R., et al., *Characterizing the performance of a do-it-yourself (DIY) box fan air filter.* Aerosol Science and Technology, 2022. **56**(6): p. 564-572.
13. Holder, A.L., H.S. Halliday, and L. Virtaranta, *Impact of do-it-yourself air cleaner design on the reduction of simulated wildfire smoke in a controlled chamber environment.* Indoor Air, 2022. **32**(11): p. e13163.
14. Srikrishna, D., *Can 10x cheaper, lower-efficiency particulate air filters and box fans complement High-Efficiency Particulate Air (HEPA) purifiers to help control the COVID-19 pandemic?* Sci Total Environ, 2022. **838**(Pt 1): p. 155884.
15. Derk, R.C., et al., *Efficacy of Do-It-Yourself air filtration units in reducing exposure to simulated respiratory aerosols.* Build Environ, 2023. **229**: p. 109920.
16. Myers, N.T., et al., *Performance evaluation of different low-cost DIY air cleaner configurations.* Aerosol Science and Technology, 2023. **57**(11): p. 1128-1141.
17. Jehn, M.L., et al., *Effectiveness of do-it-yourself air cleaners in reducing exposure to respiratory aerosols in US classrooms: A longitudinal study of public schools.* Building and Environment, 2024. **258**.
18. Schell, M. and D. Int-Hout, *Demand Control Ventilation Using CO2.* ASHRAE Journal, 2001.

19. Lu, X., et al., *The nexus of the indoor CO2 concentration and ventilation demands underlying CO2-based demand-controlled ventilation in commercial buildings: A critical review.* Building and Environment, 2022. **218**.
20. Persily, A., et al., *Simulations of Indoor Air Quality and Ventilation Impacts of Demand Controlled Ventilation in Commercial and Institutional Buildings*. 2003, National Institute of Standards and Technology.
21. ANSI/ASHRAE, *Standard 90.1-2022 - Energy Standard for Sites and Buildings Except Low-Rise Residential Buildings*. 2022.
22. American Society of Heating Refrigerating and Air-Conditioning Engineers, *ANSI/ASHRAE Standard 62.1-2022 Ventilation for Acceptable Indoor Air Quality*. 2022.
23. California Energy Commission, *Building Energy Efficiency Standards - Title 24*. 2022: Sacramento.
24. Peng, Z. and J.L. Jimenez, *Exhaled CO2 as a COVID-19 Infection Risk Proxy for Different Indoor Environments and Activities.* Environmental Science & Technology Letters, 2021. **8**(5): p. 392-397.
25. Good, N., et al., *Respiratory Aerosol Emissions from Vocalization: Age and Sex Differences Are Explained by Volume and Exhaled CO2.* Environmental Science & Technology Letters, 2021. **8**(12): p. 1071-1076.
26. Acker, B. and K. Van Den Wymelenberg, *Demand control ventilation: lessons from the field - how to avoid common problems.* ASHRAE Transactions, 2011. **117**(1).
27. Pistochini, T., et al., *Improving Ventilation and Indoor Evironmental Quality in California K-12 Schools*. 2020, California Energy Commission.
28. Fraiser, A., et al., *Standard Testing Protocols for CO2 Sensors and CO2-based Demand Control Ventilation Systems*, in *Internatoinal High Performance Buildings Conference*. 2021, Purdue University.
29. Lu, X.S., et al., *A new method for controlling CO2 in buildings with unscheduled opening hours.* Energy and Buildings, 2013. **59**: p. 161-170.
30. Schell, M., S. Turner, and O. Shim, *Application of CO2-Based Demand-Controlled Ventilation Using ASHRAE Standard 62: Optimizing Energy Use and Ventilation.* ASHRAE Transactions Symposia, 1998. **TO-98-21-1**: p. 13.
31. Seem, J.E., *A new pattern recognition adaptive controller with application to HVAC systems.* Automatica, 1998. **34**(8): p. 969-982.
32. Lu, X., et al., *Advances in research and applications of CO2-based demand-controlled ventilation in commercial buildings: A critical review of control strategies and performance evaluation.* Building and Environment, 2022. **223**.
33. Liu, H., et al., *Finding the optimal set points of a thermal and ventilation control system under changing outdoor weather conditions.* Indoor and Built Environment, 2014. **23**(1): p. 118-132.
34. Zhigang, S., L. Xuquan, and H. Songtao. *Direct feedback linearization based control of CO2 demand controlled ventilation*. in *2010 2nd International Conference on Computer Engineering and Technology*. 2010.
35. Lachhab, F., et al., *Context-driven monitoring and control of buildings ventilation systems using big data and Internet of Things–based technologies.* Proceedings of the Institution of Mechanical Engineers, Part I: Journal of Systems and Control Engineering, 2019. **233**(3): p. 276-288.
36. Zhu, J., Lauri, F., Koukam, A., Hilaire, V. *Managing Ventilation Systems for Improving User Comfort in Smart Buildings using Reinforcement Learning Agents*. in *Proceedings of European Conference on Machine Learning and Principles and Practice of Knowledge Discovery in Databases*. 2014.

37. Mande, C., *Tracer Gas Airflow Measurement System*. 2018, University of California, Davis.
38. Persily, A., *Development and application of an indoor carbon dioxide metric.* Indoor Air, 2022. **32**(7): p. e13059.
39. California Energy Commission, *Building Energy Efficiency Standards for Residential and Nonresidential Buildings*, in *Requirements for Ventilation and Indoor Air Quality*. 2019.
40. Delp, W.M., N. E; Dickerhoff, D. J; Modera, M. P. , *Field Investigation of Duct System Performance in California Light Commercial Buildings*. 2005, UC Berkeley: California Institute for Energy and Environment.
41. ASHRAE, *ASHRAE Position Document on Indoor Carbon Dioxide*. 2022: Peachtree Corners, Georgia.
42. Astrom, K., Hagglund, T., *PID Controllers: Theory, Design, and Tuning*. 2 ed. 1995, Research Triangle Park, NC: Instrument Society of America.
43. ASHRAE, *RP-1547 - CO2-Based Demand Controlled Ventilation for Multiple Zone HVAC Systems*. 2014.
44. Lu, X.Y., T; O'Neill, Z; Zhou, X, *<d-bsc20-c037.pdf>*, in *2020 Building Performance Analysis Conference and SimBuild*. 2020, ASHRAE and IBPSA-USA: Virtual.
45. O'Neill, Z.D., et al., *Energy savings and ventilation performance from CO2-based demand controlled ventilation: Simulation results from ASHRAE RP-1747 (ASHRAE RP-1747).* Science and Technology for the Built Environment, 2019. **26**(2): p. 257-281.
46. Lu, X., et al., *Advances in research and applications of CO2-based demand-controlled ventilation in commercial buildings: A critical review of control strategies and performance evaluation.* Building and Environment, 2022. **223**.
47. Ferrandez-Pastor, F.J., et al., *Deployment of IoT Edge and Fog Computing Technologies to Develop Smart Building Services.* Sustainability, 2018. **10**(11).
48. Pistochini, T., et al., *Method of test for CO2-based demand control ventilation systems: Benchmarking the state-of-the-art and the undervalued potential of proportional-integral control.* Energy and Buildings, 2023. **301**.
49. Taylor, S. and C. Cheng, *Economizer High Limit Controls.* ASHRAE Journal, 2010: p. 1-11.
50. ANSI/ASHRAE, *Standard 90.1-2010 - Energy Standard for Sites and Buildings Except Low-Rise Residential Buildings*. 2010.
51. Chiesa, G., M. Kolokotroni, and P. Heilselberg, *Innovations in Ventilative Cooling*. PoliTO Springer Series. 2021: Springer. 359.
52. Belleri, A., et al., *Evaluation tool of climate potential for ventilative cooling.* International Journal of Ventilation, 2017. **17**(3): p. 196-208.
53. American Society of Heating Refrigerating and Air-Conditioning Engineers, *ANSI/ASHRAE Standard 52.2-2017*, in *Method of Testing General Ventilation Air-Cleaning Devices for Removal Efficiency by Particle Size*. 2017.
54. American Society of Heating, R.a.A.-C.E., *Method of Testing General Ventilation Air-Cleaning Devices for Removal Efficiency by Particle Size*. 2017, American Society of Heating, Refrigerating and Air-Conditioning Engineers. p. 53.
55. Hofmann, W., *Modelling inhaled particle deposition in the human lung-A review.* Journal of Aerosol Science, 2011. **42**(10): p. 693-724.
56. Chen, J. and G. Hoek, *Long-term exposure to PM and all-cause and cause-specific mortality: A systematic review and meta-analysis.* Environ Int, 2020. **143**: p. 105974.

57. Cohen, A.J., M. Brauer, and R. Burnett, *Estimates and 25-year trends of the global burden of disease attributable to ambient air pollution: an analysis of data from the Global Burden of Diseases Study 2015 (vol 389, pg 1907, 2017).* Lancet, 2018. **391**(10130): p. 1576-1576.
58. Chen, J. and G. Hoek, *Long-term exposure to PM and all-cause and cause-specific mortality: A systematic review and meta-analysis.* Environment International, 2020. **143**.
59. World Health Organization, *WHO global air quality guidelines. Particulate matter (PM2.5 and PM10), ozone, nitrogen dioxide, sulfur dioxide and carbon monoxide*. 2021: Geneva.
60. Liu, D.T., et al., *Portable HEPA Purifiers to Eliminate Airborne SARS-CoV-2: A Systematic Review.* Otolaryngol Head Neck Surg, 2022. **166**(4): p. 615-622.
61. American Society of Heating Refrigerating and Air-Conditioning Engineers, *ASHRAE Standard 241-2023 Control of Infectious Aerosols*. 2023.
62. US Environmental Protection Agency. *Final Updates to the Air Quality Index (AQI) for Particulate Matter*. 2024; Available from: https://www.epa.gov/system/files/documents/2024-02/pm-naaqs-air-quality-index-fact-sheet.pdf.
63. Chan, W.R., et al., *Ventilation rates in California classrooms: Why many recent HVAC retrofits are not delivering sufficient ventilation.* Building and Environment, 2020. **167**.
64. US Environmental Protection Agency. *Air Quality - Cities and Counties*. 2024 [cited 2024 July 28, 2024]; Available from: https://www.epa.gov/air-trends/air-quality-cities-and-counties.
65. US Environmental Protection Agency. *Energy STAR Certified Room Air Cleaners*. 2023; Available from: https://www.energystar.gov/productfinder/product/certified-room-air-cleaners/results.
66. Tai, A.P.K., L.J. Mickley, and D.J. Jacob, *Correlations between fine particulate matter (PM2.5) and meteorological variables in the United States: Implications for the sensitivity of PM2.5 to climate change.* Atmospheric Environment, 2010. **44**(32): p. 3976-3984.
67. White Box Technologies. *Weather Data for Energy Calculations*. 2023 [cited 2023 May 26].
68. Green, C., *EPA PM2.5 Data Preprocessing*. 2024: GitHub.
69. Batterman, S., *Review and Extension of CO2-Based Methods to Determine Ventilation Rates with Application to School Classrooms.* International Journal of Environmental Research and Public Health, 2017. **14**(2).
70. Batterman, S., et al., *Ventilation rates in recently constructed US school classrooms.* Indoor Air, 2017. **27**(5): p. 880-890.
71. US Environmental Protection Agency. *Energy STAR Room Air Cleaners Key Product Criteria*. 2023; Available from: https://www.energystar.gov/products/air_purifiers_cleaners/key_product_criteria.
72. Lundgren, D.A., et al., *PM(10)/PM(2.5)/PM(1) data from a trichotomous sampler.* Aerosol Science and Technology, 1996. **25**(3): p. 353-357.
73. Haller, L., et al., *Airborne particulate matter size distributions in an arid urban area.* Journal of the Air & Waste Management Association, 1999. **49**(2): p. 161-168.
74. Geller, M.D., P.M. Fine, and C. Sioutas, *The relationship between real-time and time-integrated coarse (2.5-10 μm), intermodal (1-2.5 μm), and fine (<2.5 μm) particulate matter in the Los Angeles Basin.* Journal of the Air & Waste Management Association, 2004. **54**(9): p. 1029-1039.
75. Yin, J.X. and R.M. Harrison, *Pragmatic mass closure study for PM1.0, PM2.5 and PM10 at roadside, urban background and rural sites.* Atmospheric Environment, 2008. **42**(5): p. 980-988.
76. Zwozdziak, A., et al., *The contribution of outdoor particulate matter (PM1, PM2.5, PM10) to school indoor environment.* Indoor and Built Environment, 2015. **24**(8): p. 1038-1047.

77. Kozáková, J., et al., *The Association between Intermodal (PM1-2.5) and PM1, PM2.5, Coarse Fraction and Meteorological Parameters in Various Environments in Central Europe.* Aerosol and Air Quality Research, 2017. **17**(5): p. 1234-1243.
78. Diapouli, E., A. Chaloulakou, and P. Koutrakis, *Estimating the concentration of indoor particles of outdoor origin: a review.* J Air Waste Manag Assoc, 2013. **63**(10): p. 1113-29.
79. Zhang, Y.M., et al., *Effect of Acute PM2.5 Exposure on Lung Function in Children: A Systematic Review and Meta-Analysis.* Journal of Asthma and Allergy, 2023. **16**: p. 529-540.
80. Zhang, Y., et al., *The association of ambient PM2.5 with school absence and symptoms in schoolchildren: a panel study.* Pediatric Research, 2018. **84**(1): p. 28-33.
81. Barkjohn, K.K., B. Gantt, and A.L. Clements, *Development and application of a United States-wide correction for PM2.5 data collected with the PurpleAir sensor.* Atmospheric Measurement Techniques, 2021. **14**(6): p. 4617-4637.
82. Myers, N.T., et al., *Portable air cleaners and residential exposure to SARS-CoV-2 aerosols: A real-world study.* Indoor Air, 2022. **32**(4): p. e13029.
83. Buising, K.L., et al., *Use of portable air cleaners to reduce aerosol transmission on a hospital coronavirus disease 2019 (COVID-19) ward.* Infect Control Hosp Epidemiol, 2022. **43**(8): p. 987-992.
84. Banholzer, N., et al., *SARS-CoV-2 transmission with and without mask wearing or air cleaners in schools in Switzerland: A modeling study of epidemiological, environmental, and molecular data.* PLoS Med, 2023. **20**(5): p. e1004226.
85. Vartiainen, V.A., et al., *The effect of room air cleaners on infection control in day care centres.* Indoor Environments, 2024. **1**(1).
86. Fisk, W.J., *Health benefits of particle filtration.* Indoor Air, 2013. **23**(5): p. 357-368.
87. Allen, R.W., et al., *An Air Filter Intervention Study of Endothelial Function among Healthy Adults in a Woodsmoke-impacted Community.* American Journal of Respiratory and Critical Care Medicine, 2011. **183**(9): p. 1222-1230.
88. Bräuner, E.V., et al., *Indoor particles affect vascular function in the aged -: An air filtration-based intervention study.* American Journal of Respiratory and Critical Care Medicine, 2008. **177**(4): p. 419-425.
89. Fisk, W.J. and W.R. Chan, *Health benefits and costs of filtration interventions that reduce indoor exposure to PM2.5 during wildfires.* Indoor Air, 2017. **27**(1): p. 191-204.
90. Association of Home Appliance Manufacturers. *Find a Certified Room Air Cleaner*. [cited 2024 June 24]; Available from: https://ahamverifide.org/directory-of-air-cleaners/.
91. Kaur, K. and K.E. Kelly, *Laboratory evaluation of the Alphasense OPC-N3, and the Plantower PMS5003 and PMS6003 sensors.* Journal of Aerosol Science, 2023. **171**.
92. Sparks, T.L. and J. Wagner, *Composition of particulate matter during a wildfire smoke episode in an urban area.* Aerosol Science and Technology, 2021. **55**(6): p. 734-747.
93. Alsved, M., et al., *Size distribution of exhaled aerosol particles containing SARS-CoV-2 RNA.* Infectious Diseases, 2023. **55**(2): p. 158-163.
94. Hagan, D.H. and J.H. Kroll, *Assessing the accuracy of low-cost optical particle sensors using a physics-based approach.* Atmos Meas Tech, 2020. **13**(11): p. 6343-6355.
95. South Coast Air Quality Management District, *Field Evaluation Purple Air (PA-II) PM Sensor*. 2017.
96. Wang, Z., W.W. Delp, and B.C. Singer, *Performance of low-cost indoor air quality monitors for PM2.5 and PM10 from residential sources.* Building and Environment, 2020. **171**.

97. Park, S., et al., *Field and laboratory evaluation of PurpleAir low-cost aerosol sensors in monitoring indoor airborne particles.* Building and Environment, 2023. **234**.
98. Adams, N., *ASHRAE 52.2-2017 Test Report for Air Handler 2EKJ5 obtained from nadams@aafintl.com*.
99. Rosenthal, J., *ASHRAE 52.2-2017 Test Report for Tex-Air Filter obtained from jimrosenthal5757@aol.com*.
100. Kowalski, W.J. and W.P. Bahnfleth, *MERV Filter Models for Aerobiological Applications*. 2002.
101. Yit, J.E., B.T. Chew, and Y.H. Yau, *A review of air filter test standards for particulate matter of general ventilation.* Building Services Engineering Research & Technology, 2020. **41**(6): p. 758-771.
102. Liang, Y., et al., *Wildfire smoke impacts on indoor air quality assessed using crowdsourced data in California.* Proc Natl Acad Sci U S A, 2021. **118**(36).